universität wien

MASTERARBEIT / MASTER'S THESIS

Titel der Masterarbeit / Title of the Master's Thesis

"Dissecting kinase networks in the hyperosmotic stress response in Yeast using quantitative mass spectrometry-based and bioinformatical approaches"

verfasst von / submitted by

Marion Franziska Janschitz, BSc

angestrebter akademischer Grad / in partial fulfilment of the requirements for the degree of

Master of Science (MSc)

Wien, 2018 / Vienna 2018

Studienkennzahl lt. Studienblatt / degree programme code as it appears on the student record sheet:	A 066 834
Studienrichtung lt. Studienblatt / degree programme as it appears on the student record sheet:	Molekulare Biologie UG2002
Betreut von / Supervisor:	Prof. Dr. Gustav Ammerer
Mitbetreut von / Co-Supervisor:	Dr. Wolfgang Ludwig Reiter

Table of Contents

I. Acknowledgements

First and foremost, I thank my thesis supervisor Gustav Ammerer for giving me the chance to not only do my Master's project in his research group, but also get to know the actual everyday life of a scientist. Gustav is one of the most knowledgeable human beings I've ever known, with an impressive knack for finding interesting leads and joining dots over great distances, and he will always be exactly the kind of know-it-all I aspire to become. I am thankful to him for the opportunity to be trained in a highly educational and supportive environment and for his relentless will to make me broaden my horizon in regard to both, good scientific practise and finding my way in the professional world.

The most special of thanks go to Gustav's second-in-command, my co-supervisor Wolfgang Reiter, mentor by trade and friend by default. If it wasn't for him, I would have never made it to where (and what kind of person and scientist) I am now, and I am forever grateful that coincidence put my project into his hands - although at first chaotic, thoughtless me was a bit intimidated by his unfalteringly diligent and considerate attitude towards both, work and human interaction. Listing the countless ways this masterclass pedagogue taught, educated and fine-tuned me over the last years would fill pages, so I will resort to simply say: I am thankful to have been part of Team Dreamdestroyer, you have become a true friend to me.

When mentioning Team Dreamdestroyer, I naturally also have to mention my "oldest" if not THE friend through all of university, David Hollenstein, my predecessor Natalie Romanov, and, although a bit off the MFPL-grid, Thomas Gossenreiter - it was a pleasure working side-to-side with you lovely people and pushing the deadlines for all the great stuff we did beyond eternity together.

Of course, I also thank all the other "Ammerer-Girls" - current members Jillian Augustine-Rubak, Gabriela Gerecova, Jessica Ferrari, former member Isabella Hansmann, and my very own intern and successor Gina Varnavides for providing constant professional feedback and for turning the lab and the occasional conversation pink – as well as the mass spectrometry guardians Dorothea Anrather and Markus Hartl for input, support and an open ear for all kinds of questions.

Another round of thanks also goes to the members of Egon Ogris' research group, who made me feel so comfortable in the two adjacent labs in the second floor that I was just compelled to stay in that area for longer. Specifically, I want to thank Jiri Veis, for giving an impressive example of how to be a brilliant scientist even if surrounded by your own unbelievable chaos, for showering me with

all kinds of weird to general to actually applicable knowledge, for playing the advocatus diaboli to my personal escapades and for his always slightly different perspective on pretty much everything.

Special thanks also go to Egon Ogris himself, for providing brutally honest feedback at all times, and for giving me my first chance to amend a rough start with someone whose approval means a lot to me, to the end of being one of my examiners for this thesis. Besides Gustav Ammerer and Egon Ogris, I thank Pavel Kovarik, for accepting my proposal as third examiner so spontaneously and straightforwardly.

Finally, this thesis would have never been possible without the administrative angels Barbara Hamilton and Renate Fauland. I thank them both with all my heart for putting up with my chaos and for helping me out every single time I needed them, although I am well aware of the fact that they never really fell for my miserable-puppy-eyes.

Last, but not least, I want to thank a few people beyond my professional environment:

My best friend and nemesis, my father Franz, for giving me all the love in the world and all the tools I need to be the best version of myself, for installing within me an inexhaustible faith in myself, and for teaching me how to do the right thing when it really counts.

My beloved mother, Regina, who lives on within and through me, for all that I am.

My brother Stefan and his mother Georgine, my sister Margaux, my mother 2.0 Christine, my grandmother Antonia, my grandfather Johann and all of my aunts, uncles, cousins, nephews and nieces, for being the most wonderful, patchwork-y, loving, crazy family ever in existence.

Jenni, for being who she is. Words can’t describe what she means to me.
Sarah, for being everything anyone could ever wish for in a best friend.
Andrea, the bravest woman I have ever met, for being my spirit animal.
Julien, for being a magnificent example on how to be a bad example.
All the VBC Amateur Dramatic Club for being an endless source of laughter, love and comfort.
Lucas, for teaching me how to love genuinely.

II. Abstract

Living cells interpret and react to physicochemical stress signals using intracellular signal transduction systems, often involving post-translational modifications (PTMs) mediated by complex kinase-phosphatase networks. The high osmolarity glycerol (HOG) pathway in *Saccharomyces cerevisiae* is a paradigm for mitogen-activated protein kinase (MAPK) and stress signalling. Its central key regulator is the MAPK Hog1, a homolog of the mammalian stress-activated protein kinase (SAPK) p38, which becomes activated upon increased external osmolarity.

The Hog1-dependent hyperosmotic stress response not only includes transcriptional regulation, but also affects the global phosphorylation pattern and thereby controls diverse cellular processes, such as carbon metabolism, cell cycle regulation and the increase of the intracellular concentration of small osmolytes. However, although this pathway has been studied thoroughly for more than 20 years in regard to its purpose and function, the search for Hog1 substrates is not complete.

This work is part of a project designed to comprehensively identify substrates of Hog1. In detail, my thesis describes the impact of two kinases on the stress- and Hog1-dependent phosphorylome. First, I could widely exclude crosstalk effects of MAPK Kss1, the central regulator of the filamentous growth pathway, on the stress-responsive phosphorylation pattern. Secondly, I investigated the extent of indirect regulation of Hog1-dependent phosphorylation sites via the well-established Hog1 target Rck2, a calmodulin kinase (CaMK)-like MAPK-activated protein kinase (MAPKAPK). As a key finding I identified Rck2 as a major effector kinase downstream of Hog1. Finally, I integrated and compared the results obtained by two commonly used mass spectrometry (MS) data analysis softwares, namely MaxQuant and Proteome Discoverer, that apply differing identification and quantification algorithms. With this approach, I was able to enhance the comprehensiveness of our data even further.

III. Zusammenfassung

Zellen verarbeiten Stresssignale ihrer Umwelt mit intrazellulären Signalübertragungsystemen, die oft post-translationelle Modifizierungen beinhalten. Der „High osmolarity glycerol"-Signaltransduktionsweg (HOG-pathway) in *Saccharomyces cerevisiae* ist ein Vorzeigebeispiel für Mitogen-aktivierte Proteinkinasen (MAPK) und Stresssignalübertragung. Sein zentraler Schlüsselregulator ist die MAPK Hog1, welche bei erhöhter externer Osmolarität aktiviert wird und ein Homolog der stress-aktivierten Proteinkinase (SAPK) p38 in Säugetieren ist.

Die Hog1-abhängige hyperosmotische Stressantwort inkludiert nicht nur transkriptionelle Regulation, sondern beeinflusst auch globale Phosphorylierungsmuster und kontrolliert dadurch diverse zelluläre Prozesse (z.B. Kohlenstoffmetabolismus, Zellzyklusregulation, Osmolytenkonzentration). Die Suche nach Hog1-Substraten ist nach wie vor nicht vollständig, obwohl dieser Signaltransduktionsweg bereits seit über 20 Jahren ausführlich untersucht wird. Diese Arbeit ist Teil eines Projekts, das zur umfassenden Identifikation von Hog1-Substraten entwickelt wurde. Meine Masterarbeit beschreibt den Einfluss zweier Kinasen auf das stress- und Hog1-abhängige Phosphorylom. Erstens konnte ich mögliche Signalüberlagerungseffekte auf das stressabhängige Phosphorylierungsmuster ausgehend von der MAPK Kss1, dem Zentralregulator filamentösen Wachstums, weitestgehend ausschließen. Zweitens untersuchte ich das Ausmaß indirekter Regulation Hog1-abhängiger Phosphorylierungsstellen durch das etablierte Hog1-Substrat Rck2, eine Calmodulinkinase-ähnliche MAPK-aktivierte Proteinkinase (MAPKAPK). Als eines meiner Schlüsselergebnisse identifizierte ich Rck2 als hauptsächliche, Hog1-nachgeschaltete Effektorkinase. Drittens integrierte und verglich ich zwei üblicherweise zur Auswertung massenspektrometrischer Rohdaten verwendete Computerprogramme, namentlich MaxQuant und Proteome Discoverer, welche jeweils unterschiedliche Identifizierungs- und Quantifizierungsalgorithmen anwenden. Dadurch war ich in der Lage, die Vollständigkeit des Datensatzes weiter zu erhöhen.

IV. Introduction / Background

IV.1. How to cope with environmental stress

All living cells are exposed to varying degrees and types of physicochemical stress, which is generally compensated by activating complex intracellular signal transduction systems that regulate adaptation and enable survival. Examples can be found in all domains of life and all types of organisms, a prominent example being sessile plants that cannot elude varying environmental conditions. While perennial plants have to survive sometimes exorbitantly different climate conditions and the whole organism has to adopt differing forms and lifestyles, even annual plants have to react to daily changes in temperature and light availability. The diversity and multifunctionality of stress response systems enables plants to endure extreme conditions and creates impressively specialised niches, such as the mangrove ecosystem that tolerates high salt concentrations and alternating oxygen availability[1]. Similarly, mammal stress response systems differ between various body compartments and cover a broad range of physicochemical stress conditions that have to be counteracted for cell sustainability and survival. Our skin and mucosa, such as in the digestive system, are optimised for reacting to stress signals derived from mechanical rupture of the multicellular organ to chemical shifts like pH-changes or nutriment composition to immunological stimuli[2].

However, while stress responses in higher eukaryotes are only one of many diverse evolutional features, some of those systems are conserved and highly essential especially in free living single-cell organisms. *Saccharomyces cerevisiae* is a non-pathogenic, sugar-fermenting yeast fungus found naturally on ripe fruits and is thought to have been firstly identified as part of the waxy white film on grape and plum cuticles[3]. This natural habitat exposes yeast cells to considerable changes in environmental conditions, including temperature differences, nutrient availability and osmotic fluctuations.

The difference in hydrostatic pressure between the outside and inside of cells is balanced by the turgor pressure from within the cell and the osmotic pressure exerted on the cell by the environment[4,5]. Changes in external osmolarity thus lead to shifts in this balance and require a transmission of information from sensors that detect these changes to internal regulators that enable cells to react and adapt to the potentially life-threatening environmental conditions. Regarding osmostress, we speak of either hypo-osmotic stress, which in a natural environment may be caused by rainfall and leads to water influx and swelling of the cells, or hyperosmotic stress, where the external concentration of osmolytes is increased, for example due to sugar saturation variation in the ripening fruit[6].

The instantaneous problem yeast cells face upon hyperosmotic conditions is water loss due to the osmotic pressure, which is counterbalanced by a range of transcriptional changes and proteome-wide regulation and adaptation, often accompanied by post-translational modification. These changes are mediated by signalling pathways inducing a transient cell cycle arrest, increasing cellular osmolyte concentration, adjusting membrane permeability and stiffness, and internal reorganisation of the cell, for example via modifications of the actin cytoskeleton[7]. The main hyperosmotic stress response is regulated by the HOG-pathway, a signalling pathway initiated by osmosensors in the yeast membrane that activate the key regulator Hog1, a mitogen-activated protein kinase (MAPK), by phosphorylation via two redundant branches[8,9].

IV.2. Lessons learned from yeast: A MAPK-paradigm

MAPK pathways are essential signal transduction machineries that are unique to eukaryotic cells, but are conserved in a vast range of species from unicellular organisms like yeast to higher eukaryotes including plants and mammals[10]. The name “mitogen-activated protein

kinase" proved to be a misnomer as it became clear that MAPKs do not exclusively react to mitogens, as was believed nearly 30 years ago, when Sturgill and Ray discovered an insulin-activated serine/threonine protein kinase and labelled it microtubule-associated protein kinase at first[11]. Indeed, a diverse range of stimuli, from mitogens to heat shock, cold shock, oxygen-deprivation and inflammatory cytokine signalling to osmotic stress is integrated in the cell and processed by pathways involving MAPK-cascades. These typically consist of tightly regulated, three-tiered modules of a MAPK-Kinase-Kinase (MAPKKK), a MAPK-Kinase (MAPKK) and a MAPK that are consecutively activated by phosphorylation of their "activation loop", an C-terminal region that harbours consensus phosphorylation sites characteristic for distinct kinase families[12–14].

In yeast, there are five MAPK pathways that are described and have been investigated thoroughly, yet not in their detailed entirety: The cell wall integrity (CWI) pathway with the central regulators Pkc1 and MAPK Slt2[15,16], the sporulation pathway which activates MAPK Smk1 upon meiotic development[17,18], the filamentous/pseudohyphal growth and pheromone-sensing mating pathways under the control of the MAPKs Kss1 and Fus3[19–22], respectively, and finally the HOG pathway with the key regulator MAPK Hog1 that gets predominantly but not exclusively activated in response to hyperosmotic stress[9].

Hog1 is the ortholog of the mammalian MAPK p38[23,24], a stress-activated protein kinase (SAPK) that is involved in inflammatory cytokine, radiation, lipopolysaccharide (LPS) and also osmotic stress signalling[25,26]. This medical relevance and the easily inducible conditions make HOG signalling a classical MAPK model that provides insight into mechanics of MAPK-mediated stress signalling and post-translational modification, and enables researchers to investigate yeast signalling networks in general.

The HOG pathway is activated via two alternative branches that are initiated by different osmosensors located in the cell membrane (Fig. 1). The Sln1-branch, a classical two-component system, starts with the histidine phosphotransfer kinase Sln1 being autophosphorylated and active under basal conditions, inhibiting the redundant MAPKKKs

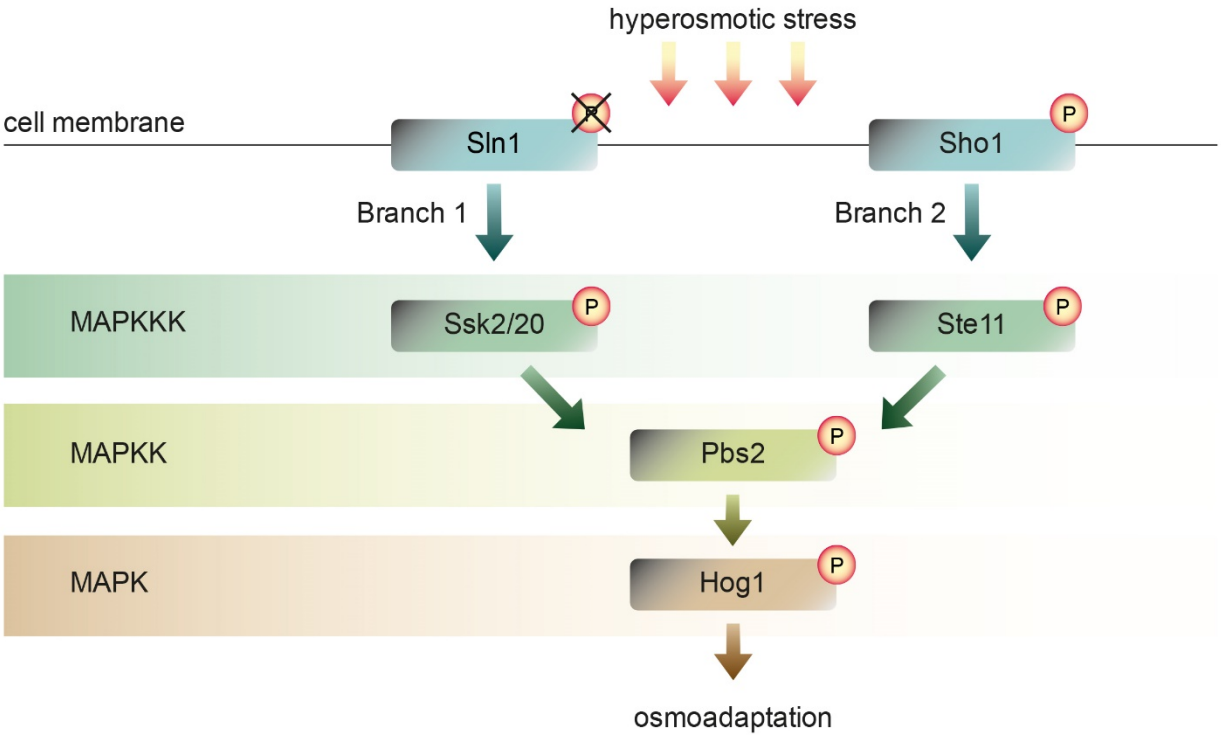

Figure 1: Schematic representation of hyperosmotic stress induced activation of the HOG-pathway.
P: phosphorylation, MAPK: mitogen-activated protein kinase; MAPKK: MAPK-kinase, MAPKKK: MAPKK-kinase.

Ssk2 and Ssk20[27,28]. Upon hyperosmotic stress, the autophosphorylation of Sln1 and inhibition of the MAPK module is lost. Osmosensor Sho1, on the other hand, activates the MAPK module together with other membrane proteins via consecutive phosphorylation of proteins that are assembled by scaffold protein Ste50, which also provides negative feedback for HOG signalling[29,30]. The MAPKKK of this branch is Ste11[31], and its phosphorylation and recruitment to the plasma membrane are crucial for the activation of the downstream MAPK-module. Both the Sln1 and Sho1 branch ultimately result in phosphorylation of the MAPKK Pbs2 on its conserved residues S514 and T518 by either Ssk2/Ssk22 or Ste11[32,33], both of which are essential modifications for the activation of the MAPKK[31]. Downstream of this integrating node, the key regulator MAPK Hog1 becomes phosphorylated by Pbs2 on its essential activation residues T174 and Y176 in the conserved MAPK TxY motif[14,24,25].

A large portion of active, phosphorylated Hog1 is transferred into the nucleus, however since it is lacking a distinct nuclear localisation sequence (NLS), the general importin α/β heterodimer is probably not involved. Instead, it has been stated that activation of the mammalian Ran GTPase homolog Gsp2 and the importin β homolog Nmd5 in combination with Hog1 phosphorylation and, notably, Hog1 catalytic activity is required for translocation[34]. MAPKK Pbs2 contains both, an NLS and a nuclear export sequence (NES), the second of which retaining the protein in the nucleus if removed, and it is thus assumed that the MAPKK shuttles between cytoplasm and nucleus as well[35]. Hog1 itself, however, is the pivotal vector to convey the hyperosmotic stress signal into the nucleus to affect the transcriptional machinery.

Hog1 activation (i.e, double phosphorylation), conjointly with its nuclear accumulation and the transcriptional changes attributed unambiguously to the kinase, can be detected within one minute after stress application, peaks at 5 minutes, and gradually reverts to basal levels within 30 minutes[33,36,37] under moderate stress conditions like for example 0.5M NaCl.

To enable recurrent functional stress sensing, the system needs to be reset to a neutral pre-stimulation state. Hog1 kinase activity itself provides a negative feedback mechanism by phosphorylating and activating phosphatases of the type 2C Ser/Thr-phosphatase family that dephosphorylate T174 (Ptc1, Ptc2, Ptc3)[38] and the protein tyrosine phosphatase family that dephosphorylate Y176: cytoplasmic Ptp3 and predominantly Ptp2, which resides in the nucleus and seems to ensure that Hog1 is only dephosphorylated after it has been activated, transferred to the nucleus and fulfilled its transcriptional regulation purpose[39,40]. The mechanism of export of dephosphorylated Hog1 is not yet fully understood, but it might require a specific factor, namely NES receptor Xpo1/Crm1[34]. Alternatively, the aforementioned observation of MAPKK Pbs2 shuttling between cytoplasm and nucleus indicates that it might be involved in the export and recycling of previously activated Hog1 as well.

Although not every detail of HOG signalling activation is decrypted, there are various extensive and far-reaching comprehensive reviews on this pathway and its functions available[7,9].

IV.3. Hog1, the hyperosmotic stress factotum

The immediate and predominant responsibility of Hog1 and HOG signalling is to re-establish the osmotic balance between the intracellular space and the environment rapidly enough to prevent desiccation and consequently cell death. This specific adjustment is primarily achieved by the accumulation of small osmolytes like glycerol, sorbitol, inositols or small carbohydrates (for example trehalose) in the cytoplasm, enabling the cells to re-establish their original volume after the initial cell shrinkage upon water loss to prevent further damage. In orchestration with this, another pivotal responsibility of HOG signalling is the activation of glycerol importer Stl1[41] via transcriptional activation of the respective *STL1* gene and the translationally regulated closure of aquaglyceroporin channel Fps1[42]. These processes help preventing the efflux of the produced osmolytes during the hyperosmotic crisis and highlight how HOG signalling incorporates both, transcriptional and translational regulation.

Consequently, Hog1 activation during hyperosmotic stress is directly related to highly increased levels of intracellular glycerol, giving the pathway its name. Glycolytic degradation of fermentable sugars and conversion of glyceraldehyde 3-phosphate (GA3P) to dihydroxyacetone phosphate (DHAP) by the triose phosphate isomerase Tpi1 provides a precursor for glycerol, which can then be reduced to glycerol 3-phosphate (G3P) by the GA3P dehydrogenase (GAPDH) Gpd1. Ultimately, the phosphate is removed by G3P phosphatase Gpp2 to produce glycerol, not only in response to hyperosmotic conditions, but also during anaerobic and oxidative stress[43,44]. During hyperosmotic stress, this process is regulated by Hog1, which enters the nucleus in dependence of its Pbs2-mediated double phosphorylation within minutes[34], as described in chapter IV.2, and acts as a transcriptional activator for the corresponding genes *GPD1* and *GPP2* as well as a range of additional transcriptional targets that are amongst others involved in cell cycle regulation and transcriptional elongation[45,46].

One can distinguish different mechanisms for the MAPK to provide transcriptional regulation:

i) Hog1 might deliver osmostress-specific DNA-binding transcription factors to the nucleus, ii) the initiation of a DNA-bound transcription factor's transactivation function might be regulated by Hog1-binding, iii) the general transcription machinery itself might be recruited to a structural docking platform provided by Hog1-dependent chromatin remodelling, or iv) components of the transcriptional machinery might become directly phosphorylated and activated by Hog1[47]. Notably, Hog1 indeed provides transcriptional regulation via combinations of all these mechanisms for various subsets of osmostress-associated genes. In the case of *GPD1*, Hog1 interacts with Hot1, a transcription factor that effectively traps the kinase at the gene's promoter. Not only does Hog1 phosphorylate Hot1, but the MAPK itself has been shown to bind to the *GPD1* DNA region in its activated state, recruiting the transcription machinery including RNA Pol II and TFIIB exclusively in the presence of Hot1[37,48,49]. This mechanism is highly similar for the prototypically Hog1-Hot1-dependent transcriptional regulation of *STL1*, which codes for glycerol membrane symporter protein Stl1 and is activated in response to hyperosmotic stress to facilitate glycerol uptake[41], thereby supporting the cell's efforts to increase osmolyte levels by initiating glycerol synthesis and glycerol retention within the cell.

Other transcription factors that associate with Hog1 are the redundant zinc-finger-like transcription factors Msn2/4 and Msn1, which are general stress-associated factors and also involved in the regulation of a large set of osmo-responsive genes[50], the ATF/CREB-related transcriptional repressor Sko1[51,52] which is turned into an activating transcription factor recruiting SWI/SNF and SAGA complexes by Hog1 via direct phosphorylation[53], and Smp1, a MEF2-like transcription factor that becomes phosphorylated by Hog1 on residues in its transactivation domain to exert its function[54]. Additionally, activated Hog1 interacts with nucleoporins and other factors associated with the nuclear pore complex, thereby regulating export of transcribed mRNAs to the cytoplasm as yet another mechanism of transcriptional regulation[46]. Taking into account the fundamental and highly versatile function of Hog1 as a part transcription factor, part mediator-like regulator of transcription, the effects of a Hog1-knockout under hyperosmotic conditions or the introduction of a constitutively active Hog1

(either through a hyperactive Pbs2-variant or an *SLN1*-deletion[27,33]) under basal conditions are expectably fatal for yeast: Constitutively active Hog1 leads to a lethal hypo-osmotic crisis, where cells enter a cell cycle arrest that isn't released anymore. The impaired reset of the HOG signalling cascade leads to unnecessarily high intracellular concentrations of glycerol and, induced by the difference in osmotic pressure, influx of water. This results in cell swelling and ultimately cell wall disruption[6,15]. Interestingly, attempts to rescue this lethal phenotype by deleting classically Hog1-dependent transcription factors (Msn2/4, Hot1…) were not successful[48], and Hog1 hyperactivation could only be counteracted, when essential factors of the entire transcription machinery like for example the RSC chromatin remodelling complex were targeted[55,56]. Contrarily, deletion of the established Hog1 downstream target kinase Rck2 indeed rescues the lethal phenotype[57–59], indicating a specific and individual role of this kinase in the hyperosmotic stress response, as will be elaborated on later in this thesis.

On the other end of the spectrum of Hog1 activity, *hog1*Δ cells that do not show any prominent growth defects on yeast extract peptone (YEP) full medium plates, or liquid cultures containing 2% glucose, are hardly able to survive when small osmolytes like NaCl, KCl or Sorbitol are added to the plates/liquid culture. A concentration of 0.5M NaCl is sufficient to abort proliferation of *hog1*Δ cells almost completely. However, rewiring the central HOG response by expressing *GPD1* and *GPP2* under a Kss1/Fus3-dependent promoter in *hog1*Δ cells showed the upregulation of glycerol to be sufficient for cell survival upon hyperosmotic stress[60]. This raises the question why the complex and resource-intensive HOG machinery is activated at all, and whether the bare minimum of regulating two genes that allow survival would be more beneficient for cell persistence. To answer this, one has to refrain from understanding the HOG response as an independent event, but instead consider the consequences of the initial water loss for the whole single-cell organism. Firstly, cells exposed to hyperosmotic stress have to re-organize their internal compartments according to the decreasing space. Secondly, to provide successful re-establishment of the osmotic balance, cells have to adapt metabolically and switch from a proliferating to a glycerol-producing setting, which,

consequently, also includes changes in the expression of genes producing enzymes involved in the regulation of glycolysis and a temporary cell cycle arrest[7,45,46,61]. Indeed, studies that investigated gene expression on a global level proved Hog1 to be responsible for as much as ~80% of the overall osmostress-induced genes. A large portion of these genes are part of the so-called environmental stress response (ESR) which is characterised by differential transcriptional changes of about 300 – 600 genes that do not only occur upon hyperosmotic stress, but also in a variety of other stress conditions like DNA damage, heat shock and oxidative stress, and are mostly involved in processes regulating protein synthesis and cell growth[61–63]. Finally, it stands to reason that some of the effects of the HOGresponse are regulated by redundant fail-safe mechanisms that may even be regulated on completely different levels of adaptation, but provide a similar or even identical outcome. For example, Westfall *et al.* showed that yeast cells are viable and survive hyperosmotic stress conditions if Hog1 is tethered to the plasma membrane and merely kept from entering the nucleus instead of being knocked out[64]. Classical gene expression changes associated with nuclear localisation of Hog1, including genes described here, did not occur in strains that were expressing membrane-tethered Hog1, although these strains were still able to increase cellular glycerol concentration. This indicates that cytosolic processes of the hyperosmotic stress response might be just as efficient as transcriptional regulation and suffice to ensure cell survival[42], although on a decidedly different level of adaptation. While cells increase glycerol production via *GDP1/GPP2* expression levels and activate glycerol uptake from the surroundings via *STL1* expression levels[41], the consideration of posttranslational regulation as an equally important and effective survival mechanism is reflected in the maintenance of high glycerol concentrations in the cytoplasm: Part of safeguarding the cellular osmotic balance is the opening of aquaglyceroporin channel Fps1 to release glycerol upon high turgor pressure, and its closure upon exposure to increased extracellular osmolarity to prevent glycerol efflux[65,66]. Positive regulators Rgc1 and Rgc2 are bound to the cytoplasmic C-terminal domain of Fps1 to keep it in its open state, while dissociation of these factors leads to channel closure,

a process that is to a large extent dependent on Hog1[42]. Lee *et al*. were able to show a remarkable mechanism for the release of Rgc2 and subsequent Fps1 closure, where hyperosmotically activated Hog1 binds to a MAPK-docking site in the cytoplasmic N-terminal domain of Fps1 and phosphorylates Rgc2, initiating its removal from the Fps1 C-terminus[42]. Additionally, proteome-wide mass spectrometry shotgun experiments have already shown the changes in phosphorylation patterns upon hyperosmotic stress to be vast and complex and comprise non-transcriptional regulation as well as transcriptional changes besides glycerol production[67–69].

Taken together, these findings suggest that the HOG response involves not only essential survival mechanisms, but initiates an entire machinery of fine-tuned intracellular processes that might contribute to advantages under competitive growth or repeatedly occurring stress environments.

IV.4. Railroading kinase networks: Pathway insulation and crosstalk

Phosphorylation is the most abundant type of post-translational modification in cell signalling and regulation. As described above, MAPKs are involved in several important regulatory processes including the cell cycle, metabolic optimisation, mating, sporulation and stress signalling, and thus the orchestration of kinase-phosphatase interaction networks to ensure signal fidelity is crucial to cell survival. The 3-dimensional structure of most protein kinases exhibits a specific fold, with two lobes that make up the nucleotide binding and catalytic center enclosing a deep cleft that contains the adenosine-triphosphate (ATP) binding pocket in a so-called “closed” conformation[70,71]. In the case of many protein kinases, and also MAPKs, a specific peptide-binding surface loop on the C-terminal domain of the kinase is phosphorylated to initiate catalytic activation. Substrate binding at this “activation loop” then leads to a

conformational shift that makes the ATP-binding pocket accessible and enables the transfer of a phosphate from bound ATP to the designated substrate motif[14]. Specifically for proline-directed Ser/Thr-kinases like MAPKs, the consensus motif of the substrate consists of a phospho-accepting serine or threonine (S/T) and a proline (P) at position +1 relative to the phosphorylation site (p+1)[72–75], proline being preferred here due to its ability to place the side chains of the substrate peptide away from the kinase surface in its favoured backbone position. A family of close relatives of MAPKs, the cyclin-dependent protein kinases (CDKs) which regulate the cell cycle, also recognize such S/TP motifs[73,76–78]. Considering the presence of various MAPKs and CDKs in the cell which all recognize the same motifs, the question arises how signal fidelity is maintained[79], especially since there are indeed MAPK that not only recognize the same motifs as Hog1, but even share components of the HOG signalling pathway[9,80]. Thus, several mechanisms exist that allow the cell to integrate responses to extracellular stimuli independently of each other, ensuring adaptation to the respective environmental situation.

One of the most straight-forward mechanisms is the separation of signalling pathways via distinct upstream activation processes. The CWI-pathway with the central MAPK Slt2[15,16] is activated when sensor proteins in the membrane detect stretching of the cell membrane, as is the case during proliferation-induced morphologic changes, treatment with diverse membrane-disrupting agents or oxidative stress[81,82]. The MAPK-module of this pathway consists of MAPKKK Bck1, MAPKK Mkk1/2 and MAPK Slt2, and is activated by protein kinase C (PKC) signalling[13]. Here, crosstalk between hyperosmotic response and cell wall stress response are unlikely and both pathways are able to activate a distinct set of target proteins, conveniently, as hyperosmotic conditions cause cell shrinkage as opposed to cell wall stretching and require contrary adaptational processes. Differentially, Ras-related GTPase Cdc42, p21-activated protein kinase (PAK) Ste20, adaptor protein Ste50 and MAPKKK Ste11[29–31,83–85] are used in the upstream activation cascade of the HOG pathway, the filamentous growth (FG) pathway and the pheromone response (PR) pathway[9,19–22]. In this case, crosstalk has to be prevented

by other means to ensure activation of the correct set of proteins necessary for adaptation to either hyperosmotic conditions (HOG-pathway, MAPK Hog1), nutritional deprivation (FG-pathway, MAPK Kss1) or mating encouragement (PR-pathway, MAPK Fus3). For Kss1 and Fus3 differentiation seems to be particularly difficult, since both pathways use a Ste20-Ste11-Ste7 cascade to phosphorylate their respective MAPK[9], however, Fus3-activation requires binding of the scaffold protein Ste5 to connect the three-tiered MAPK-module and increase the otherwise low affinity between Ste7 and Fus3, whereas Kss1-activation does not[86–90]. Besides this static mechanism involving a scaffolding protein, Fus3 signalling also leads to inactivation of the Kss1 pathway by regulating downstream factors. While phosphorylated Fus3 and Kss1 both inhibit transcriptional repressors Dig1/2[9,22] and thereby convey i) Dig1/2-dissociation from the transcriptional complex and ii) phosphorylation of transcriptional transactivator protein Ste12[22,91,92], their targeted transcription elements differ: Homodimers of phosphorylated Ste12 control pheromone responsive elements (PRE), while a heterodimer of Ste12 and TEA/ATTS-DNA binding transcription factor Tec1 is required for the expression of filamentation-responsive-elements (FRE)[93]. Upon FG and PR pathway activation by pheromones, however, active Fus3 directly phosphorylates Tec1, marking it for ubiquitination and degradation, and thus inhibits Kss1-dependent expression of FREs[94–96].

A more direct way of pathway insulation can also be established by effectors actively intercepting other pathways, as is the case for Kss1-inhibition upon hyperosmotic stress signalling. Adaptor protein Ste50, as described earlier, is shared by various pathways, and its complex formation with Ste11 leads to both, Hog1 and Kss1 activation. In the absence of Hog1, cells show to develop filamentous growth regardless of the stress stimulus being HOG- or FG-specific, indicating that HOG signalling is required to prevent the activation of the Kss1-MAPK-module in response to hyperosmotic stress[97,98]. Besides again disrupting Tec1 function by inhibiting its DNA binding ability[99], Hog1 actively phosphorylates Ste50, leading to inhibition of Kss1 activity[29,30,97] (Fig. 2). Phosphorylation of Ste50 dampens signalling in all three, PR, FG and HOG pathways, making negative regulation of the Ste50 phosphorylation by Hog1

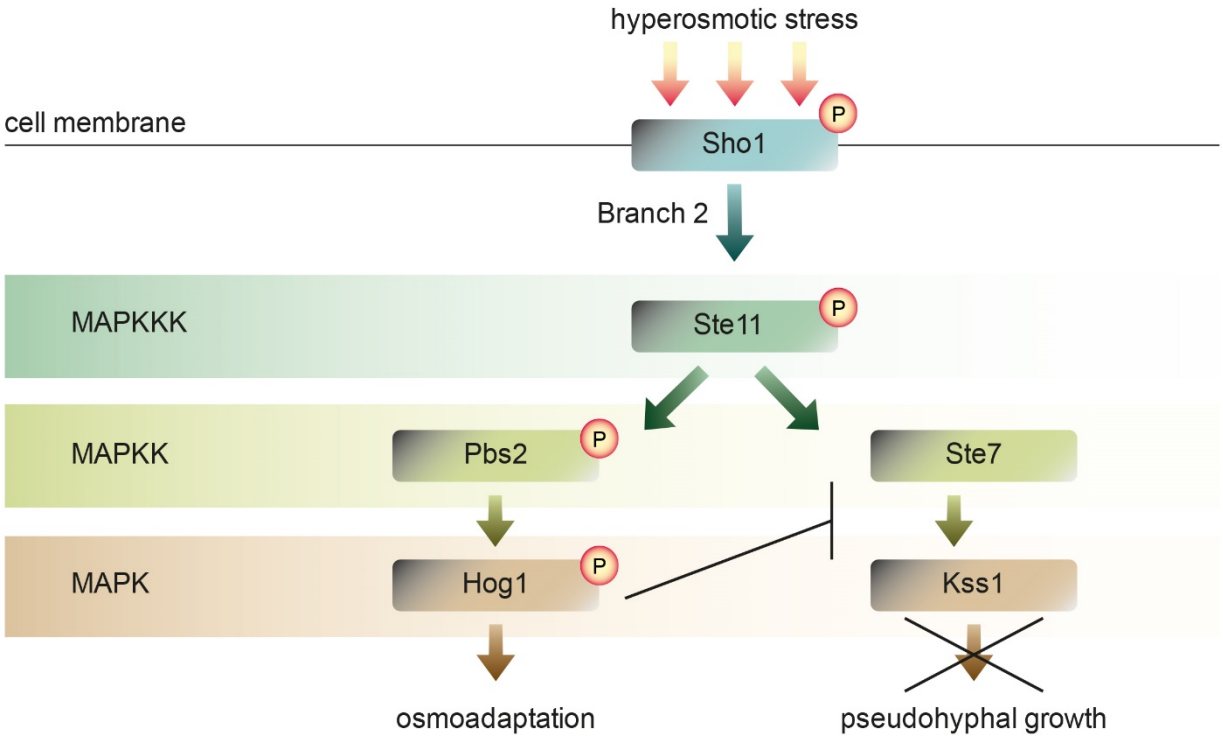

Figure 2: Schematic representation of the Hog1-mediated inhibition of Kss1 activation upon hyperosmotic shock. MAPK: mitogen-activated protein kinase; MAPKK: MAPK-kinase, MAPKKK: MAPKK-kinase.

seemingly counterproductive for the HOG response too. Yet this depicts another aspect of pathway insulation, where the kinetics of activation are taken into account: While Kss1 activation has to be prolonged and sustained to promote filamentous growth, HOG signalling is intrinsically short-termed and needs to be replenishable, thus negative regulation is desirable for Hog1, but temporarily abrogates Kss1 (and Fus3) activation and thus prevents crosstalk between the pathways[100]. Another, yet more complex and hard to monitor mechanism is the activation of phosphatases by the MAPK itself, which specifically dephosphorylate other kinases or their targets, thus providing negative feedback loops that can enhance signal fidelity even further.

Not only downstream phosphatases contribute to the complexity of kinase-phosphatase networks, but also target kinases that are directly activated by the respective MAPK, so-called

MAPK-activated protein kinases (MAPKAPK), regulate their own set of substrates. A prominent example of such a kinase in HOG signalling is the calmodulin-like kinase (CaMK) MAPKAPK Rck2[57–59]. Bilsland-Marchesan *et al.* and Teige *et al.* not only confirmed the interaction between Hog1 and Rck2, establishing its residues T379 and S520 as hallmarks of HOG signalling, but also observed that deletion of Rck2 rescues the lethal phenotype of cells carrying a hyperactive Hog1 allele[58,59]. As mentioned in chapter IV.3, it is noteworthy that the overproduction of osmolytes and accompanying transcriptional and translational changes that lead to the lethal phenotype of hyperactive Hog1 is not rescued by deleting classical Hog1-associated transcription factors like Msn2/4 and Hot1[48], indicating that Hog1-activated Rck2 plays a crucial and individual role as a major effector kinase of the hyperosmotic stress response, as will be emphasised by my results presented in chapter VI.2.

Rck2 itself, being of the CaMK family, is not a proline-directed Ser/Thr-kinase but recognizes an R/KxxS/T-motif, which is similar to motifs recognized by both the cAMP-activated kinase (PKA) family and AMP-activated protein kinase (AMPK) family[72–75,101], for example Snf1[102]. Again, overlapping substrate specificities emphasize the importance of signal fidelity on every level and exhibit the enormous scientific challenge posed by the complexity of these extensive kinase-phosphatase networks.

One approach to disentangle kinase-substrate interactions on a proteomic scale are bottom-up tandem mass spectrometry shotgun experiments that enable researchers to monitor phosphorylation pattern changes in varying experimental conditions[67–69,103–107]. By inhibiting or removing specific kinases upon stress treatment, one can integrate data from sets of dynamic phosphorylation sites and compile comprehensive interaction networks. Analysing the phosphorylome of MAPK Hog1 and MAPKAPK Rck2 in an hyperosmotic environment, for example, shows increased phosphorylation of key residues in Rck2's activation loop in dependence of Hog1, as Rck2 is a direct substrate of Hog1 in hyperosmotic stress[58,59,69]. However, this example shows that in addition to these primary dynamic PTMs, activated substrates of Hog1 can also be kinases who in turn phosphorylate indirect or secondary targets

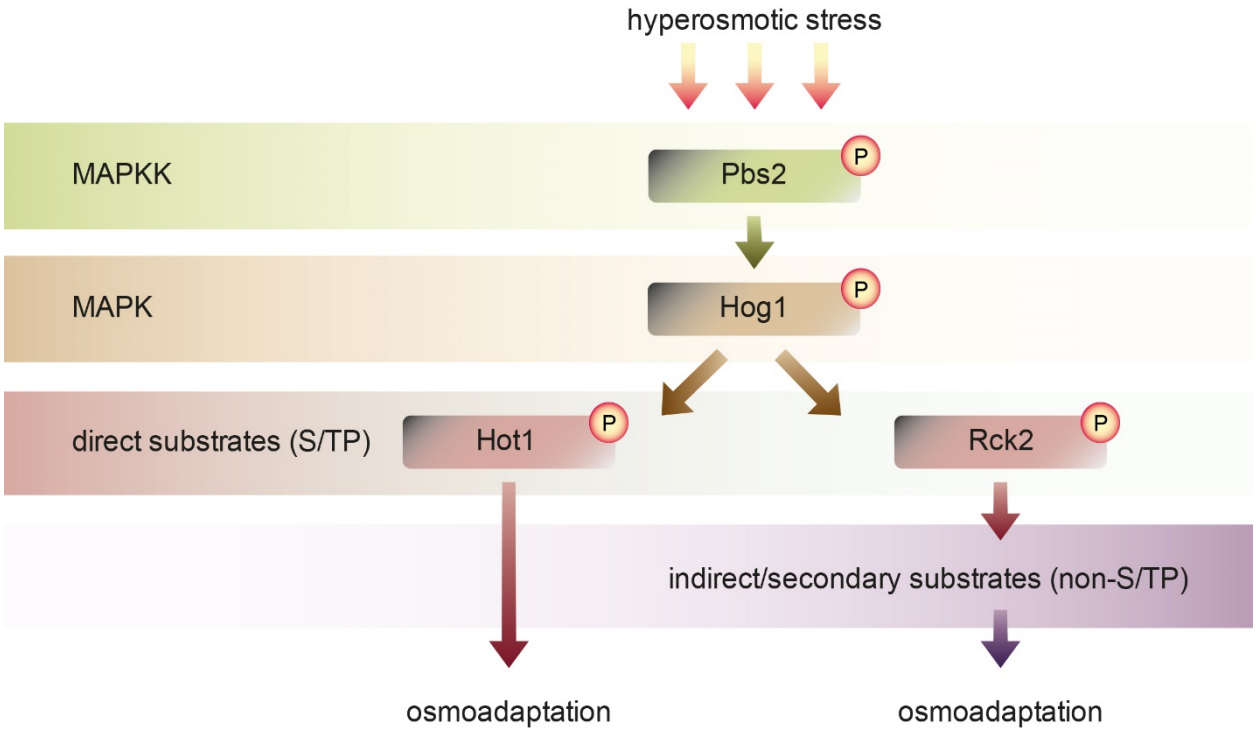

Figure 3: Schematic representation of the directly Hog1-dependent (primary) and indirectly Hog1-dependent (secondary) HOG response that contribute to osmoadaptation. MAPK: mitogen-activated protein kinase; MAPKK: MAPK-kinase, S/TP: Ser/Thr-Pro-motif

of the HOG response, enhancing the complexity of osmoadaptation even further. (Fig. 3).

When speaking of kinase networks, we are not only considering direct interactions between pathways, but instead include combined outcomes of various pathways that interconnect at various signalling nodes or contribute to a shared result. For example, the Hog1-mediated phosphorylation (and subsequent dissociation) of Rgc1 and Rgc2 mentioned in chapter IV.3 is not the only regulating mechanism for Fps1 channel closure. Muir *et al.* were able to show that Fps1 closes even in *hog1*Δ cells, indicating the presence of some additional Hog1-independent regulatory process[108]. Indeed, they reported Ypk1, a TORC2-dependent kinase which usually phosphorylates sphingolipid homoeostasis factors Orm1/2[109–111], to target Fps1 under basal conditions. Upon hyperosmotic stress, however, they showed that TORC2-dependent Ypk1-phosphorylation is downregulated, leading to a loss of phosphorylation of Fps1, which causes

the channel to close even if Rgc1/2 release is not mediated by Hog1[108]. This is an example of pathway orchestration where insulated pathways integrate signals and lead to a safe-guarded, multi-faceted outcome, ensuring adequate adaptation to environmental conditions, and interactions like this can be hinted at by performing proteome-wide analysis of phosphorylation pattern changes using quantitative mass spectrometry.

IV.5. The small ABC of mass spectrometry

High-throughput screening is a powerful tool to analyse biological processes and their origins as well as testing an increasing number of specifics (pharmaceuticals, interaction partners, bioinformatical parameters), thereby generating enormous amounts of data (e.g. RNA-Seq, genetic shotgun screening) in a short time, using less material, and economically optimising working conditions. The need for appropriate terminology describing the analysis of an entire biological system, in the sense of considering all its constituents, led to the development of "-omics" research fields, with genomics being among the first terms to be coined in the early 1920ies. Much later, in the mid-1990ies, after it had become clear that RNA levels do not necessarily reflect protein content due to alternative splicing and post-translational modifications that affect protein stability and turn-over, the term proteomics was being spread. Today, advances in quantitative mass spectrometry techniques made bottom-up proteomics with liquid chromatography of digested peptides coupled to tandem mass spectrometry (LC-MS/MS)[112,113] a highly effective method to analyse the proteome of cells, including PTMs under varying experimental conditions, thus enabling us amongst other to do large-scale phosphoproteomics. Classically, proteins are extracted from cells and digested with a site-specific protease such as Lys-C or trypsin. Originating peptides can then be separated according to hydrophobicity on a reversed-phase high-pressure liquid chromatography

(rpHPLC) column, which is coupled to a mass spectrometer. At the interface between rpHPLC and mass spectrometer, the solvent evaporates and eluted peptides are ionized by an electrospray ionisation (ESI) source which establishes a positive charge on the solvent-deprived peptides. The mass spectrometer can for example be a linear trap quadropole (LTQ) device which traps ions of a specific mass/charge-ratio (m/z-values) in an electric field generated by its two-dimensional quadropole structure, or an even more powerful orbitrap, which detects the ion current resulting from the captured ions oscillating along the long axis of and orbiting around a central, spindle-shaped electrode. In the mass spectrometer, peptides are quantified according to their ion signal intensity as a function of their m/z-value. The result is a full scan, the so-called MS1-spectrum, which reflects the peptides, or "precursors", present in the sample at a specific point of time, with the composition of an MS1 scan depending on the peptides' physical properties and thus retention time on the rpHPLC. Identification of the amino acid sequence of a specific peptide requires selection and isolation of the precursor according to its m/z-value and subsequent collision with an inert gas to break the peptide at its fragmentation-sensitive peptide bonds to produce characteristic fragment ions. These so-called MS2-spectra, generated by either collision-induced dissociation (CID)[114,115] or higher-energy C-trap dissociation (HCD)[116], can now be matched to an in-silico dataset containing all peptides and fragments potentially produced by the applied protease. Matching MS2-spectra are scored by software-specific algorithms that take into account charge, intensity and deviation of a potentially identified peptide from its expected m/z-values (for both, peptide and fragments). Although such MS search engines are constantly improved, these peptide spectrum matches (PSMs) have a probability of being wrongly assigned, which increases with for example low quality of the spectrum. Low quality spectra might be generated due to degradation of the peptides present in the sample (leading to for example "non-tryptic peptides" in a trypsin-digested sample that are interpreted wrongly due to the missing arginine/lysine) or low signal-to-noise-ratios of an ion intensity peak. Also, increasing length of peptides complicates the unambiguous matching of an MS2-spectrum to an in-silico template, and

unconsidered modifications that change the m/z-value of a peptide might lead to misinterpretations of the fragmentation pattern. Finally, on protein level, special mindfulness has to be attributed to protein identifications that are quantified in the sample using information from only a single precursor peptide or fragmentation, as the reliability of an identification event increases with the assignment of several PSMs to a specific protein.

Since the number of lower scores for correctly matched spectra does quite substantially overlap with higher scores for wrongly assigned spectra, MS-data should be statistically validated to be able to set a score-threshold that neither eliminates too many true positive PSMs nor yields a large number of false positive PSMs. However, assigning p-values as a measure of statistical significance to each individual PSM doesn't do the trick as we run into the multiple testing problem[117], where a p-value of < 0.05 would result in a 5% overall chance of PSMs being false positives - a notion that is acceptable for a single test, but results in exorbitantly high numbers when applied to a dataset of for example 4000 proteins, where 200 false positives would be expected just by chance already. To circumvent this problem, a so-called target-decoy approach[118,119] is commonly used to calculate a false discovery rate (FDR) which is more representative of the actual global population error rate. Here, a devised duplicate of the in-silico set of possible peptides is generated by reversing the sequence of every peptide, doubling the database to be searched for PSMs. The (clearly labelled) decoy database should be similar to the (real) target database in regard to amino acid distribution to ensure scoring stability, but there should be no overlaps between target sequences and decoy sequences to be able to unambiguously differentiate between both databases. Fragmentation spectra that are matched against these decoy peptides therefore have to be wrongly assigned and enable us to estimate the number of potential false positives in the actual target database. By using the FDR, we can calculate the likeliness of an event being true (the PSM being genuine) on the base of a null-hypothesis (all PSMs being random matches) in a score-dependent manner. This is established by sorting PSMs according to their score, and individually calculating the fraction of all false positives (matched to decoy sequence) over all

true positives (matches to target sequence) that have a higher score than the respective PSM to be evaluated. This results in a score-specific parameter called q-value (FDR-adjusted p-value) that describes the minimum FDR-threshold at which an individual PSM can be accepted[120]. The q-value allows individual comparison of PSMs between different experiments, making it especially advantageous for large-scale datasets. MS-datasets presented in my thesis were processed using a stringent q-value/FDR threshold of 1%.

IV.6. Of phosphoproteomics and isotopic labelling

The focus of my thesis is the proteome-wide capture of kinase-dependent phosphorylation pattern changes using quantitative MS-based experimental approaches. When dealing with phosphorylated proteins, and subsequently peptides in the MS analysis, several peculiarities must not be neglected.

First of all, the mass of a phosphopeptide and its fragmentation pattern are distinctly different from its unphosphorylated version, and have to be considered when creating the in-silico target and decoy databases and the information has to be passed to the device and software algorithm detecting, identifying and matching the individual m/z-values to a sequence. Second, phosphopeptides can be phosphorylated at multiple sites, which makes differentiation of those additional moieties on the peptide difficult even with modern, high-resolution devices and assignment algorithms. Additionally, as with variable modifications like methionine oxidation, phosphorylated peptide-species per se increase the number of possible peptides and fragmentation patterns. This becomes especially challenging when cleavage sites for the digesting protease are close to the large phosphate group, which might lead to steric hindrance and an increased probability of a missed cleavage and thus even more peptide variants. Besides these experimental difficulties, the physical properties of phosphopeptides make them

prone to biased results. For example, information about the stoichiometry of the phosphorylation is often missing, making it difficult to differentiate between biologically relevant changes and “noise” from random or non-functional phosphorylation[121]. Also, the tendency of phosphopeptides to stick to surfaces during sample preparation as well as in the rpHPLC-MS setup[122,123], along with a questionable stability of their ionisation efficiencies[124,125] has to be considered. The same is true for varying digestion efficiency, which, as said, can be impaired in close vicinity to phosphate groups[126], making phosphopeptides hard to analyse in complex samples, also because of their low relative abundance in whole cell protein extracts. To circumvent the latter, enrichment techniques using for example affinity chromatography (TiO_2) are necessary to increase the relative fraction of phosphopeptides in a sample. Additionally, strong cation exchange (SCX) chromatography can be employed to decrease a sample’s complexity collecting and measuring individual peptide fractions, making it possible to analyse peptides with lower abundance. On top of that, phosphorylations are often substoichiometric, thus only the relative abundance of the phosphopeptide over the unphosphorylated peptide can be quantified. In the experimental setups presented in my thesis, we used stable isotopic labelling with amino acids in cell culture (SILAC) as a method to quantify dynamic behaviour of phosphorylation sites, allowing us to deduce regulation of these sites in regard to various experimental conditions[127].

To obtain samples that can be used to compare the effects of an experimental condition to an untreated control later, cell populations are cultured in media which are identical but contain either ^{12}C- or ^{13}C-labelled arginine and lysine (‘light’ or ‘heavy’ isotopic labelling). After extraction, proteins are digested using e.g. Trypsin protease, which cuts C-terminally of Arg and Lys, giving rise to peptides that contain at least one (sometimes two or three, if cleavage sites are missed, very seldom more) 6-C-amino acid that is isotopically labelled as heavy or light. Such isotopically labelled peptides are chemically identical, and differ only in regard to by their mass, which leads to distinguishable m/z-values that can be identified in the MS analysis. Thus, they can be traced back to either the experimental or control culture and used

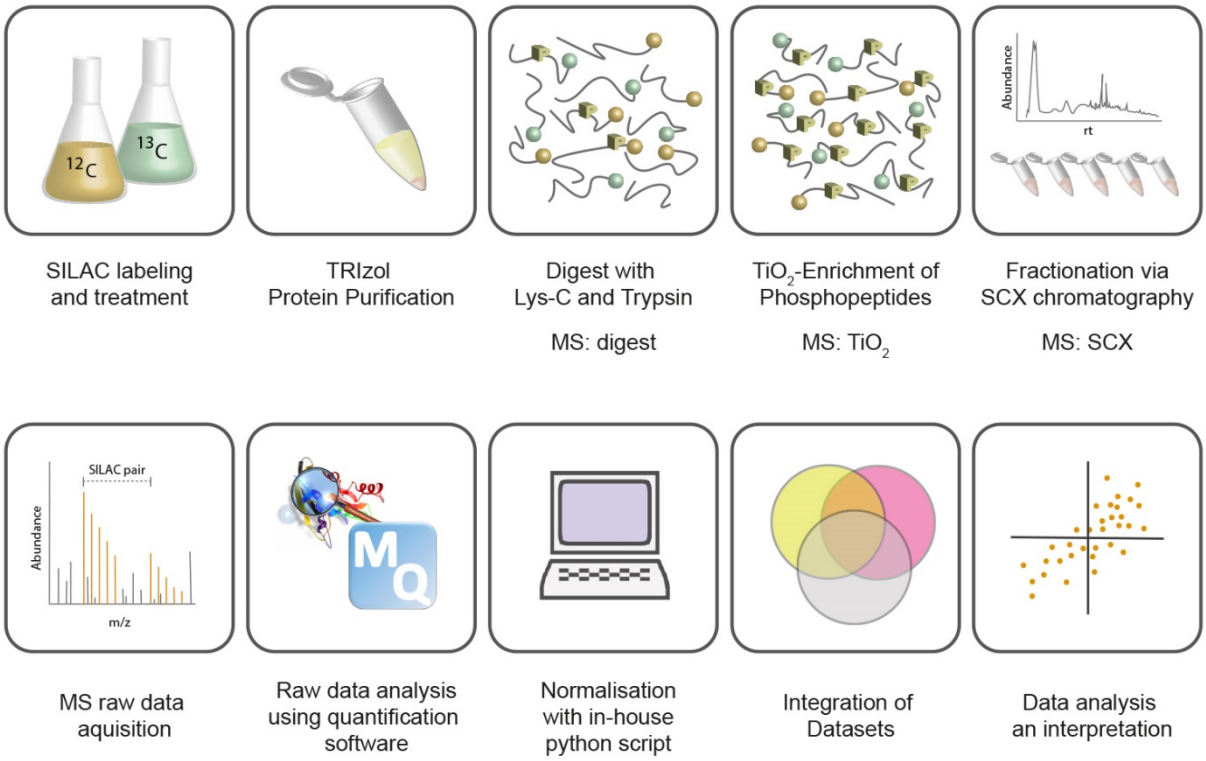

Figure 4: Experimental workflow for LC-MS shotgun experiments. Experiments were performed as described in the main text. SILAC: stable isotope labelling with amino acids in cell culture, MS: mass spectrometry, TiO_2: titanium oxide, SCX: strong cation exchange

for analysis of dynamic changes in phosphorylation between conditions. Additionally, Lys and Arg are both positively charged and obtain a second (sometimes third, seldom more) charge via the ESI source upon elution from the rpHPLC, leading to a specific pattern of m/z-values and light and heavy ion intensity peaks that is characteristic for isotopically labelled and respectively digested peptides. These “SILAC-pairs” can be directly quantified in relation to each other and generate a corresponding light-to-heavy ratio (L/H-ratio) which is used as a measure of phosphopeptide abundance fold change between experimental and control samples in our project. Fig. 4 summarizes the experimental procedure from sample preparation to bioinformatical analysis.

IV.7. The Hog1-dataset: Romanov et al. (Appendix X.1)

The HOG-pathway and its activation's result, the transcriptional and translational hyperosmotic stress response (HOG response), serve as a paradigm for MAPK-signalling, and several target proteins of the key regulator MAPK Hog1 have been described already[7]. As reviewed in chapter IV.3, research regarding Hog1 targets has been centered for a long time around transcriptional regulation of the cell cycle and enzymes influencing the cell's carbon metabolism, especially to preserve intracellular glycerol concentrations. With the rise in mass spectrometry-based phosphoproteomic experiments, however, it became clear that Hog1 should be regarded as more than a transcription factor and massively influences the phosphoproteome in hyperosmotically challenged cells, levelling its major role in the transcriptional stress-response with its importance in post-translational regulation.

Still, while quantitative phosphoproteomics studies conducted for example by Kanshin *et al.* and Soufi *et al.*[67,68] provide an excellent overview of the scale and dynamics of osmostress-induced changes of proteome-wide phosphorylation patterns, the unambiguous assignment of substrates to a specific kinase remains challenging in the complex, interconnected kinase-network that is activated upon hyperosmotic stress. Our research group has addressed this problem (as described in Romanov *et al.*[69], a copy of the publication is attached in Appendix X.1 of my thesis) by dissecting the hyperosmotic stress response in regard to Hog1 kinase activity, thereby creating an extra dimension of resolution that allowed us to integrate information about both, stress-association and Hog1-dependency, of dynamically regulated phosphorylation sites. This dataset, hereafter referred to as "Hog1 dataset (Romanov *et al.*)", comprises the starting point for the experiments and findings described in my thesis.

To determine phosphorylation site induction that is i) dependent on hyperosmotic stress and ii) dependent on Hog1 kinase activity, two different quantitative SILAC MS experiments have been designed. In a first SILAC-experiment, termed setup SR ("Stress Response"), changes

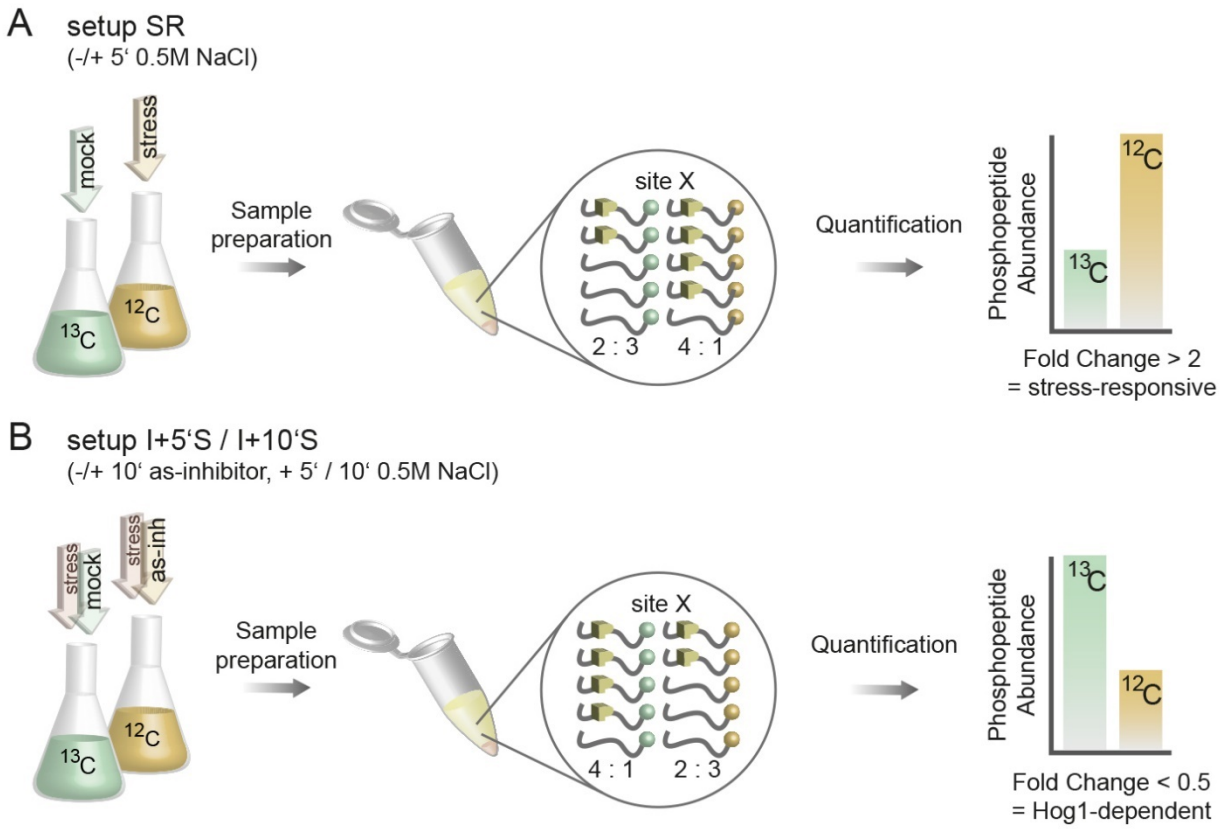

Figure 5: Schematic representation of experimental setups generating the Hog1 dataset. A) Setup SR (“stress response”), increase or decrease in phosphopeptide abundance by more than 2-fold was considered significant, corresponding phosphorylation sites were classified as stress-responsive, relevant stress-responsive behaviour of a theoretical phosphorylation site X is depicted. B) Setup I+5’S/I+10’S (“inhibitor + 5’/10’ stress”), increase or decrease in phosphopeptide abundance by more than 2-fold was considered significant, corresponding phosphorylation sites were classified as inhibitor-susceptible, relevant inhibitor-susceptibility (i.e., Hog1-dependency) of a theoretical phosphorylation site X is depicted. as-inhibitor: Hog1-specific adenosine-triphosphate-analog-sensitive kinase inhibitor.

in the global phosphorylation pattern in wildtype W303 cells after a 5’ treatment with 0.5M NaCl were analysed relatively to mock-treated cells, to provide the first layer of information (Fig. 5A). Secondly, the Hog1-dependency of dynamic phosphorylation sites was determined by abolishing Hog1-kinase activity during hyperosmotic stress in cells carrying an endogenous analogue sensitive allele of *HOG1* (*HOG1as*). The gene product expressed from this allele (Hog1as) harbours a point mutation (T100G) in the adenosine 5′-triphosphate (ATP) binding pocket, rendering it sensitive to 1-isopropyl-3-(phenylethynyl)-1H-pyrazolo[3,4-d]pyrimidin-4-

amine, an ATP-analog also known as SPP86. This inhibitor can be added to liquid culture pre-stress, and specifically diminishes Hog1 kinase activity[128]. Comparing the global phosphorylation pattern in SPP86-treated cells to that of control cells that were mock-treated with dimethyl sulfoxide (DMSO) enabled us to identify Hog1-dependent phosphorylation. For the SILAC-based experiments described in Romanov *et al.* (Appendix X.1), the inhibitor was added 10 minutes prior to stress application, and global phosphorylation pattern changes were measured after 0', 5' and 10' of hyperosmotic stress, designated setups I+0'S, I+5'S and I+10'S, ("Inhibitor + X minutes Stress") respectively (Fig. 5B). Integration of setup SR with these inhibitor experiments can be visualised in a two-dimensional scatter plot that can be separated in 8 fields corresponding to phosphorylation site behaviour (Fig. 6A-D, adapted from Romanov *et al.*). To consider a protein a putative direct Hog1-substrate in the hyperosmotic stress response, corresponding peptides had to meet three criteria. In regard to dynamic phosphorylation behaviour, the phosphopeptide has to i) show a ≥ twofold increase in abundance in setup SR, and ii) show a ≥ twofold decrease in abundance in either setup I+5'S or setup I+10'S. As depicted in Fig. 6D, peptides that meet these criteria are located in behavioural field 1, and can be considered as both, stress-associated and Hog1-dependent. Additionally, peptides had to iii) harbour the MAPK consensus motif S/TP at their phosphorylation site, to establish them as being able to be directly phosphorylated by Hog1.

These criteria were true for 36 phosphorylation sites which attributes to over 25 new putative Hog1-substrates. To validate these candidate substrates, we used a protein-protein-proximity-assay called M-Track, which is based on the enzymatic labelling[129,130].

For our M-Track strategy, we tagged every candidate protein C-terminally with a histone3-lysine9-methyltransferase (HKMT), which was then, upon substrate-Hog1-proximity, able to methylate the lysine on a histone 3 (H3) tag we attached to the C-terminus of Hog1. H3-methylation was subsequently used to quantify proximity-signals, and we were able to obtain positive proximity signals and thereby validate almost all putative Hog1 substrates. Closer assessment of the Hog MS dataset regarding the composition of the various

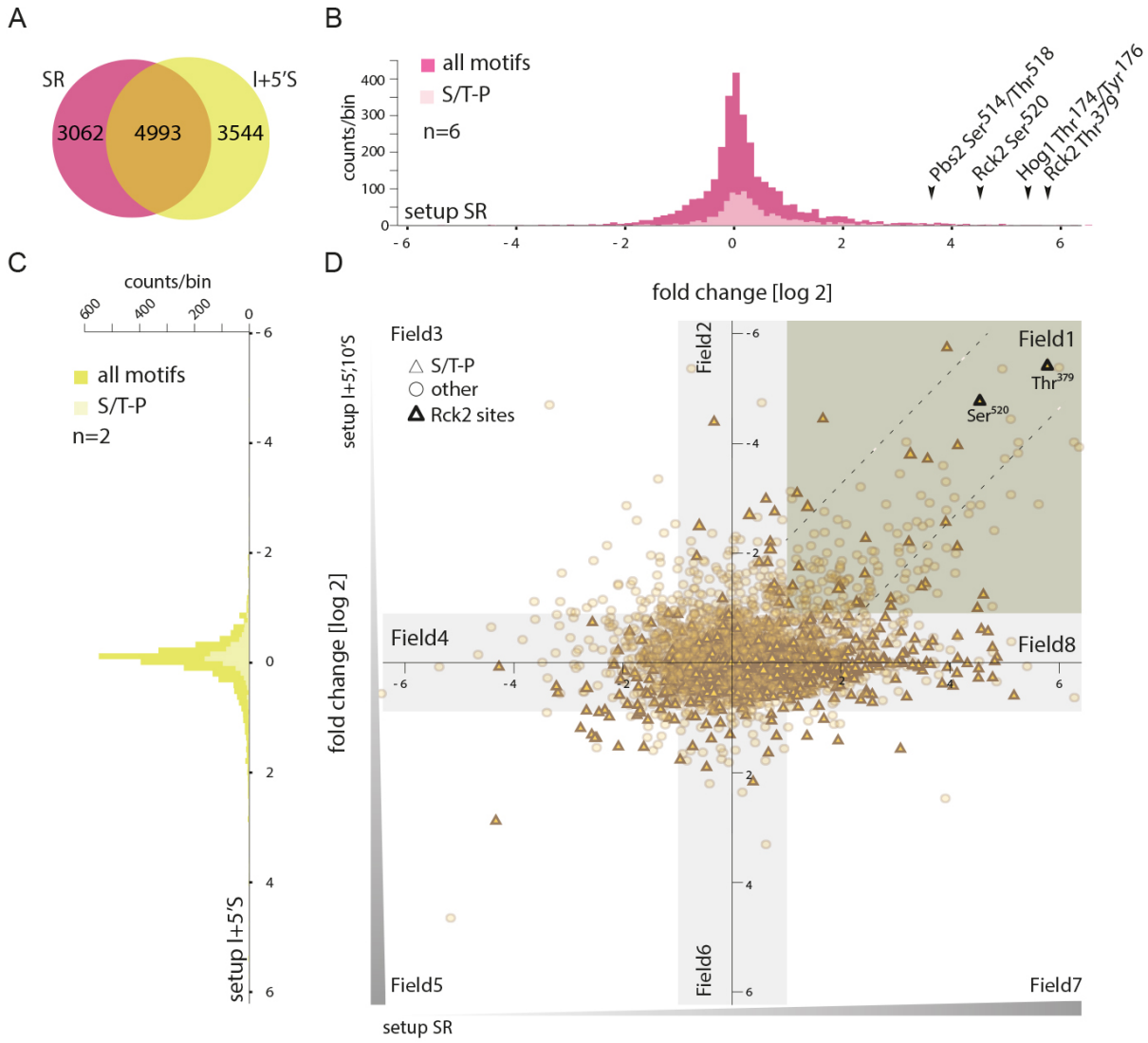

Figure 6: The Hog1 dataset. Setup I+10'S not shown. A) Venn diagram showing overlap of unique phosphorylation sites between setups SR (pink) and I+5'S (lilac) B) Histogram of ratio distribution (log2-transformed) of setup SR, light pink bins indicate S/TP motifs, dark pink bins indicate other motifs. Hallmarks of HOG signalling are indicated by arrowheads C) Histogram of ratio distribution (log2-transformed) of setup I+5'S, light lilac bins indicate S/TP motifs, dark lilac bins indicate other motifs. D) 2-dimensional distribution of ratios (log2-transformed) quantified in setups SR and I+5'S, triangles indicate S/TP motifs, circles indicate other motif, black triangles indicate hallmark Rck2-peptides.

behavioural fields, however, gave rise to additional experimental leads which are presented in the results-section of my thesis and have been integrated into Romanov *et al.* (Appendix X.1).

V. Aims Of The Thesis

My thesis is part of a project using quantitative mass spectrometry approaches to identify direct and indirect targets of the key regulator MAPK Hog1 upon hyperosmotic stress. Several results described and discussed here overlap in terms of content with some of the chapters in "Identifying protein kinase–specific effectors of the osmostress response in yeast" by Romanov *et al.* (Appendix X.1), as they were integrated in the manuscript by my co-authors and myself during my participation in the project.

The aims of the thesis can be separated into three distinct aspects:

1. Identification of potentially crosstalk-masked Hog1-targets.

A large number of phosphorylation sites comprising a threonine or serine followed by a proline at position p+1 (S/TP motif) become phosphorylated upon hyperosmotic stress, which is the characteristic recognition motif of proline-directed kinases, such as MAPKs. However, a surprisingly large portion of S/TP sites quantified in the original Hog1-dataset is phosphorylated independently of Hog1 kinase activity and must therefore be targeted by other proline-directed kinases. Crosstalk from the MAPK Kss1 which is usually inhibited by Hog1 kinase activity might play a role here and produce false negative results upon Hog1-inactivation. Introducing the quantitative MS-shotgun approach I used to address assumptions about this set of phosphorylation sites and its results is the first aim of my thesis.

2. Extent of indirectly Hog1-dependent regulation mediated via Rck2.

I also investigated the set of stress-associated phosphorylation sites that can not be directly targeted by Hog1 itself, since they do not harbour an S/TP motif, but still were dependent on Hog1 kinase activity. An analysis of predominant phosphorylation motifs in this set hinted us

towards the well-established Hog1 target Rck2, a MAPK-activated protein kinase (MAPKAPK) of the CaMK-like protein kinase family, that recognizes and phosphorylates serines or threonines preceded by an arginine or lysine at position p-3 (R/KxxS/T motif). A second aim of this work is to present the quantitative MS-approach I used to investigate the effect of Rck2 on the stress-associated, indirectly Hog1-dependent set of phosphorylation sites and to report Rck2 as a as major signalling hub and effector kinase downstream of Hog1.

3. Effects of differences in software algorithms on bioinformatic data interpretation.

Finally, my thesis also aims to address bioinformatic effects on quantitative MS data interpretation and aims to extend the comprehensiveness of the Hog1 dataset (Romanov *et al.*).

Using two different popular identification and quantification software packages, I analysed the same extensive raw dataset resulting from all our MS-shotgun experiments and compared the outcome. The analysis pinpoints some of the advantages and pitfalls of maximising the information that can potentially be gained from proteome-wide MS shotgun approaches.

VI. Results

VI.1. Crosstalk from the filamentous growth pathway potentially masking Hog1 targets is negligible in the Hog1 dataset

Quantitative MS-based approaches using SILAC labelling enable us to analyse phosphorylation pattern changes under various experimental conditions on a proteomic scale. The Hog1-dataset (Romanov *et al.*), as defined in chapter IV.7, consisting of a stress experiment (SR) and experiments analysing phosphorylation patterns upon Hog1 inhibition (I+0'S, I+5'S, I+10'S), displayed 36 S/TP sites in the designated behavioural field 1 (Fig. 7) which are increasedly phosphorylated upon hyperosmotic stress in dependence of Hog1 kinase activity. While validation of these putative targets via the protein-protein-proximity assay M-Track revealed more than 25 new Hog1 targets proteins, most S/TP sites that showed increased phosphorylation upon hyperosmotic stress were not dependent on Hog1 kinase activity and resided in behavioural field 8 (Fig. 7). As described in Romanov *et al.* (Appendix 1.X), we hypothesized that upon Hog1 inhibition some of these S/TP sites might be targeted by Kss1-mediated crosstalk, Kss1 being the central MAPK of the filamentous growth pathway which is inhibited upon Hog1-activation in wildtype cells[97,98]. These phosphorylation events would thus be masked by Kss1 activity and wrongfully assigned as Hog1-independent. To determine the extent of a potential bias introduced in the dataset by Kss1-crosstalk, we designed an MS shotgun experiment using a strain that carries the *HOG1as* allele in a *kss1*Δ

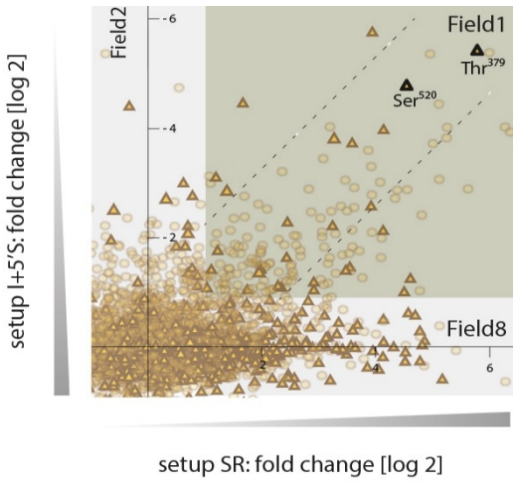

Figure 7: Most S/TP-sites are phosphoryated independently of Hog1. Close-up from Fig. 6D. Triangles: S/TP motifs, circles: other motifs, black triangles: Hog1-dependent Rck2 activation sites

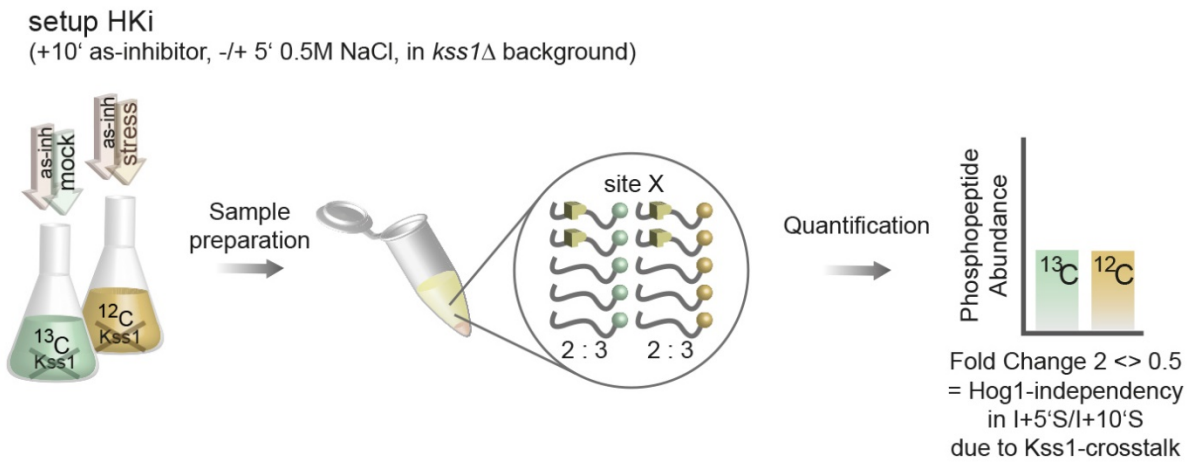

Figure 8: Schematic representation of experimental setup HKi. Setup HKi, inhibition of Hog1as (10’ prior to stress) in a *kss1*Δ background as described in the main text, increase or decrease in phosphopeptide abundance by more than 2-fold was considered significant, corresponding phosphorylation sites were classified as stress-responsive (i.e. Hog1- and Kss1-independent), relevant stress-unresponsiveness of a theoretical phosphorylation site X that was masked by Kss1-crosstalk and assumed to be Hog1-independent in setup I+5’S is depicted (this behaviour should be true for all Hog1-dependent phosphorylation sites).

background. In this setup, designated HKi, I compared phosphorylation patterns of unstressed and stress-treated cells (5’, 0.5M NaCl) in the absence of Hog1 and Kss1 kinase activity (Fig. 8, setup HKi). Truly Hog1-dependent S/TP motifs assigned to field 8 that didn’t show inhibitor-susceptibility due to Kss1-crosstalk (and thus would have reduced the comprehensiveness of the list of putative Hog1 targets) would show static behaviour in this setup. The same static behaviour should be observed at phosphorylation sites that had already been deemed Hog1-dependent according to setup I+5’S. Phosphorylation sites that are still dynamically phosphorylated upon stress in this strain background may be considered as regulated by other kinases independently of both, Hog1 and Kss1. The HKi setup generated a total of 6747 quantified phosphorylation sites (Supplemental Table 1, adapted from Romanov *et al.*, Supplemental Table S2), approximately 18% of which were responsive to stress treatment. In comparison, the dynamic stress response in setup SR comprised roughly 23% of all quantified phosphorylation sites. Setups SR and HKi provided a 32% overlap to be analysed, and subsequent integration with setup I+5’S allowed me to categorise these sites into a Hog1-dependent and a Hog1-independent set. Phosphorylation changes at S/TP motifs

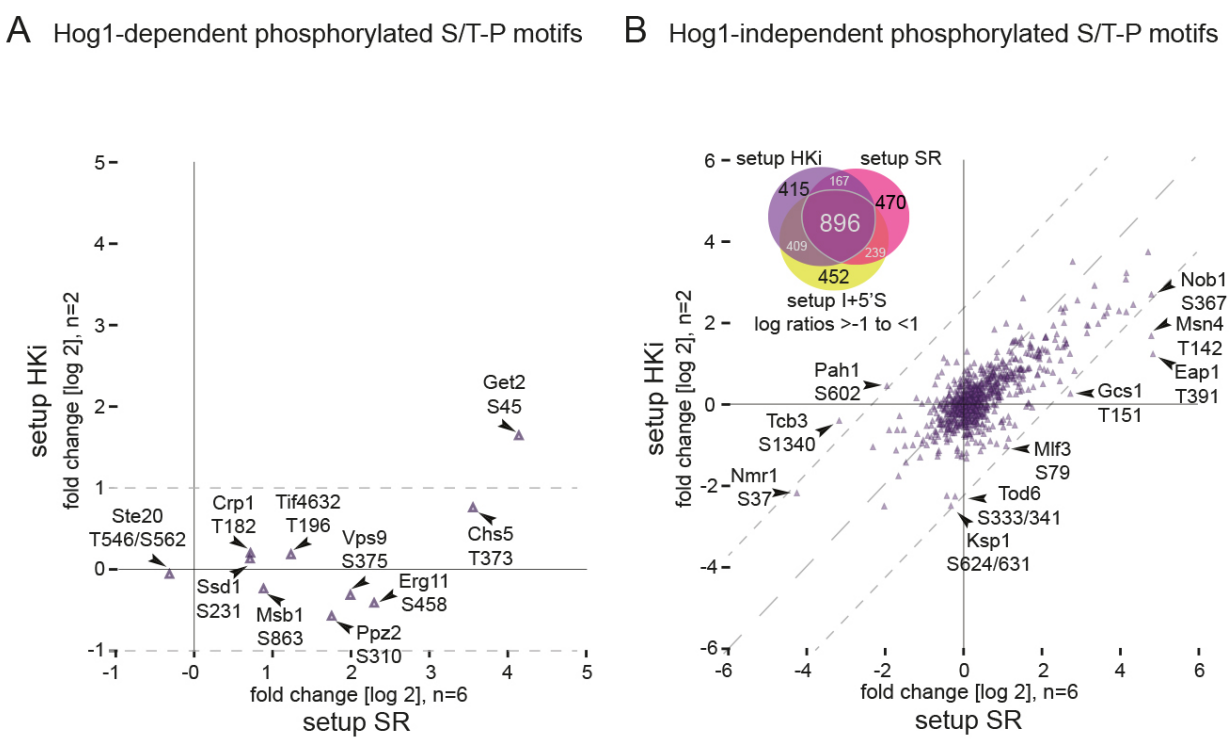

Figure 9, adapted from Romanov *et al.*, Supplemental Fig. S2: Behaviour of Hog1-dependent and Hog1-independent S/TP sites in setup HKi. A) SILAC ratios of Hog1-dependent S/TP motifs overlapping between setups SR and HKi showed distribution along x-axis within a deviation range of 2. B) Venn Diagram of overlap and SILAC ratio distribution of Hog1-independent S/T-P sites (less than 2-fold regulated in setup I+5'S) responding to stress (0.5M NaCl, 5 minutes) in wild type (setup SR) and in a strain in which both, Hog1 (inhibited: as-allele) and Kss1 (deletion mutant: *kss1*Δ) were inactivated.

that were Hog1-dependent according to setup I+5'S, as expected, remained static in setup HKi and did not correlate when compared to setup SR, except for S45 of Get2 (Fig. 9A, adapted from Romanov *et al.*, Supplemental Figure S2). This site, however, was not only determined as a highly reliable Hog1-dependent target by our phosphoproteomic data with a fold change of approximately 0.2 in both, setup I+5'S and I+10'S (Supplemental Table 1, adapted from Romanov *et al.*, Supplemental Table S2), but we were also able to show Get2 to come into proximity of Hog1 during the hyperosmotic stress response, as validated by a weak, but still significant M-Track signal (Romanov *et al.*, Fig. 4E). Noteworthy, its adverse behaviour in the HKi setup is less pronounced (roughly 6 times less than in setup SR), and might thus be explainable by cumulative side effects of the inhibition of Hog1as and deletion of *KSS1*. As a

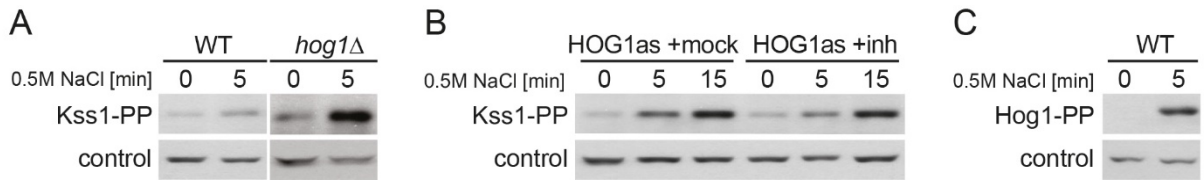

Figure 10: Detection of Kss1-PP and Hog1-PP. A) Kss1 phosphorylation upon hyperosmotic stress in wildtype and *hog1*Δ background B) Kss1-phosphorylation upon hyperosmotic stress in mock- and inhibitor-treated cells carrying the *HOG1as* allele. C) Hog1-phosphorylation upon hyperosmotic stress in wildtype

proof of principle, I can therefore state that Hog1-dependent sites almost invariably behave likewise in setup HKi as they do in setup I+5'S, adding to the evidence of Hog1-involvement. Regarding the Hog1-independent set (i.e., assigned to field 8 according to setup I+5'S), a linear correlation (R = 0.61) of stress-responsiveness could be observed between setups HKi and SR for more than 90% of sites in this set (Fig. 9B, adapted from Romanov *et al.*, Supplemental Figure S2), indicating that these phosphorylation changes are predominantly independent of Hog1 and Kss1. Consequently, I can assume that the high portion of S/TP sites previously residing in field 8 is indeed regulated independently of Hog1 and the Hog1 dataset (Romanov *et al.*) does not disregard considerable amounts of potential Hog1-targets. The findings of this MS-shotgun experiment are in line with results of a Western blot analysis, where I investigated the activation status of Kss1 by monitoring the increase in Kss1 phosphorylation at its characteristic MAPK TxY motif upon hyperosmotic stress in i) wildtype cells, ii) cells carrying the *HOG1as* allele and iii) a *hog1*Δ background. As expected and shown previously[97,98], Kss1 phosphorylation was strongly induced in comparison to its behaviour in wildtype cells after 5' of stress treatment (0.5M NaCl) when *HOG1* was deleted and thus pathway-crosstalk-inhibition was abolished (Fig. 10A). Nevertheless, neither mock- nor inhibitor-treatment in Hog1as-cells resulted in a comparably high phosphorylation increase at the same point of time after stress application (Fig. 10B). Detected Kss1 phosphorylation exceeded the increase in stress-treated wildtype cells only after 15' of stress application, indicating that Kss1 inhibition

was not abolished in our Hog1 inhibition experiments. Also, the minor activation of Kss1 in wildtype cells (or mock-/inhibitor-treated Hog1as cells) is negligible if compared to the strong induction of Kss1 phosphorylation that I observed in a *hog1*Δ background, and similarly when compared to the much more pronounced signal increase in western blots detecting Hog1 phosphorylation (Fig. 10C). This again is in line with the quantification of dynamic Kss1 phosphorylation observed in setup SR. Here, even in wildtype cells with intact pathway-crosstalk-inhibition, the Kss1 activation motif is dynamically phosphorylated, however, only with a fold-change ≤ 5 between unstressed and stressed samples, confirming the slight but negligible activation of Kss1 in both, a Hog1-active and Hog1 inhibited situation. Contrarily, Hog1 activity as measured by stress-induced phosphorylation at its MAPK TxY motif exceeds Kss1 activation by far, with a ~70-fold increase in abundance of the respective double-phosphorylated peptide in setup SR (Supplemental Table 1, adapted from Romanov *et al.*, Supplemental Table S2).

Taking all aspects of this analysis into account, my experiments show that Kss1-crosstalk is not masking Hog1-dependent sites in the original dataset to any considerable extent, and I am able to state that the set of S/TP sites that are phosphorylated directly by Hog1 is indeed smaller than previously expected. My findings implicate that the increased phosphorylation of Hog1-independent S/TP sites upon hyperosmotic stress is regulated by an unknown mechanism that might involve other proline directed kinases, or is affected by the inactivation of phosphatases that preferentially dephosphorylate S/TP motifs under basal conditions.

VI.2. Hog1-dependent non-ST/P sites are regulated indirectly via a major kinase signalling hub

Considering previous studies regarding the effect of hyperosmotic stress on phosphorylation patterns on a proteomic scale, the number of S/TP sites showing Hog1-dependency, although

providing an impressive gain in information, was surprisingly small. Amongst confirmed Hog1-substrates, however, are various kinases and phosphatases that might affect global phosphorylation patterns under the control of Hog1. Indeed, of all phosphorylation sites that showed stress-responsiveness and Hog1-dependency, 82.4% were non-S/TP sites (residing in field 1, Fig. 11A), indicating a distinct indirect effect of Hog1 on stress-associated phosphorylation. Biologically, it stands to reason that a key regulator like Hog1 would delegate some of its responsibility to secondary regulators, which gave rise to two interesting questions: i) Is the observed indirect Hog1 response distributed across various direct substrates or are we able to discern an additional level of regulation downstream of Hog1? and ii) are the secondary responses merely supporting the directly Hog1-dependent phosphorylome or do they have distinct biological purposes, covering autonomous branches of the HOG response? Attempting to narrow down potentially involved kinases that might convey Hog1-dependent regulation, we analysed this set of sites in regard to their phosphorylation motif to see whether we could deduce putative kinase dependencies from motifs that were repeatedly found in the set. A MotifX search[131,132] revealed that R/KxxS/T and S/TxxxL motifs were significantly enriched amongst field 1 phosphorylation sites (Fig. 11B+C), which hinted us towards basophilic kinases (Fig. 11D). This group of kinases, which includes members of the protein kinase A, C and G (PKA, PKC, PKG) and casein kinase I (CK1) families as well as calmodulin-like protein kinases (CaMK), recognizes serines and threonines preceded by an arginine or lysine at position -3 (R/KxxS/T)[72–75]. An additional leucine at position +4 (R/KxxS/TxxxL) constitutes an even more specialised motif that is recognized by the AMPK subgroup of CaMK with Snf1[101,102] and Sch9[133,134] as prominent representatives.

A hallmark of HOG signalling that was regarded as one of various quality controls of our experimental approach in Romanov *et al.* (Appendix X.1) was the phosphorylation of Rck2, a MAPKAPK that is also part of the CaMK family[57]. Rck2 is a well-described downstream substrate of Hog1 that is phosphorylated at its two characteristic activation sites T379 and S520 upon hyperosmotic stress[58,59], which led us to hypothesise that a subset of field 1

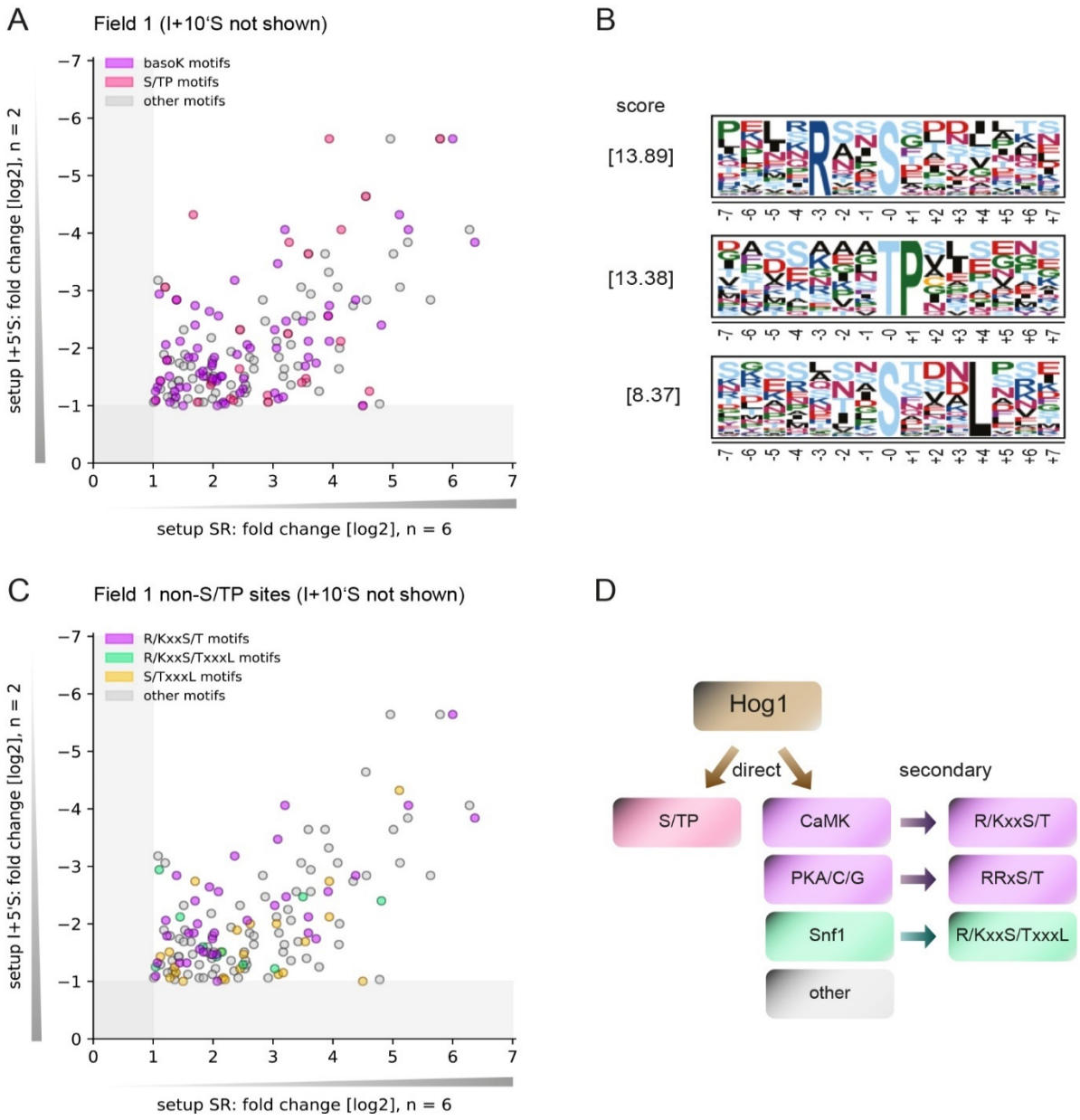

Figure 11: A secondary kinase-network downstream of Hog1. A) non-S/TP sites are predominant in field 1, pink circles represent S/TP motifs, purple circles represent basophilic kinase motifs, grey circles represent other motifs. B) Overrepresented motifs in field 1 provided by MotifX enrichment analysis, in order of score: RxxS, TP, SxxxL. C) field 1 non-S/TP sites colourcoded by motif D) Schematic representation of a possible directly and indirectly Hog1-dependent HOG response. Potential effector kinase families are suggested.

basophilic kinase sites might be targeted by this kinase. To determine to what extent Rck2 influences global phosphorylation patterns and field 1 phosphorylation sites in response to hyperosmotic stress, we designed another SILAC experiment where I compared stressed wildtype cells to stressed cells lacking Rck2 (5', 0.5M NaCl), designated setup *rck2*Δ (Fig. 12).

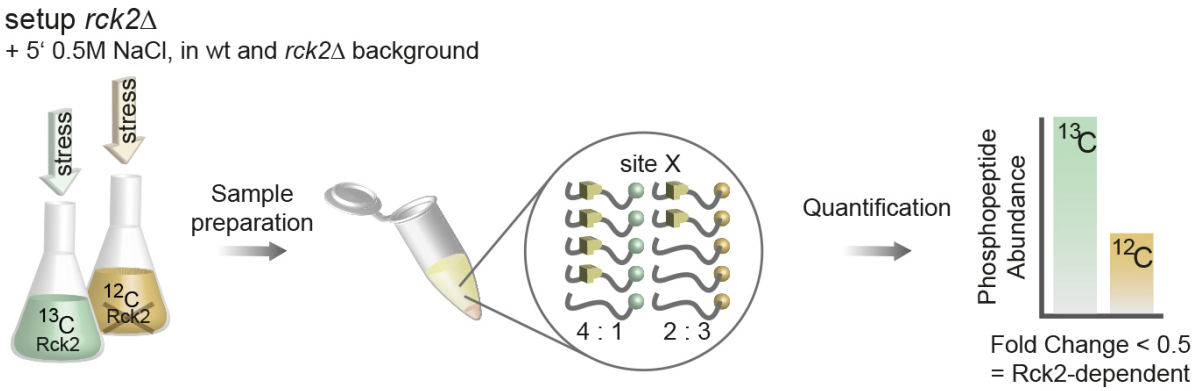

Figure 12: Schematic representation of experimental setup *rck2*Δ. Stress application in a *rck2*Δ background as described in the main text, increase or decrease in phosphopeptide abundance by more than 2-fold was considered significant, corresponding phosphorylation sites were classified as *rck2*Δ-responsive, relevant *rck2*Δ-responsiveness (i.e., Rck2-dependency) of a theoretical phosphorylation site X is depicted.

While the use of an *RCK2*-deletion strain is more prone to produce potential artifacts than a strain where kinase activity is specifically inhibited, as operated in the Hog1-inhibited datasets in Romanov *et al.* (Appendix X.1), this methodology is commonly used and perfectly suitable to generate an overview of kinase effects.

The MS shotgun of setup *rck2*Δ exceeded our expectations and demonstrated that deletion of *RCK2* results in changes of the stress-associated phosphoproteome that are comparable to the size of the effect of Hog1 inhibition. In setups I’+5’S as well as I+10’S, roughly 10% of all quantified phosphorylation sites were susceptible to Hog1 inhibition in either direction (more/less phosphorylated), which attributes to around half the percentage of sites found to be generally responsive to hyperosmotic stress in setup SR (~22%). In setup *rck2*Δ, 13.4% of all quantified phosphorylation sites showed dynamic behaviour upon *RCK2*-deletion (Fig. 13A). Of a total of 4834 phosphorylation sites corresponding to 1479 proteins quantified, 318 sites (220 proteins) were less phosphorylated in response to hyperosmotic stress when compared to wildtype cells, thus being *RCK2*-dependent. Notably, 142 of these sites (113 proteins) were harbouring basophilic kinase motifs. To investigate the impact of Rck2 activity on the Hog1-

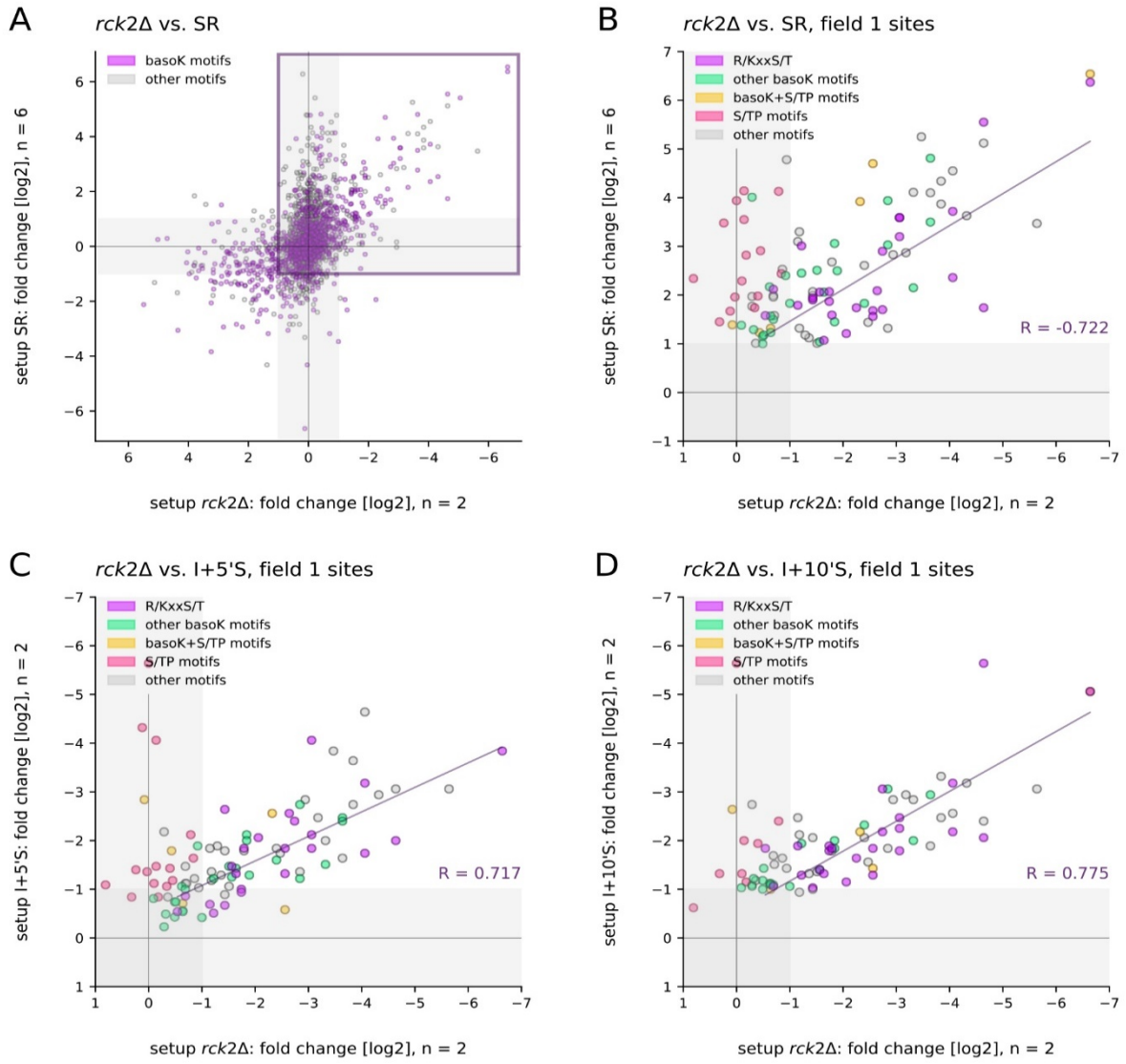

Figure 13: The Rck2-dataset. A) Overlap between setup SR and setup *rck2*Δ. *RCK2*-deletion affects a large number of phosphorylation sites. The violet square indicates the section depicted in B-D; purple circles: basophilic kinase motifs, grey circles: other motifs B) Overlap between field1 sites in setup SR and setup *rck2*Δ (violet square in A); phosphorylation of most Hog1-dependent non-S/TP motifs is Rck2-dependent; phosphorylation of solely S/TP motifs is not Rck2-dependent. C-D) Overlap between field1 sites in setup I+5'S (C) / I+10'S (D) and setup *rck2*Δ, phosphorylation of most stress-responsive non-S/TP motifs is Rck2-dependent; solely S/TP motifs are not affected by *RCK2*-deletion. Purple and green circles: basophilic kinase motifs, yellow circles: S/TP and basophilic kinase motifs, pink circles: solely S/TP motifs, grey circles: other non-S/TP motifs; correlation of potentially directly Rck2-targeted R/KxxS/T motifs is depicted; basoK = basophilic kinase

dependent phosphorylome, I analysed the overlap between setup *rck2*Δ, SR and I+5'S, covering 106 of 203 of all field 1 sites (52.4%) regardless of their motif. The effect of *RCK2*-deletion on field 1 was impressively high, as 60 of the 83 covered non-S/TP sites (72.3%)

- including every single one of the 41 R/KxxS/T sites in this set - showed a decreased phosphorylation status upon hyperosmotic stress treatment in the *rck2*Δ background (Fig. 13B). By this evidence, I can propose that Rck2 is a master regulator of HOG signalling. Besides these 60 phosphorylation sites whose diminished phosphorylation could be attributed to the lack of Rck2 activity, I also reviewed phosphorylation events that might potentially be field 1 sites, but have only been quantified in either stress or inhibitor experiments. By doing this, I identified 39 additional non-S/TP sites (Supplemental Table 1, adapted from Romanov *et al.*, Supplemental Table S2) showing decreased phosphorylation in setup I+5'S (i.e., Hog1-dependency) and 9 additional non-S/TP sites showing increased phosphorylation in setup SR (i.e., stress-responsiveness) that were also less phosphorylated in setup *rck2*Δ (i.e., Rck2-dependency). To provide a proof of principle for the *rck2*Δ setup, I also investigated the behaviour of the set of directly Hog1-dependent S/TP sites which should not be affected in setup *rck2*Δ. Within the overlap between field 1 S/TP sites and setup *rck2*Δ, no significant correlation was found between either stress-responsiveness (*rck2*Δ vs. SR, Fig. 13B) or Hog1-dependency (*rck2*Δ vs. I+5'S / I+10'S, Fig. 13C / D), however, 5 of the 23 S/TP sites in the overlap showed dynamic behaviour upon *RCK2*-deletion. Closer examination of these sites revealed that all of them harbour a basophilic kinase site in combination with the previously determined S/TP motif (Fig. 11B-D, yellow circles), emphasising the possibility of promiscuous phosphorylation sites that are targeted by more than one kinase at the same time. Taken together, these findings confirm that a large part of the Hog1-dependent stress response upon hyperosmotic stress is indirectly mediated via kinase networks. Additionally, it answers my first question, by dismissing a broad distribution of Hog1-derived cues across all its direct targets. Instead, my data proposes a distinct novel tier of regulation downstream of Hog1 with Rck2 as a major effector kinase of HOG signalling. However, while the Rck2-dependent set of phosphorylation sites included several suggested interactors of Rck2[102,135,136] I was also able to show Rck2-dependency for more than 25 protein kinases from various families, like Gin4, Hsl1, Kcc4, Sch9 and Snf1. These kinases are all prominent basophilic

kinases, and it is reasonable to assume that their Rck2-dependency is co-responsible for the large amount of dynamically phosphorylated basophilic kinase motifs found in setup *rck2*Δ. This would introduce additional tiers of regulation into the HOG-Rck2-network which could be followed up and dissected stepwise into even smaller sections of kinase-specific interactions.

To shed further light on the potential range of cellular processes influenced by Rck2 activity, I performed a gene ontology (GO) enrichment analysis using the online Functional Annotation tool DAVID[137,138]. For my analysis I used the level 4 biological process GO-terms associated with the Saccharomyces Genome Database (SGD) identifiers of different sets of proteins and clustered GO-terms according to the semantic similarity algorithm of the online tool REVIGO[139]. Fig. 14 shows statistically significant (fold changes with $p < 0.05$) GO-term enrichments for protein sets derived from i) Rck2-dependent field 1 sites that harbour an R/KxxS/T motif, i.e., sites that are potentially directly targeted by Rck2 (lane 1), ii) all Rck2-dependent field 1 sites, i.e., including sites that are potentially targeted by kinases downstream of Rck2 (lane 2), iii) Hog1-dependent sites harbouring an S/TP motif, i.e. sites that are potentially directly targeted by Hog1 (lane 3) and iv) all Hog1-dependent non-S/TP sites, i.e. sites that are targeted by kinases (including Rck2) downstream of Hog1 (lane 4). Revision of the functional annotation showed that proteins harbouring S/TP motifs cover GO-terms classically associated with Hog1 (lane 3), i.e. glycerol transport and the osmotic stress response, while indirect/secondary Hog1-targets harbouring non-S/TP motifs seem to cover functional processes related to membrane budding/vesicle-mediated transport and also specific metabolic processes (lane 1 & 2). It is however worthwhile to stress the point that lane 4 contains the set of proteins derived from all field 1 non-S/TP sites, and therefore includes proteins (almost 50%) that are not covered in the *rck2*Δ setup. Still, considering the impressively high percentage of Rck2-dependence in the *rck2*Δ/field 1 overlap, it is justifiable to expect an equally large effect of Rck2 on sites currently not covered in setup *rck2*Δ. This allows me to speculate that GO terms exclusively associated with the lane 4 protein set might

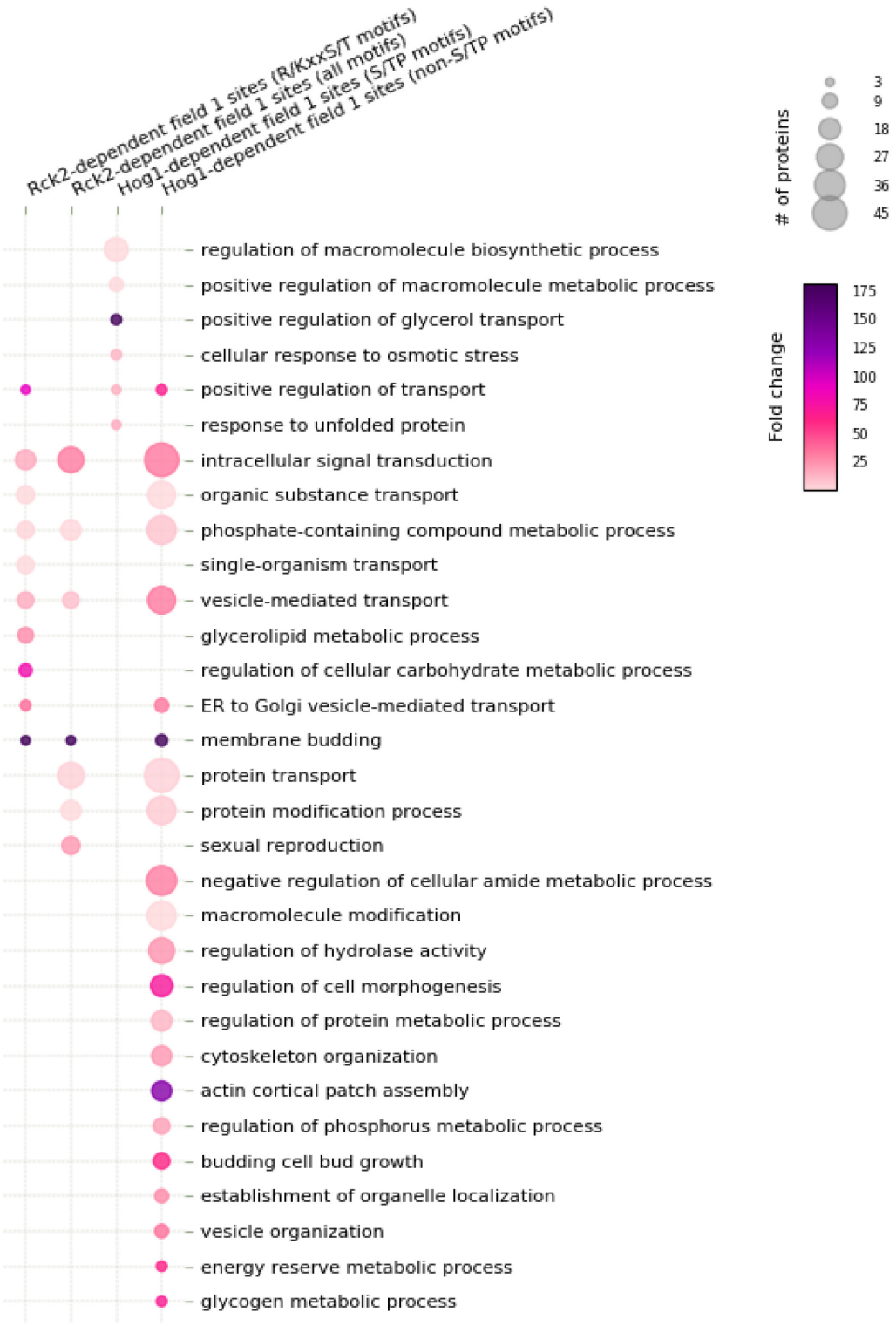

Figure 14: GO-term enrichment in various sets of proteins. GO-term enrichment (level 4 biological processes) and clustering of semantically similar GO-terms was performed as described in the main text and chapter VIII.6, lane 1: protein set derived from Rck2-dependent field 1 sites harbouring an R/KxxS/T motif, lane2: protein set derived from all Rck2-dependent field 1 sites regardles of their motif, lane 3: protein set derived from field 1 S/TP sites, lane 4: protein set derived from all field 1 non-S/TP sites regardless of coverage in setup *rck2*Δ.

hint towards other Rck2-related functions, possibly again in an indirectly regulated manner. Indeed, functional annotations of lane 4 proteins tend to be related to cell morphology and membrane organisation, supporting the hypothesis of Rck2 being in charge of regulating aspects of these processes downstream of Hog1. Additionally, although the fold change significance cut-off might exclude some relevant GO-terms due to the small number of proteins (~30) in the sets depicted in lane 1 and lane 2, I observed remarkably distinct differences between lane 3 (derived from directly Hog1-dependent sites) and the others (derived from indirectly Hog1-dependent sites). Applying my criteria as described, I found “positive regulation of transport” to be the only GO-term assigned to both the putative direct and indirect/secondary Hog1-substrates.

Thus, I can conclude that Rck2 indeed serves as key regulator of autonomous processes during the hyperosmotic stress response as opposed to merely being a supportive addition to the direct Hog1-phosphorylome.

VI.3. Testing for osmosensitive phenotypes of putative direct Hog1-substrates

I next wanted to test whether the newly identified direct substrates of Hog1 assume an individual physiological role in a hyperosmotic environment by analysing survival and growth rates of strains lacking the respective protein. To do so, I compared growths rates of deletion mutants for each of the putative Hog1-substrates in liquid cultures for 4-5 generations (400’ on average) after hyperosmotic stress treatment (0.5M NaCl) to mock treated samples (Fig. 15A, from Romanov *et al.*, Fig. 5A). The difference between growth rates was scored relatively to the difference in a wildtype strain and a *hog1*Δ strain. 9 of the tested deletion mutants showed decreased growth rates upon hyperosmotic stress treatment that was outside the fluctuation margin of the wildtype strain (Fig. 15B, from Romanov *et al.*, Fig. 5B): *hal5*Δ*, vps9*Δ*, chs5*Δ*,*

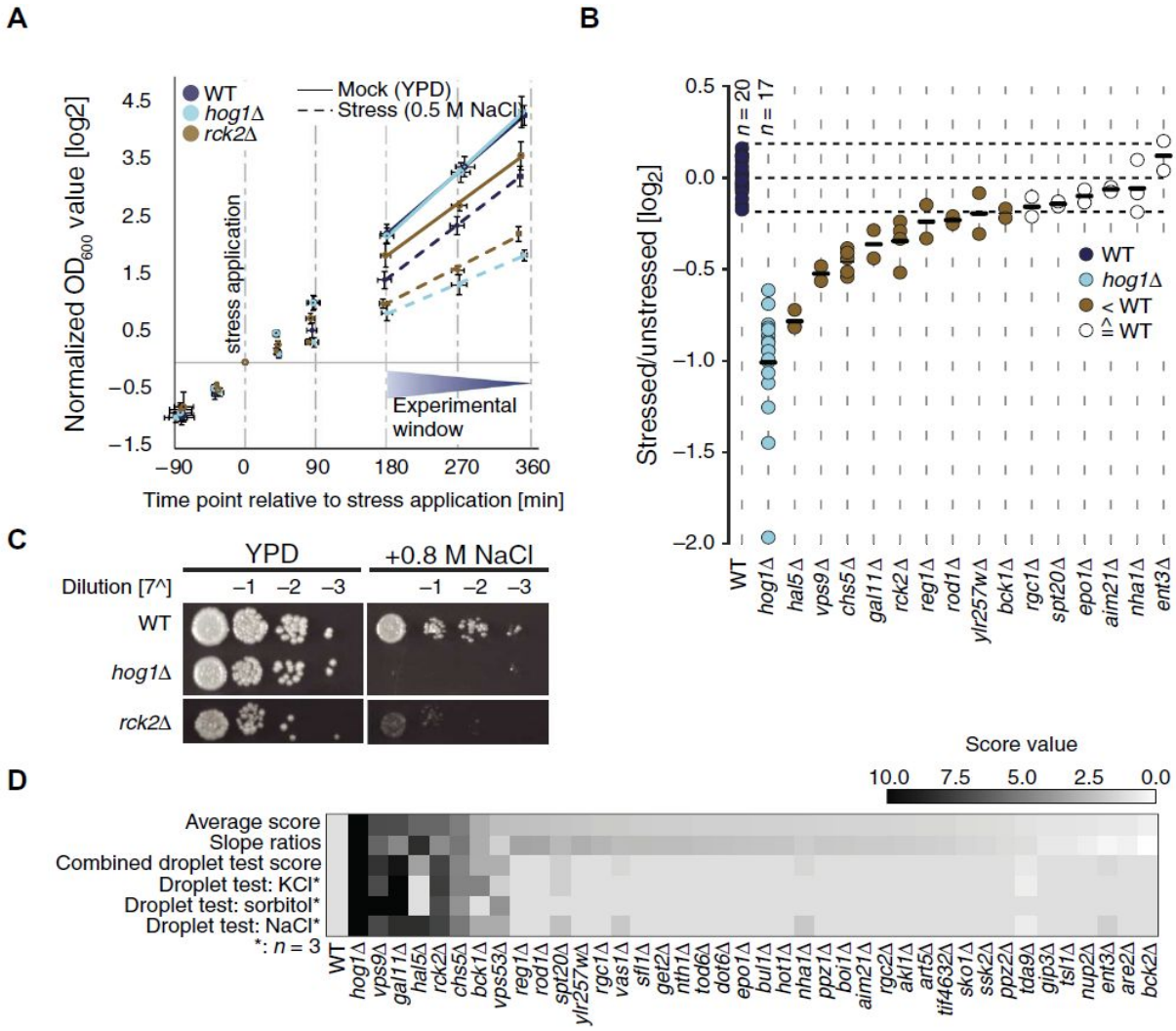

Figure 15: Characterization of osmosensitive phenotypes. A) Log2-transformed growth curves of wild-type (WT), *hog1*Δ, and *rck2*Δ cells in the absence of hyperosmotic stress and after induction of hyperosmotic stress. OD600: optical density at 600nm. B) Stressed/unstressed (mock) ratios of log-transformed growth curve slopes depicted in (A); n ≥ 2 replicates per sample. C) Serial dilution droplet test of the individual deletion mutants on YPD plates on YPD + 0.8MNaCl. D) Heatmap illustrating scaled scores from growth curve analysis (slope ratios) and dilution droplet tests under different conditions. Rows are sorted according to combined average score (0 to 10).

*gal11*Δ*, rck2*Δ*, reg1*Δ*, rod1*Δ*, ylrw257w*Δ, and *bck1*Δ. Of the respective 9 proteins, 4 hadn't been described in the context of HOG signalling yet, namely Reg1, Rod1, Vps9 and Ylr257w. The decreased growth rates in response to stress indicate that these proteins indeed might play a role in short-termed adaptation to hyperosmotic environments. Additionally, I determined long-term effects of hyperosmotic stress on cells lacking the putative Hog1 substrates by a serial dilution droplet test. Here, I analysed growth of deletion mutants after 1-4 days compared

to wildtype and *hog1*Δ cells on full medium YEP plates containing one of the following stressors: 0.5 M NaCl, 0.8 M NaCl, 1.2 M NaCl, 0.8M KCl, 1.2M KCl, or 1.2M sorbitol. While *hog1*Δ cells were almost inviable already at low concentrations of osmolyte, wildtype cells and most of the deletion mutants showed little sensitivity to low to medium concentrations of osmolyte. Growth was scored using an arbitrary scoring system, taking into account the concentration of osmolyte and differentiating between no sensitivity (0), slight sensitivity (1) and strong sensitivity (2) to hyperosmotic stress (Fig. 15C, from Romanov *et al.*, Fig. 5C). Concentrations of 1.2M of either osmolyte slowed down cell growth almost invariably, even in wildtype cells. However, 4 strains, namely *chs5*Δ*, gal11*Δ*, rck2*Δ and *vps9*Δ, could be considered as highly osmosensitive with this setup (Romanov *et al.*, Supplemental Fig. S8, all osmosensitivity tests of one replicate, representative for all triplicates), and *hal5*Δ cells were highly osmosensitive on plates containing NaCl, which is consistent with the involvement of kinase Hal5 in sodium tolerance. Three additional strains showed weak osmosensitivity, namely *bck1*Δ, *spt20*Δ and *vps53*Δ. The results of individual osmolyte scores, average serial dilution droplet test scores and growth curve scores were integrated and are summarized in Fig. 15D (from Romanov *et al.*, Fig 5D).

Overall, my analysis showed that several proteins, when lacking, do indeed affect fitness of cells in a hyperosmotic environment. This finding is rather straightforward for proteins like Rck2, since it is a major signalling hub downstream of Hog1, and *RCK2* deletion would thus be assumed to be prone to affect osmoadaptation in a similar manner as Hog1 inactivation. The same is true for Gal11, which is a subunit of the RNA Polymerase II mediator complex, and thus affects transcription in general in the deletion mutant, leading to impaired growth already before stress treatment. Still, it is noteworthy that some deletion mutants showed impaired or restricted osmoadaptation even if the respective proteins were not involved in maintaining or increasing osmolyte concentration. For example, *VPS9* and *VPS53* deletion both showed to slightly to strongly affect growth in a hyperosmotic environment but hadn't been directly connected to HOG signalling previously. Both of the respective proteins are involved

in vacuolar and Golgi-endosome trafficking, and deletion mutants show abnormal vacuole morphology and transport[140–142]. This abnormal vacuole phenotype can also be observed in *CHS5* deletion mutants[140], along with decreased hyperosmotic stress resistance, as has been described in the literature[143,144] and confirmed in my growth test analysis. Although it is not completely precluded that some of the newly identified Hog1 targets are by-stander substrates, my observation of growth deterioration for some of the deletion mutants indicate again that translational regulation via HOG signalling comprises more than just the regulation of internal osmolyte concentrations and that these processes might indeed be physiologically relevant for cell fitness and survival in hyperosmotic environments. It also stands to reason that physiological effects of the deletion of a single relevant factor might be minor in comparison to combined suspension of a whole set of Hog1-dependent substrates[145]. Additionally, physiological effects of subtle changes in the phosphoproteome might also become more relevant if cells are exposed to repeatedly fluctuation of the osmotic balance or affect competitive fitness[146].

VI.4. Extending the original Hog1 dataset by using different raw MS data processing softwares

This work and the referenced project describe quantitative MS-based phosphoproteomics approaches to capture the effects of kinase-phosphatase-networks and analyse their interconnectivity on a proteomic scale. One limitation of this methodology is the necessity of creating overlaps between datasets to follow changes in the phosphorylation pattern upon individual experimental conditions. Conclusions can then be drawn about specific phosphorylation sites that become more valid the more information on the respective peptide is collected and confirmed, both globally (i.e., behaviour of the phosphorylation site in different experimental setups) and individually (i.e., several PSMs that cover the same peptide and

occurence of the quantified SILAC ratio in several biological replicates). As described in chapter IV.5, peptide spectra are collected, identified and quantified using software tools which take into account various parameters like amino acid modifications, false positives, contaminants and signal-to-noise-ratios.

While the choice of software for analysing a specific dataset is mainly subject to the technical and methodological constraints of the experiment as well as research group conventions (e.g. for reasons of experience and reproducibility), it stands to reason that the use of a broader range of tools might lead to valuable new information (e.g. in terms of applicability of the individual softwares, but also in terms of proteome coverage).

The Hog1 dataset (Romanov *et al.*) has been analysed using the commonly used MS quantification software Proteome Discoverer (PD, version used: 1.3), which uses an automated workflow integrating search tools like SEQUEST and Mascot[147,148]. The second commonly used search engine for experimental setups like ours is MaxQuant (MQ, version used: 1.5.2.8)[149,150], where developers recently introduced a new feature called “Requantify”, allowing calculation of SILAC ratios (see chapter IV.6) where the signal of either the heavy or light labelled peptide can’t be quantified as a peak over noise due to very low abundance and thus low signal intensities. Instead of processing only SILAC signals identified as pairs, the software captures putative SILAC peptide intensities individually and calculates a ratio using the noise signal of the missing peak as baseline. The advantage of this method is especially productive if, for example, in setup SR a peptide in the mock-treated sample (^{13}C SILAC signal) is not or substochiometrically phosphorylated and thus not present in a high enough abundance in the MS sample after TiO2-phosphopeptide enrichment, while the same peptide is phosphorylated post-stress (^{12}C SILAC signal), thus enriched and easily quantified. Additionally, MQ and PD use different algorithm pipelines, which may lead to different outcomes regarding which peptides are identified and quantified.

I wanted to know whether I would be able to increase the coverage of the proteome and thus potentially the overlap between our experiments by re-analysing all our generated raw MS

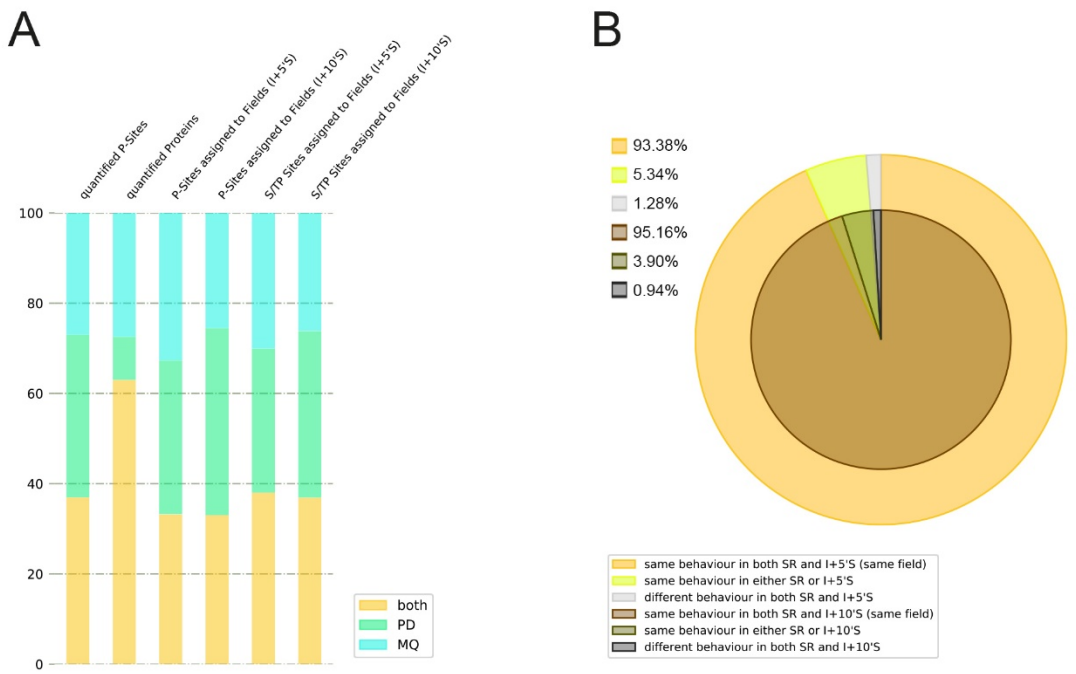

Figure 16: Comparison of quantified phosphorylation sites in PD and MQ. A) Percentage of different sets of phosphorylation sites (respectively proteins, lane 2) in MQ (turquoise), PD (green) or both (orange). B) Percentage of phosphorylation fileds with same behaviour in either SR or I+5'S (light colour-code) / I+10'S (dim colour-code), same behaviour in both dimensions (orange), one dimension (yellow) or no dimension (grey). P-sites: phosphorylation sites, PD: Proteome Discoverer, MQ: MaxQuant

datasets using MQ. On average, PD and MQ shared 35.6% of quantified peptide hits (Fig. 16A) for various sets of phosphorylation sites and proteins. Both softwares, however, added a roughly equal share of individual quantifications (PD average: 36.1% / MQ average: 28.3%) to the dataset. This shows how data mining can lead to an increase of proteome coverage by (in our case) one third when re-analysing the raw data using an alternative algorithm. Notably, the overlap between softwares rises to 59,7% when comparing protein coverage instead of phosphorylation site coverage. This difference in overlap size presumably results from the fact that proteins often harbour more than one affected phosphorylation site. These might be quantified individually by either software, but converge on the same protein, thereby also increasing the reliability of a suggested putative substrate. As a measure of quality, I analysed

behavioural field assignment of phosphorylation sites as described in Chapter IV.7 and depicted in Figure 6D, i.e. peptide hits quantified in setup SR and at least one inhibition setup (I+5'S/I+10'S). Of the 2191 (I+5'S) / 1384 (I+10'S) sites that had been assigned to any behavioural field in both the PD and MQ dataset, 93.38% (I+5'S) / 95.16% (I+10'S) were assigned to the same field, an additional 5.34% (I+5'S) / 3.9% (I+10'S) were assigned to fields that prompt the same behaviour in at least one dimension (either stress dependency or inhibitor susceptibility) and only 1.27% (I+5'S) / 0.59% (I+10'S) were assigned to entirely opposed fields, i.e. show different behaviour in both SR and the respective inhibitor dataset according to one or the other software (Fig. 16B). To investigate the comparability of both softwares further, I analysed the correlation between all peptide ratios quantified by PD and MQ for setups SR, I+5'S and I+10'S, obtaining correlation coefficients of R = 0.88, R = 0.79 and R = 0.89, respectively (Fig. 17A-C). An even more distinct correlation can be seen in the histograms in Fig. 17D-F, where individual ratio differences for setups SR, I+5'S and I+10'S are calculated as MQ-ratio(log2) - PD-ratio(log2). While 93.43% (SR) / 96.76% (I+5'S) / 98.12% (I+10'S) of all peptide ratios resided within a cutoff of +/-1 quantification difference (q.d.) between PD and MQ, only 6.57% (SR) / 3.33% (I+5'S) / 1.88% (I+10'S) were outside these boundaries. With an even stricter cutoff of +/-0.5 quantification difference, I still obtained 82.92% (SR) / 89.78% (I+5'S) / 92.31% (I+10'S) within boundaries.

Since I observed a notable accumulation of peptides in setup I+5'S that seem to be dynamic in the MQ analysis but static in the PD analysis, I compared the quantification difference (q.d.) of the peptides found to be outside of the cutoff in either as dataset with their quantification difference in the other two datasets, respectively. If the observed discrepancy between MQ and PD was due to a difference in the softwares' power to quantify specific peptides, I would expect a similarly differential behaviour in all three datasets and it would then be interesting to analyse common properties of this set of peptides. However, Fig.17G-I shows that almost all analysed peptides that were found to have quantification differences greater than +/-1 in one dataset actually reside within the cutoff and show a very good correlation in the other two

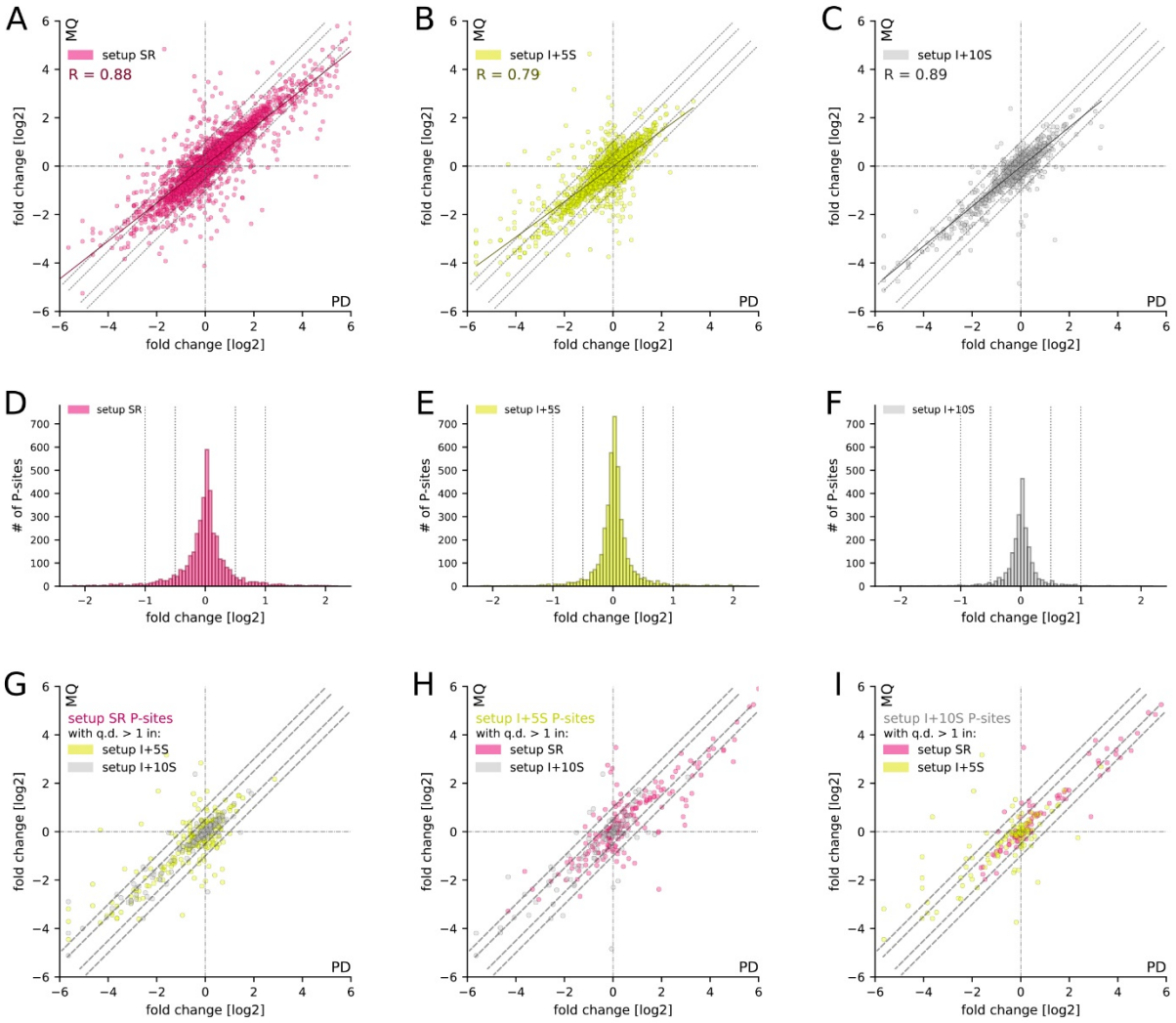

Figure 17: Ratio correlation between PD and MQ. A-C) log2-ratio correlation for all quantified phosphorylation sites in setups SR (A, pink), I+5'S (B, yellow) and I+10'S (C, grey). Dotted grey lines indicate cutoff for quantification differences of > 0.5, respectively > 1. D-F) Histograms of log2-ratio quantification difference (calculated as MQratio[log2] – PDratio[log2]) distributions in setups SR (A, pink), I+5'S (B, yellow) and I+10'S (C, grey). Dotted grey lines indicate cutoff for quantification differences of > 0.5, respectively > 1. G-I) log2-ratios of phosphorylation sites with quantification differences > 1 in one setup (G: setup SR, pink; H: setup I+5'S, yellow; I: setup I+10'S, grey) vs their log2-ratio correlation in the respective other setups. Dotted grey lines indicate cutoff for quantification differences of > 0.5, respectively > 1. P-sites: phospohorylation sites; q.d.: quantification difference.

datasets. This result indicates that even ratios that differ by more than +/-1 between PD and MQ in one dataset don't have to be immediately disregarded. In conclusion, I can thus assume that quantifications of both softwares are stably comparable and individual quantifications of either software can be regarded as valid additional peptide hits.

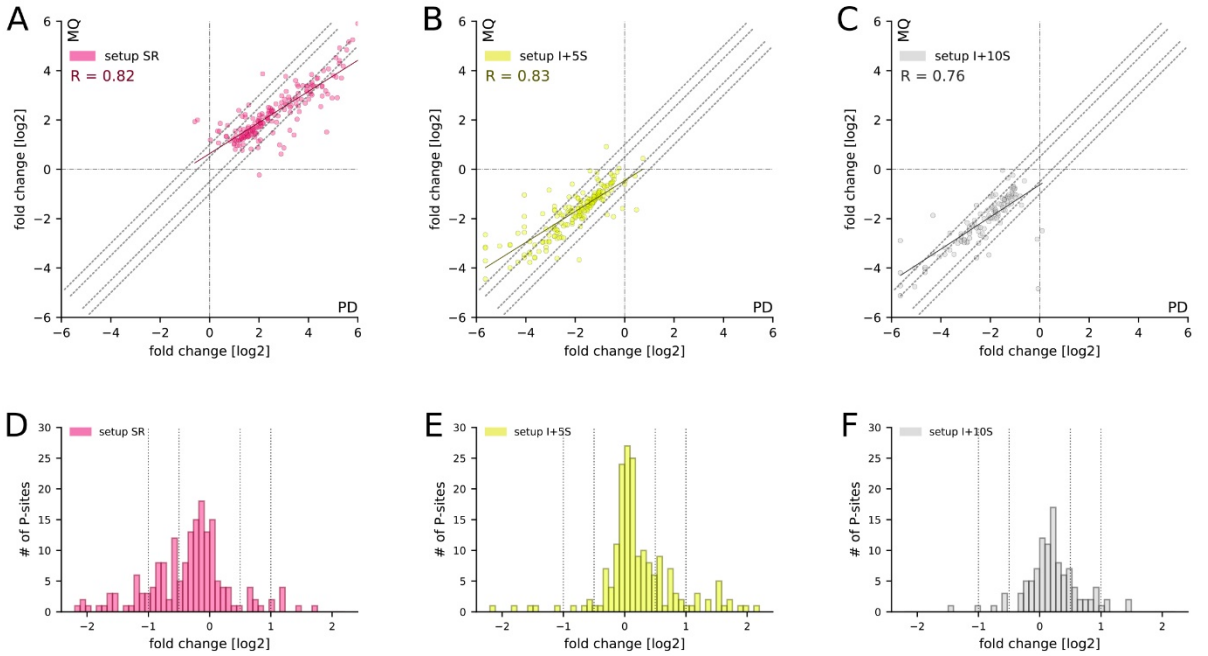

Figure 18: Ratio correlation between PD and MQ for field 1 phosphorylation sites. A-C) log2-ratio correlation for all quantified field 1 phosphorylation sites in setups SR (A, pink), I+5'S (B, yellow) and I+10'S (C, grey). Dotted grey lines indicate cutoff for quantification differences of > 0.5, respectively > 1. D-F) Histograms of log2-ratio quantification difference (calculated as MQratio[log2] – PDratio[log2]) distributions in setups SR (A, pink), I+5'S (B, yellow) and I+10'S (C, grey). Dotted grey lines indicate cutoff for quantification differences of > 0.5, respectively > 1. P-sites: phospohorylation sites; q.d.: quantification difference.

I then wanted to know how the analysis with an additional software affects the Romanov *et al.* dataset of Hog1-dependent phosphorylation sites, i.e phosphorylation sites residing in field 1 according to PD. First, and equivalently to my previous quality control, I analysed ratio correlation and quantification differences between PD and MQ quantifications for all sites residing in field 1 according to PD. I obtained linear correlation coefficients of R = 0.82 (SR) / R = 0.83 (I+5'S) / R = 0.76 (I+10'S) (Fig. 18A-C) and 77.84% (SR) / 85.56% (I+5'S) / 89.19% (I+10'S) of sites with quantification differences of less than +/-1 (Fig. 18D-F). Interestingly, when analysing the smaller set of field 1 phosphorylation sites, it becomes obvious that MQ quantifications result in generally lower ratios than PD quantifications.

Of the 203 field 1 phosphorylation sites (149 proteins) quantified by the PD software, 80.3% (163 sites, 124 proteins) were covered in the MQ analysis (Fig. 19, left piechart). 68.1%

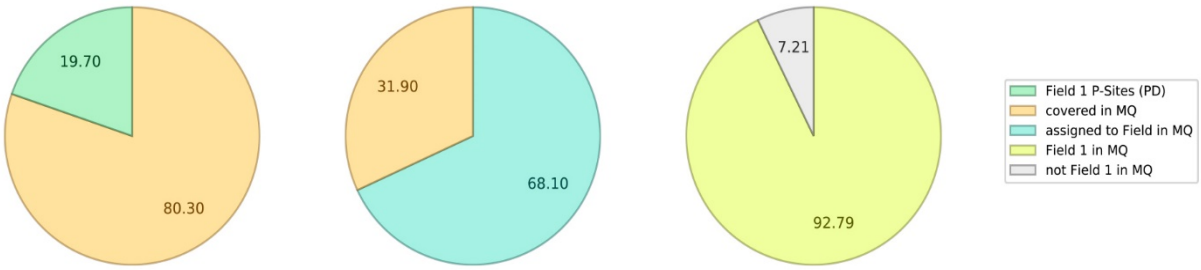

Figure 19: PD Field 1 Phosphorylation Sites as quantified in MQ. Left piechart: MQ-coverage of PD Field 1 P-Sites. Center piechart: Depiction on MQ-covered PD Field 1 P-Sites, assignment to any field (i.e., quantification in setup SR and either I+5'S or I+10'S). Right piechart: Field assignment of PD 1 P-Sites in MQ. MQ: MaxQuant; PD: Proteome Discoverer; P-Sites: Phosphorylation sites.

(111 sites, 89 proteins) of these sites were also assigned to a behavioural field in MQ (Fig. 19, center piechart), with field 1 being assigned in 92.79% (103 sites, 82 proteins) of all cases (Fig. 19, right piechart). The 100 additional phosphorylation sites (86 proteins in total) that were not covered in MQ and resided in field 1 according to PD added another 67 proteins that hadn't been covered by sites within the overlap. The analysis using MQ also yielded 172 unique field 1 sites (134 proteins in total, 111 proteins not covered by sites within the overlap) that hadn't been covered by PD, increasing the field 1 protein set even further. Finally, subtracting the proteins that were added to the list by both softwares via individual, non-overlapping phosphorylation sites, I was able to identify the 82 proteins in the overlap, plus 54 additional proteins assigned to field 1 individually by PD, and 98 additional proteins assigned to field 1 individually by MQ. These numbers add up to a total of 234 proteins in field 1, enhancing the original dataset for this field by almost 60%.

Considering this increase in information, I assumed that the list of putative Hog1 substrates, i.e. proteins that are directly phosphorylated upon hyperosmotic stress by Hog1, could also be extended by combining the PD and MQ analysis. I therefore again focussed on phosphorylation sites in field 1 that harboured an S/TP motif. Indeed, I found 42 S/TP sites residing in field 1 according to MQ, 20 of which haven't been covered or assigned to field 1 in

the PD dataset (Supplemental Table 1, adapted from Romanov *et al.*, Supplemental Table S2). These sites correspond to 17 proteins, with four (Hot1, Rck2, Sko1, Ste50, all confirmed interactors of Hog1) having been already assigned to field 1 via different sites in the PD dataset, prompting us to take a closer look at these sites. First, for Hot1, the classical Hog1-dependent catalytic site S153 was assigned to field 1 in the PD analysis, but showed only Hog1 inhibitor susceptibility in the MQ analysis, while its stress-responsiveness fell slightly below our strict 2-fold cut-off. Instead, according to MQ, Hot1 site T360[104] was assigned to field 1. Second, HOG signalling hallmarks and Rck2-activating sites T379 and S520[58,59] were quantified and assigned to field 1 in both the PD and MQ analysis, together with another previously described but not further characterised site, T350 (currently investigated by Jiri Veis, Egon Ogris research group). According to MQ, also the behaviour of the peptide carrying the double-phosphorylation of S515 and S520 was assigned to field 1. Next, Sko1 had been assigned to field 1 in the PD analysis due to stress responsive and Hog1-dependent phosphorylation on T215, a site that has so far only been characterised in a study investigating co-occurence of ubiquitylation and phosphorylation upon proteasome inhibition by Swaney et al.[151]. The MQ analysis however covered the classical Hog1-dependent catalytic sites S108 and T113 of Sko1[52] as well, assigning their behaviour to field 1. According to MQ, the peptide carrying the double phosphorylation of S108 and T113 is stress-responsive and inhibitor-susceptible, while both peptides carrying only one of these phosphorylations are less abundant upon stress treatment, and, in the case of S108, also more abundant upon inhibitor treatment. These seemingly reversed dynamics of the single-phosphorylated peptides are most likely due to the predominant double-phosphorylation upon stress application, and are in line with phosphorylation dynamics described for peptides of confirmed Hog1 targets like Tsl1 (Romanov *et al.*). Fitting its established role in HOG signalling, T94 of Sko1, a catalytic site that is targeted by Hog1-activated CDK Cdc28[78], was also assigned to field 1 according to MQ. Finally, of the various catalytic sites of Ste50 that mediate the negative feedback loop of prolonged Hog1 activation by inhibiting Ste50-Opy2 interaction in the regulatory pathway

Protein	P-Site	Descr_short
Far8	T132	involved in recovery from pheromone-induced cell cycle arrest
Gcs1	S157 / T161	ADP-ribosylation factor GTPase activating protein (ARF GAP), involved in ER-Golgi transport
Hsf1	T97	heat shock TF, involved in diauxic shift, monitors translational status of cell through an RQC (Ribosomal Quality Control)-mediated translation-stress signal
Kic1	S625, T1073	PAK/Ste20 family, necessary for cell integrity, role in RAM (cell polarity) signalling
Orm2	T18	mediates sphingolipid homoeostasis, reacts to DNA replication stress and also hyperosmotic stress
Psp2	S340	cytoplasmic suppressorof intron-splicing defects
Sog2	T214	RAM-signalling, essential for cell morphology and separation after mitosis
Tfg1	T673	subunit of TFIIF, involved in RNA PolyII initiation and elongation
Ubp13	S261	Protease that cleaves ubiquitin-protein-fusions
Ysp2	S336	retrograde sterol-transport from plasma membrane to ER, conserved across eukaryotes
Tsa1	T174	highly abundant ribosome-associated and cytoplasmic antioxidant chaperone, reacts to DNA replication stress

Table 1: Putative direct substrates of Hog1 according to MQ. List of putative Hog1 substrates as described in the main text. Short protein descriptions are collected from the Saccharomyces cerevisiae database (https://www.yeastgenome.org/).

upstream of Hog1, T244 and T341[78,152–154] were assigned to field 1 in the MQ analysis, whereas PD only yielded the former. Of the residual 13 proteins on the field1 list according to MQ, the phosphatase Ppz1 was already included in the former list of putative Hog1 substrates in Romanov *et al.* (Appendix X.1) due to its stress responsiveness and sites of its paralog Ppz2 being found in field 1 in the PD dataset. Furthermore, the field 1 list according to MQ contained two additional known interactors of Hog1 that haven't been covered in the PD analysis: the nucleoporin Nup2[46] and the cytoskeleton regulatory complex protein Pan1 which has been previously reported to become phosphorylated by Hog1 at S1225 by our lab[155]. It should be noted that the inherent incompleteness of MS shotgun studies may result in known dynamic phosphorylation sites to not be covered, however, in agreement with other studies[67,156], I could observe that various reported Hog1 target sites were not responsive to stress or inhibitor treatment. While many of these sites were established as Hog1 target sites by performing in vitro-kinase assays, and therefore it might be questionable if they are genuine in-vivo

substrates of Hog1, I could still confirm many nuclear factors and targets that are involved in cell cycle progression and elongation, which are also validated in part by point mutation experiments. Thus, I can assume that my analysis can be seen as complementary to these kinase assays, again highlighting the importance of assembling comprehensive datasets from various methodological approaches. Finally, the list of putative direct substrates of Hog1 according to MQ (Table 1) contains 9 proteins that have, to our knowledge, not been investigated in relation to hyperosmotic stress and HOG signalling previously. These proteins (Far8, Gcs1, Hsf1, Psp2, Sog2, Tfg1, Ubp13, Ysp2, Tsa1) would be interesting hints for validation by our protein-protein-interaction assay, assessment of physiological relevance upon hyperosmotic conditions and further research. One additional protein from the p21-activated kinase (PAK)/Ste20 family, Kic1, has been mentioned as an interactor of Hog1 in a high-throughput study from 2011 aiming to investigate phosphatase Ptc1 function[157], but its involvement in hyperosmotic stress hadn't been further investigated as well. To us, this protein was interesting, since according to the PD dataset it harbours two sites that are either stress-responsive (T625) or susceptible to Hog1 inhibition (S723), but couldn't be identified as Hog1 substrate due to lacking overlaps between setups. T625 is now covered in the MQ-analysis and can indeed be assigned to field 1, together with a second site, T1073. Another interesting finding was the stress-responsive and inhibitor-susceptible dynamic phosphorylation of T18 of Orm2, a protein that has been described in the context of the TORC1/2- and Ypk1-mediated sphingolipid homeostasis and the Hog1-independent hyperosmotic stress response[109,158]. Indeed, in our dataset the phosphorylation of various sites of Ypk1 are downregulated (Supplemental Table 1, adapted from Romanov *et al.*, Supplemental Table S2), which is in line with Orm2-phosphorylation and activation, however, our data implicates a direct dependency on Hog1 of at least one of Orm2's sites. Following the validation strategy of Romanov *et al.* (Appendix X.1), Gina Varnavides from our research group is currently testing these newly identified putative Hog1 substrates using the M-Track protein-protein-proximity assay in the course of her Master's thesis, and preliminary results (data not shown) indicate that we will be

able to extend our list of validated putative Hog1 substrates. However, for Orm2 and Ysp2 we had to adapt our M-Track strategy due to the proteins' transmembrane domains which prevent the HKMT-tagged C-terminus of the candidate substrate from interacting with the H3-tag of Hog1. To circumvent this problem, we N-terminally tagged Orm2, Ysp2 and Nup2 (as positive control) with HKMT expressed under a triose phosphate isomerase (TPI) promoter[159], and, as in the original strategy, compared the proximity signal between unstressed conditions and hyperosmotically challenged cells. Again, preliminary data kindly provided by Gina Varnavides (data not shown) indicate that both proteins show a significantly enhanced Hog1-proximity signal upon hyperosmotic conditions, indicating they are true substrates of the MAPK.

Finally, to illustrate further advantages of using two different quantification algorithms on the same raw dataset, I performed a GO-term analysis on the original (PD) dataset, the new (MQ) dataset and the combined (PD + MQ) dataset to gain information about the role of the HOG response in biological processes. Fig. 20 shows the distribution of proteins found in different sets over GO-terms collected by the online Functional Annotation Tool DAVID[137,138]. To depict GO-terms with a high level of specificity, I chose level 4 of biological processes, at the same time minimising redundancy by clustering semantically similar GO-terms using the online tool REVIGO[139]. Lane 1 (upper legend) shows GO-terms associated with the original set of putative Hog1 substrates, i.e. proteins harbouring field 1 S/TP sites according to the PD analysis, while lane 2 (upper legend) shows the same for the protein list derived from combining the MQ analysis with the PD analysis. Due to the low number of proteins in these two sets, fold enrichment numbers are not evaluated statistically and data points are supposed to only indicate general overrepresentation of the respective GO-terms. Lane 3 and 4 (upper legend) show overrepresentation of GO-term enrichment with significant ($p < 0.05$) fold change in the entire field 1 according to either PD or MQ. As a representation of background enrichment of the GO-terms found for lanes 1-4, lane 5 and 6 (lower legend) depict enrichment with significant ($p < 0.05$) fold change of the respective GO-terms in the middle field, i.e. the list of proteins that harbour sites unaffected by either stress or Hog1 inhibition. Notably, none

of the GO-terms of the middle field reaches a fold enrichment higher than 2.8-fold, although their protein count per GO-term exceeds that of lanes 1-4 by an average factor of 100. Besides the obvious and expected increase in found GO-terms when combing the PD with the MQ analysis (lane 2 vs. lane 1), the MQ dataset alone yielded more GO-terms than the PD dataset (lane 4 vs. lane 3), which is not surprising, considering it also contributed almost double as many individually assigned proteins to field 1 as the PD dataset. However, GO-terms that are covered in both softwares are comparably stable in protein count and fold-change between PD and MQ, which strengthens my assumption of comparable validity of data derived individually from either one of the two softwares. Biologically, Fig. 20 shows that field 1 proteins are to a high extent functionally associated with signal transduction and osmolyte transport regulation, which is in line with the general understanding of the HOG response. Additionally, I found GO-terms regarding a broad range of metabolic regulation as well as protein localisation and organisation, including vesicle-mediated transport and endo/exocytosis, fortifying our previous suggestion of Hog1 being a regulator for metabolic fine-tuning, potentially via autonomous downstream signalling of Rck2, which I showed to be a major effector kinase of Hog1 (chapter VI.2). As in the functional annotation analysis in chapter VI.2, where I concentrated on potentially Rck2-related GO-terms, processes associated with cell movement and polar growth were also enriched in the entire field 1, with cell budding and establishment of cell polarity even showing up in the S/TP site containing and therefore presumably directly Hog1-dependent set of proteins. With this finding, one could hypothesise that Hog1 might even play a role in stress prevention by means of chemical sensing and attempting to escape local stressor concentrations. However, phosphorylation does not necessarily lead to activation of the substrate, therefore it would be necessary to collect further evidence regarding the characteristics of the affected phosphorylation sites of the proteins contributing to the GO-term list to be able to make assumptions about the biological background. This is evident, for example, as the key regulators responsible for pseudohyphal growth and pheromone sensing, Kss1 and Fus3, are inhibited upon Hog1-activation, as described and analysed in chapter VI.1.

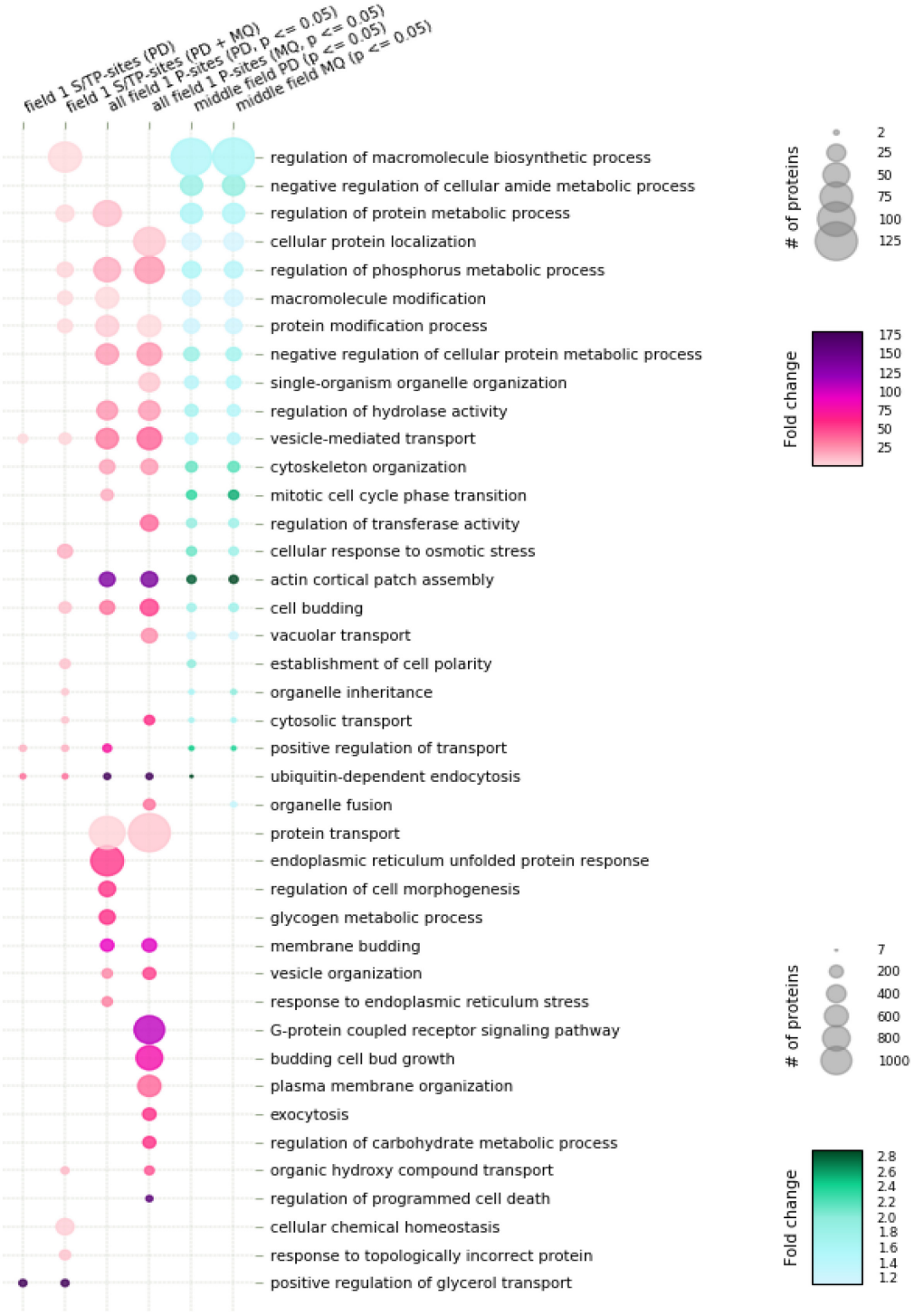

Figure 20: Biological processes enriched in various sets of proteins. GO-term enrichment (level 4 biological processes) and clustering of semantically similar GO-terms was performed as described in the main text and chapter VIII.6, lane 1: protein list derived from directly Hog1-dependent phosphorylation sites as quantified by PD, lane 2: protein list derived from directly Hog1-dependent phosphorylation sites as quantified by either PD or MQ, lane 3: protein list derived from all field 1 phosphorylation sites as quantified by PD, lane 4: protein list derived from all field 1 phosphorylation sites as quantified by MQ, lane 5: protein list derived from static phosphorylation sites (middle field) as quantified by PD, lane 6: protein list derived from static phosphorylation sites (middle field) as quantified by PD.

Here, it might intuitively be more reasonable to suggest that Hog1 could have an inhibitory effect on targets of these pathways to enhance signal fidelity even further.

In conclusion, I was able to show that an individual analysis with either PD or MQ is qualitatively comparable and information gained from either analysis is equally valid, and that combination of two different softwares can increase the output of raw quantitative MS-data, thus being a reasonable approach for proteomics-scale screening experiments. Nevertheless, the divergence between both analyses emphasises the incomprehensiveness and individuality of MS shotgun data, and confirms the choice of software to be a tangible parameter when comparing interlaboratory results.

VII. Discussion

This work is based on a comprehensive MS-shotgun study identifying direct and indirect substrate proteins of MAPK Hog1, the central element of the HOG signalling pathway, and presents approaches to unravel a complex kinase network. Using different experimental setups, we analysed the impact of three key kinases on the *S. cerevisiae* phosphoproteome upon hyperomostic stress conditions and found that i) MAPK Hog1 directly regulates a comparably small set of substrates (36 S/T-P motifs), while most stress-responsive S/T-P motifs are affected in a Hog1-independent manner (Appendix X.1), ii) the effect of Kss1-crosstalk on the phosphoproteome upon Hog1 inhibition is negligible (Chapter VI.1), and iii) MAPKAPK Rck2 constitutes a major effector kinase in the HOG signalling network, controlling a substantial part of Hog1 secondary/indirect targets (Chapter VI.2). I also tested whether any of the newly identified direct Hog1 targets were of physiological relevance in a hyperosmotic environment by analysing short-term and long-term effects of a range of stress conditions on cell growth of the respective deletion mutants, indeed identifying several Hog1-regulated proteins to affect osmoadaptation (Chapter VI.3). Furthermore, I aimed and succeeded to expand the output of our MS-shotgun approaches by re-analysing the original Hog1 dataset using a second quantification software (Chapter VI.4).

VII.1. Occam's razor failed: Who, if not Kss1?

In Romanov *et al.* (Appendix X.1), we presented more than 25 new substrates that are phosphorylated upon hyperosmotic stress and directly dependent on Hog1. By analysing the dataset using a different software package, we were even able to increase this set of new putative Hog1 targets by about 30%. Furthermore we could confirm that phosphorylation of

several established Hog1 targets is affected Hog1-dependently upon hyperosmotic stress conditions, namely Hot1[160], Rck2[161], Rgc1, Rgc2[42], Rtg3[162], Sko1[53], Ssk2[163] and Ste50[88,153]. As described in Romanov *et al.* (Appendix X.1), GO-enrichment analyses on the dataset even revealed Hog1-involvement in cellular processes that haven't previously been associated with HOG signalling, for example the Exomer and GET complexes in vesicular transport to the Golgi, as well as SAGA and Mediator complexes and trehalose metabolism (Appendix X.1, Fig. 6). In addition to phosphorylation dynamics that point towards direct interaction between Hog1 and its substrates, we also analysed Hog1-dependent stress-responsive phosphorylations that can't be directly exerted by Hog1 due to the lack of a consensus motif at the phosphorylation site, showing the great extent of secondary effects of the kinase on proteome-wide phosphorylation changes. To our knowledge, our study is to date the most comprehensive screen analysing the hyperosmotic stress response in Yeast. However, it is indispensable to note that the stochastic nature of the method renders MS shotgun data inherently incomplete. Examplatory, a few known targets of Hog1 and upstream regulators, like for example the relevant phosphorylation sites of osmosensor Sho1, weren't included in our dataset. While this fragmentary lack of information is not surprising, we took specific interest in phosphorylation sites that were described previously in association with hyperosmotic stress and were covered in our dataset with contradictory results. Indeed, some proteins that have been previously reported as targets of Hog1 by performing in-vitro kinase assays showed no phosphorylation dynamics in our analysis in response to stress treatment or Hog1 inhibition. This is in agreement with other observations[67,156], and might challenge the notion that all targets established in these in-vitro assays are genuine in-vivo targets of the kinase. On the other hand, our analysis can be seen as a complementary approach to comprehensively dissect kinase-phosphatase-networks, as many factors, especially associated with cell cycle and elongation, were canonically found and validated as direct substrates of Hog1 in various experimental approaches. Our findings therefore also emphasise the importance of integrative data analysis, and points out the problem of overlaps between

experiments as the limiting step of proteome-wide MS screens. Such pitfalls can be partially circumvented by thorough data mining, an example of which can be seen in Romanov *et al.* (Appendix X.1), where our group combined phosphorylation data that was only available for one experimental set up with published lists of other laboratories, or in the aforementioned expansion of the dataset by analysing the same raw MS data with different software packages. Still, even taking the increase in information by varying search algorithms into account, the direct effects of Hog1 seem surprisingly small for a key regulator when compared to the large set of S/TP sites that were phosphorylated in stress, but showed no Hog1-dependency (field 8 S/TP sites). An explanation for this phenomenon might be due to pathway crosstalk by the activation of a related kinase, like filamentous growth MAPK Kss1, an option I addressed by performing a stress response MS-shotgun with Hog1 inhibited in a *kss1*Δ background (setup HKi). However, more than 90% of all field 8 S/TP sites (responsive to stress but not dependent on Hog1) in setups SR and I+5'S were still phosphorylated in response to stress in setup HKi, indicating that the influence of Kss1 is negligible in the original Hog1 dataset. This finding is supported by the minor phosphorylation increase of activating key residues of Kss1 in a Hog1-inhibited stress experiment as compared to the situation in a *hog1*Δ background.

Although I was able to rule out Kss1 activity as potential origin of impaired Hog1 substrate identification, I still wondered if there are other kinases responsible for phosphorylation at shared targets sites. Considering the chance for crosstalk between pathways that activate kinases with identical consensus phosphorylation motifs, I investigated the behaviour of the other MAPKs systems present in yeast. Firstly, activation key residues T180 and Y182 of Fus3 have been reported to not become significantly phosphorylated during early timepoints (5') of the hyperosmotic stress response before[154], which is in line with the aformentioned kinetic insulation between the hyperosmotic stress, filamentous growth and pheromone response pathways. Using data from setups SR, I+5'S and HKi, I also found Fus3 to be only minorly phosphorylated in a Hog1-inhibited background, analogous to Kss1-behaviour, suggesting that the involvement of this kinase in the hyperosmotic stress response upon Hog1-inhibition is

indeed negligible. Smk1, the MAPK of the sporulation pathway, is not expressed upon vegetative growth and could be excluded upfront from the list of potential candidates for a hypothetical masking effect[17]. Regarding the CWI MAPK Slt2, it has been reported previously that Slt2 activating phosphorylation is not affected in early timepoints (0-30') by hyperosmotic stress conditions[60,164], a notion I could confirm by Western Blot experiments that showed no increase in phosphorylation of the MAPK in either a wildtype, Hog1-inhibited or *hog1*Δ background. Furthermore indicating that Slt2 crosstalk is not active and masking potential Hog1 targets, we found established targets of Slt2, namely S238 of Swi6[165], S160 of Rcn2[166] and several S/TP motifs on Rlm1[167,168], to be static in our dataset in both the stress and inhibitor setups. Collectively, these findings indicate that none of the other MAPK systems becomes considerably activated in a Hog1-inhibited situation, and thus the phosphorylation pattern of field 8 S/TP sites in hyperosmotically challenged cells is genuinely not directly dependent on Hog1. To explain the Hog1-independent phosphorylation of this large portion of field 8 S/TP sites, I entertain two principal possibilities:

i) other proline-directed kinases, for example CDKs, might be involved. While CDKs are mainly known for regulating the cell cycle, some of them are indeed associated with cell-cycle independent stress responses, for example Pho85, a CDK that responds to phosphate starvation. Since CDKs do not share the mechanisms of MAPK signalling, is it less plausible that potential masking effects of Hog1-targets are due to crosstalk between pathways, but rather might be a result of interconnected or redundant physiological processes.

ii) phosphatases that selectively dephosphorylate S/TP motifs under basal conditions could be affected. Inhibition of a phosphatase upon hyperosmotic stress conditions could potentially explain the high percentage of Hog1-independent S/TP phosphorylation. An interesting candidate for these hypothesis is PP2A (D. Hollenstein, W. Reiter, personal communication), a phosphatase that has been associated with the transcriptional response to hyperosmotic stress[169]. The role of this phosphatase upon hyperosmotic conditions is currently investigated in another project in our group.

VII.2. Indirect responses - pulling strings for the mastermind

The predominant aim of Romanov *et al.* (Appendix X.1) was to describe the directly Hog1-dependent phosphorylome upon hyperosmotic stress. Indeed, we were able to challenge the previous assumption of Hog1 regulating the major part of stress-associated S/TP phosphorylation and to narrow this notion down to a relatively small validated set of putative direct Hog substrates. However, our data revealed an impressively large portion of Hog1-dependent phosphorylation sites that can't be directly regulated by Hog1 due to their lack of an S/TP motif. To be precise, 82.4% of all stress-responsive and Hog1-dependent phosphorylation dynamics quantified in the overlap of our stress and inhibitor experiments were non-S/TP motifs, hinting towards important downstream mechanisms that take over the cue from Hog1 to phosphorylate substrates on their own. The sheer size of this set of Hog1-indirect, or secondary, responses is in line with the broad range of cellular processes that are affected and have to be adjusted upon a hyperosmotic stress situation. As described in Chapter IV.2, our motif analysis of non-S/TP sites residing in field 1 showed a significant increase of basophilic kinase phosphorylation motifs in this set. This fuelled our investigation and confirmation of Rck2 as a major regulator and introduction of a distinct regulatory tier of secondary Hog1-dependent responses. According to my data, it is safe to assume that Rck2 regulates most of the basophilic kinase motifs contributing to the secondary HOG response, since 72% of all field 1 non-S/TP motifs and 100% of all field 1 R/KxxS/T motifs covered in the *rck2*Δ setup were affected by the *RCK2* deletion. However, as the R/KxxS/T motif is recognised by other basophilic kinase families as well, the many Rck2-dependent sites in the field 1 overlap might not all be direct targets of Rck2. Instead, equivalently to Rck2 mediating a whole range of Hog1-downstream regulation, other kinases might do the same for and act downstream of Rck2. As mentioned in chapter VI.4, besides calmodulin-like kinases (CaMK), also cAMP-activated protein kinase A (PKA) family members like Tpk1-3 recognise a

Protein	Short Description	Function		Interesting network partners
Alk1	haspin-like S/Tkinase	spindle-formation, cell polarity		
Cki1	choline/ethanolamine kinase	first step in phosphatidylcholine synthesis (Kennedy pathway)	genetic physical	Gcs1, Ptk2
Fpk1	S/T-kinase of the Kin82-subfamily	phospholipid translocation, inhibits upstream inhibitory kinase Ypk1	physical genetic physical genetic, physical genetic, physical genetic, physical	Akl1, Art5, Ptk2, Ste50, Cdc42, Cdc24, Ypk1/2, Tor2 (interconnected), Yck2, Rtg3, Syp1 (interconnected), Cdc28, Pho85, Gin4, Sic1 (interconnected)
Hrk1	S/T-kinase	ion homoeostasis	genetic	Snf1
Lcb5	Diacylglycerol kinase (DAGK)	phosphorylates sphingoid long-chain bases	genetic genetic	Get2, Snf1
Mss4	Phosphoinositol-4phosphate-5kinase (PI4P5K)	cytoskeleton organisation, cell polarity	genetic	Pan1, Tor2, Cdc42 (interconnected)
Nnk1	S/T-kinase	implicated in proteasome function, phosphorylates Gludependent dehydrogenase Gdh2	genetic genetic, physical	Get2, Ask10, Tpk1/3, Tor2, Cdc24, Pkh1, Pkc1 (interconnected)
Pcl6	Cyclin of Pho85 kinase holoenzyme	activates PP1/2 via Glc8 inactivation, glycogen storage	genetic, physical	Slt2, Bck1, Cdc28, Sic1, Swi6 (interconnected)
Psk2	PAS-domain containing S/Tkinase	sugar metabolism and translation, shift from glycogen synthesis to glucan synthesis	genetic genetic, physical	Bul1, Get2, Slt2, Tor2, Rtg3 (interconnected)
Sch9	AGC family kinase	growth control pathway, transactivates osmostressresponsive genes, intergrates nutrient signals and sphinolipid-mediated signals, regulates Slt2 activity	physical genetic, physical genetic, physical	Pkh1/2 Hog1, Sko1 (interconnected) Bck1, Rim15, Msn2/4, Snf1, Sic1, Hsf1, Pho85 (interconnected)
Vac7	kinase activator (vacuolar membrane protein)	activates PI(3,5)Pkinase Fab1 upon hyperosmotic shock, vacuolar segregation, inheritance and morphology		

Table 2: Rck2-dependent kinases. List of putative Rck2-downstream acting kinases as described in the main text. Short protein descriptions, function descriptions and interaction information are derived from the Saccharomyces cerevisiae database (https://www.yeastgenome.org/) and PhosphoGrid (https://phosphogrid.org/).

specialised version of the motif with an arginine/lysine on position -2 ([R/K][R/K]xS/T). Even more specialised, the CaMK-subfamily of AMP-activated protein kinases (AMPK) like Sch9 and Snf1 recognise the R/KxxS/T motif with an additional leucine on position +4

(R/KxxS/TxxxL). When analysing which proteins contributed to the R/KxxS/T enrichment in field 1 according to the MotifX search, I found sites of 38 proteins besides Rck2, 6 of which were kinases (Romanov *et al.* and Wolfgang Reiter, personal communication). For five of these six kinases, at least one stress-responsive and Hog1-dependent R/KxxS/T motif that also shows to be Rck2-dependent in the *rck2*Δ setup was covered, yet none of them was characterised as conveying catalytic activity: Cki1 (S14[106]), Fpk1 (S227, S414[170]), Nnk1 (S65[170]), Psk2 (S156[171]), and Sch9 (S290[172]) (Table 2). Since for none of these kinases known catalytic phosphorylation sites (i.e., in the activation loop of the kinase) were covered in the *rck2*Δ setup, I am only able to propose an unspecified connection with secondary HOG signalling. Nevertheless, the *rck2*Δ setup yielded six additional kinases (respectively kinase subunits or well-established kinase activators) that harbour stress-responsive and Rck2-dependent basophilic kinase motifs: Alk1 (S212[151]), Hrk1 (S139[106]), Lcb5 (S202[171]), Mss4 (S341[170]), Pcl6 (S124[151]), and Vac7 (S164[78]) (Table 2). Again, for all of these kinases catalytic sites were either not characterised or not covered in our setup. When investigating these 12 kinases in regard to their functions and suggested interaction partners, I consistently found processes related to cell wall integrity, cell polarity and membrane budding (including vesicle-mediated transport and vacuolar organisation), but also hints to cell cycle regulation. This finding reproduces the results of our GO-term enrichment analysis in chapter IV.2, and suggests that the interface between HOG signalling and cell cycle arrest might be regulated autonomously by Rck2. Specifically, I repeatedly encountered the Snf1-complex (and its associated factors) which is known to negatively regulate HOG signalling[173,174]. Although the respective activating sites of Snf1 were not covered in our experiments, a NetworKIN-analysis performed for Romanov *et al.* (Appendix X.1) had suggested Snf1 as one of the most probable effector kinases downstream of Rck2. Taken together, these findings suggest that even incomprehensive data from various experiments, when combined, can lead to new insights into kinase-phosphatase networks. One specific example would be the regulation of potassium transporter Trk1[135,175,176] by its regulator kinase Hal5 and regulator phosphatases Ppz1/Ppz2,

which have never before been connected to HOG signaling. In detail, S63 of Hal5 was found to be Rck2-dependent, while Ppz1/2 would possibly constitute direct targets of Hog1 (Supplemental Table 1, adapted from Romanov *et al.*, Supplemental Table S2). The action of these regulatory events might explain changes in the phosphorylation pattern of Trk1 as we found S412 and S414, two non-S/T-P motifs, to be up-regulated in a stress- and HOG-dependent manner. S414 additionally showed susceptibility to deletion of *RCK2* supporting a regulatory role for the kinase in potassium transport.

In conclusion, my analysis shows how several hierarchical tiers of signalling contribute to the HOG response and emphasise the importance of dissecting these kinase-phosphatase networks in a step-by-step-wise manner to be able to make detailed assumptions about the regulation of a specific protein.

VII.3. Two bottom-up tandem mass spectrometry quantification softwares are better than one

While defined and reproducible sample preparation is essential to minimize divergence between MS experiments, it is still not evitable to introduce minor systematic errors at various points of the experimental procedure and sample preparation. For our experiments, potential error sources have to be controlled already at harvesting, where medium variability may introduce slight changes in cell growth, and the optical density at 600nm (OD_{600nm}) is used as a tool to determine the number of cells in liquid culture, potentially leading to variability in cell volume - however, in experiments using SILAC-labelling these differences between conditions can be normalized bioinformatically with our in-house python script processing (David Hollenstein). Reproducibility of cell breakage and protein isolation as well as stability of PTMs is subject to buffer conditions and temperature and can be counteracted by denaturing reagents or inhibitors of proteases and phosphatases. Furthermore, when analysing peptides

digested with Lys-C and Trypsin, as is the case in our experiments, one has to account for variation originating from missed cleavage sites by adjusting MS-parameters to recognize peptides harbouring more than one lysine or arginine[155,177], resulting in double- or triple-charged peptides to be analysed. Also, loss of information during enrichments for a specific subset of peptides, here phosphopeptides, may occur in part due to interaction between biological material and surfaces of plastic ware and laboratory utensils. Finally, even if artifacts generated by these origins of systematic error are minimized using optimised and reproducible protocols, datasets procured from experiments like the ones described here are large and as complex as the biological context they are derived from, and they require sophisticated bioinformatic processing to ensure valid data interpretation.

As experiments are combined to deduct information, a highly limiting parameter is the overlap between those experiments. On average, even technical replicates overlap by only 35-60% with the complexity of the sample not having any tangible effect on peptide hit reproducibility[178]. This inherent incomprehensiveness of tandem mass spectrometry leads to heightened sensitivity to other parameters affecting the repeatability of experiments and has become one of the most important technical borders for researchers to push at. While increasing the number of technical and biological replicates thus certainly helps increasing overlaps and quality of identifications and quantifications, experimental shotgun setups as sophisticated as the ones presented here hamper these efforts by requiring multiple overlaps between multiple experiments. In addition to the sources of systematic error described before, sample preparation, processing and evaluation of one experiment to decide on our next steps usually costs a large amount of money and time, thereby inevitably introducing fluctuations in device performance and environmental factors as well. This emphasises the increasing importance of considerate experimental design, proper execution and validation of this kind of stochiometric data, as it was done in out study, to be able to trust and replicate results. Our research group has been working on projects investigating the HOG response using tandem mass spectrometry shotgun approaches for over 10 years and we thus have a large amount

of data at our disposal, with increasingly improved methods to achieve higher reproducibility. According to the evaluation of intralaboratory repeatability between experiments (technical and biological replicates) that has been conducted by Natalie Romanov during her Master's thesis, the collected data are highly reproducible with ratio correlation coefficients of 0.7-0.9 (Natalie Romanov, "Screening for novel targets of the MAPK Hog1 using quantitative proteomics"), providing us with a highly stable and ample dataset for further bioinformatical analysis. As of today, we analyse raw MS data using the commonly used quantification software MaxQuant, while earlier studies, including Romanov *et al.* (Appendix X.1), have been conducted using the also commonly used software Proteome Discoverer. Since both softwares use different algorithms and processing pipelines to identify and quantify peptides from raw mass spectrometry data, I wondered what our results would look like if I was analysing the same raw MS data with either one of the softwares. As described in chapter VI.4, I was indeed able to extend the list of putative Hog1-targets using MaxQuant as a second quantification software and give better claim to previously ambiguous hints. I was also intrigued by the fact that different bioinformatic analyses seem to constitute a similar range of individuality as a biological replicate, as the overlap between peptide hits quantified by either software amounts to an average of 35.6% and the overlap between proteins reaches almost 59.7%. Ratios in the overlap were again highly correlative (R = 0.7-0.9), indicating that individual phosphorylation site quantifications from either software can be considered valid MS shotgun data. In the end, I found 13 proteins harbouring Hog1-dependent S/TP sites that were not covered in the PD analysis. These proteins (with the exception of the published Hog1 interactors Nup2 and Pan1[46,155]) are currently validated using the M-Track protein-protein-proximity assay (Gina Varnavides, work in progress, data not shown). Preliminary results already show that we will be able to extend the substrate candidate list that has been published in Romanov *et al.* (Appendix X.1), emphasising how bioinformatical processing of raw data with different quantification softwares is a valuable tool to exploit the hidden potential for higher comprehensiveness of MS shotguns.

Two proteins, however, sparked my interest specifically, namely the PAK/Ste20 family protein kinase Kic1 and Orm2, which mediates sphingolipid homeostasis together with its paralog Orm1. According to preliminary protein-proximity data by Gina Varnavides, both proteins can be validated by a positive M-Track signal. Kic1 has already been characterised as essential kinase of the highly conserved centrin homolog Cdc31 and regulator of spindle pole body duplication and cell wall integrity in the late 1990ies, but since then only a small number of studies regarding this protein have been conducted. While the CWI pathway and its key regulator MAPK Slt2 are actively inhibited by Hog1 upon a hyperosmotic stress situation (chapter II.4), our study showed factors functionally annotated with cell polarity and budding site establishment, cell morphology, and membrane organisation to be enriched in the entire field 1 and even in the presumably directly Hog1-dependent set of substrates. In chapter VI.2, I investigated downstream kinases of Rck2, indeed confirming that these processes are highly represented within the set of proteins harbouring R/KxxS/T and thus potentially directly Rck2-dependent phosphorylation sites, suggesting an Rck2-regulated interface between HOG signalling and CWI/cell polarity/morphology related processes. Notably, Kic1 harbours not only directly Hog1-dependent non-catalytic sites T625 and T1073, but also a field 1 R/KxxS/T motif (S511). This site hasn't been characterised at all so far, but also hasn't been covered in setup *rck2*Δ unfortunately. Nevertheless, with the field 1 list according to MQ yielding Kic1 (and also Sog2), as putative direct substrate of Hog1, I additionally provide indication of an interconnection between direct HOG signalling and the RAM signalling network[179]. This raises the question if non-catalytic phosphorylation of thusly related factors is assisting in crosstalk prevention between the HOG-pathway and signalling cascades preparing cells to cell wall straining situations like proliferation, mating, and hypoosmotic stress processing. Another evidence for this hypothesis could be the finding that *KIC1* and *PBS2* expression levels (Pbs2 = MAPKK upstream of Hog1) seem to have anticorrelating effects on cell wall stability[180]. Alternatively, Hog1 targeting factors like Kic1 (and Sog2), thereby interconnecting direct HOG signalling with a virtually independent process (i.e, RAM-signalling), is curiously

reminiscent of its direct action on proteins that establish links to carbon metabolism and cell cycle. Reportedly, Hog1 induces a G1 cell cycle arrest upon hyperosmotic conditions via activation of cyclin dependent kinase inhibitors (CKI) Sic1 and Cip1[45,181,182], and it directly affects a range of metabolic processes supporting and influencing cell cycle arrest and release. An example for this is the neutral trehalase Nth1 which degrades stored trehalose to be accessible for active carbohydrate metabolism at G1/S transition[183] and which we could validate as a direct substrate of Hog1 in Romanov *et al.* (Appendix X.1). Therefore, assuming Hog1 has an active role in the effects of metabolism and cell cycle progression on each other, and taking into account literature that connects membrane perturbation to cell cycle arrest[184], it would stand to reason that cell wall integrity in terms of cell polarisation and budding is directly affected by HOG signalling as well.

This new evidence of Hog1 directly co-regulating virtually independent cellular processes that are nevertheless essential for osmotic adaptation also sparked my interest in Orm2 and its paralog Orm1. These ER membrane proteins that have only been characterised and become targets of thorough investigation a few years ago are conserved from yeast to humans (ORMDL genes) and crucial to sphingolipid homoeostasis[185–187]. They exert their function by inhibiting the first and rate-limiting step of sphingolipid biosynthesis via interaction with serine palmitoyl coenzyme A transferase (SPT), but become heavily phosphorylated and inhibited themselves upon compromised sphingolipid synthesis. This process integrates various signals and is mediated by sphingolipid levels that are responsive to ER and heat stress. Also, sphingolipid homoeostasis is subject to a sensor- and feedback loop provided by TORC2-dependent phosphorylation of a kinase module consisting of Ser/Thr-kinases Pkh1 and subsequently Ypk1. In turn, Ypk1 is known to i) regulate components of the CWI pathway[188] and ii) have its phosphorylation counteracted by phosphatase PP2A[109,189]. Both of these aspects have been mentioned earlier in this chapter and other chapters in the context of HOG signalling. This includes the Ypk1-dependent phosphorylation of Hog1-interaction partner Fps1[108] introduced in chapter IV.4, which provides yet another connection between Ypk1- and

HOG signalling. Indeed, while TOR-dependent site T662 and Pkh1-dependent site T504 of Ypk1 were not covered in either our PD or MQ analysis, I found several known but uncharacterised phosphorylation sites in close proximity to these sites (and as well at the N-terminal end of Ypk1) to be downregulated in setup SR (Supplemental Table 1, adapted from Romanov *et al.*, Supplemental Table S2). Interestingly, although the relevant phosphorylation sites for Ypk1 interaction are also not covered in our datasets, we found Ser/Thr-kinase Fpk1, a downstream target that also phosphorylates and inhibits Ypk1, among the Rck2-dependent kinases (chapter VII.2). Equally interesting, the PKA/PKG/PKC (AGC) family protein kinase Sch9, known interactor of Hog1[133] and shown to be one of the presumable downstream effector kinases of Rck2 (chapter VII.2), is also targeted by Pkh1/2 and activated by phytosphingosine together with Ypk1[134,190]. Ultimately, this proposed Pkh1/2-Ypk1-Sch9 network might also be relevant when considering the endocytosis, vesicle-/vacuole-related and starvation-signalling-related GO-terms enriched in the Hog1-Rck2-network (Romanov *et al.,* Fig 2E and Fig. 6), as it is also targeted by TORC1-signalling (together with Snf1) and might establish additional connections from HOG signalling to even more distantly related processes like nutritional stress, oxidative stress and CO2-sensing[191–193].

In conclusion, my thesis is clearly able to show that today's sophisticated proteomics and computational methods enable us to extract increasingly complex network data even from a pathway as well-characterised and thoroughly studied as the HOG-pathway. Romanov *et al.* (Appendix X.1) is to our knowledge the most comprehensive study investigating direct and indirect substrates of Hog1 that has been conducted so far, and the work presented here shows that pushing the frontiers not only technically but also bioinformatically is a valid approach to increase the comprehensiveness of quantitative MS shotguns. It remains to be decided which of the many leads provided by a catalogical study like Romanov *et al.* (Appendix X.1) and the follow-up manuscript covering the combination and comparison of PD and MQ softwares will be followed up.

VIII. Materials & Methods

Disclaimer:

The following materials and methods are exclusively described in Appendix X.1:

- Strains, sample preparation, and processing of MS-shotgun setups SR, I+0'S, I+5'S, I+10'S
- Bioinformatic parameters and processing of MS-shotgun data using Proteome Discoverer
- M-Track validation performed for putative Hog1-substrates

VIII.1. Yeast strains / Plasmids

Standard methods for genetic manipulation were used. Plasmids used for strain construction are listed in Table VI.9.i. Table VI.9.ii summarizes all strains used in the MS-shotgun setups HKi and *rck2*Δ and for osmosensitivity testing. Construction of SILAC strains used in this thesis for MS-shotguns was performed as follows: Hog1 wildtype SILAC strains (WR209, WR 210) were obtained by crossing as described in Reiter *et al.*[155]. Hog1as SILAC strains (WR557, WR564) were obtained by crossing as described in Romanov *et al.* (Appendix X.1, Supplemental Material, Yeast strain and plasmid construction). Hog1as *kss1*Δ SILAC and Hog1 wildtype *rck2*Δ SILAC strains (MJ043, MJ243) were obtained by transforming Hog1as SILAC strain WR557 with a *KSS1*-deletion cassette, respectively Hog1 wildtype SILAC strain WR209 with an *RCK2*-deletion cassette. Cloning was performed analogously to deletion mutants described below. Construction of deletion mutants used for osmosensitivity testing was performed by replacing the ORF of the respective gene to be deleted in Hog1 wildtype strain WR557 with a deletion cassette carrying a HIS3-marker by homologous recombination after transformation as described in Reiter *et al*. and earlier[155,194–196]. Deletion cassettes were cloned from plasmid pGA2260 using primer annealing sequences 5'-tcc ggt tct gct gct ag-3'

and 5'-cct cga gga cag aag ac-3' and 53bp homologous recombination sites ~200-500bp upstream and downstream of the respective gene. Construction of strains for M-Track assays was performed as follows: Hog1-H3-HA HKMT(-) M-Track strains (WR1242, WR1249) were obtained from transformation and backcrossing as described in Romanov *et al*. (Appendix X.1, Supplemental Material, Yeast strain and plasmid construction). Hog1-H3-HA M-Track strains carrying the respective C-terminally HKMT-tagged candidate gene were obtained by transforming WR1242 and WR1249 with a myc-HKMT tagging cassette[67] which was cloned from plasmid pJA31, a modified version of plasmid pCK900 (unpublished material, kindly provided by Jillian Augustine-Rubak), using primers designed with the same primer annealing sequences used for the aforementioned deletion mutants and 53bp homologous recombination sites directly upstream of the respective gene's ORF's stop codon and ~50-100 bp downstream of the stop codon[103,195]. Hog1-H3-HA M-Track strains carrying the respective N-terminally HKMT-tagged candidate gene were obtained as described for C-terminally tagged candidate gene strains with 53bp homologous recombination sites ~50-100bp upstream of and in frame with the gene's start codon.

VIII.2. Growth Conditions

For MS-shotgun experiments, cultures were inoculated in synthetic SILAC medium (2% yeast nitrogen base, 2% glucose, amino acids as required, excluding auxotrophic markers according to genetical setup and $^{12}C/^{13}C$-labelling amino acids arginine and lysine). SILAC labelling[127]: Experimental and control samples were differing only in regard to ^{13}C-labelled arginine (0.05mg/mL of L-arginine-HCl, Eurisotop) and ^{13}C-labelled lysine (0.05mg/mL of L-lysine-2HCl, Eurisotop). ^{12}C-Proline (L-Proline, Eurisotop) was added in excess to minimize arginine-to-proline-conversion. For western blots, cultures were inoculated in YEPD full medium (1% yeast extract, 2% peptone, 2% glucose, amino acids as required, excluding auxotrophic markers according to genetical setup). Cells were grown shaking at 30°C (200rpm) for at least seven

generations to mid-log phase (OD_{600nm} ~1) and then exposed to experimental/control conditions. Conditions for growth assays are described in Romanov *et al.* (Appendix X.1, Materials & Methods, Growth tests).

VIII.3. Experimental/control conditions for MS-shotgun experiments

Setup HKi: Inhibitor (1-isopropyl-3-(phenylethynyl)-1H-pyrazolo[3,4-d]pyrimidin-4-amine, called SPP68) - a gift from M. Grøtli at the University of Gothenburg - was added 10' prior to stress treatment at a final concentration of 5µM in DMSO to both, experimental (W303 Hog1as *kss1*Δ) and control (W303 Hog1as *kss1*Δ) sample identically. The inhibitor ensures full inactivation of kinase activity at the Hog1*as* allele used in this experiment by binding in vicinity to the ATP-binding pocket in the kinase cleft and prohibiting ATP-binding[128]. The experimental sample was then treated with NaCl at a final concentration of 0.5M for 5', the control sample was mock-treated with isotonic medium. Setup *rck2*Δ: Both experimental (W303 *rck2*Δ) and control (W303 wildtype) sample were treated with NaCl at a final concentration of 0.5M for 5'.

VIII.4. Protein purification, phosphopeptide enrichment and MS analysis

HKi and *rck2*Δ: MS shotgun experiments were performed identically to setups SR, I+0'S, I+5'S, and I+10'S, as described in Romanov *et al*. (Appendix X.1) and earlier[155]. After harvesting cells by filtration and cell breakage by bead-beating in a FastPrep®-24 device (MP Biomedicals), a TRIzol (Invitrogen) protocol[197] was used to extract proteins which were then resuspended in ABC-urea buffer (50mM ammonium bicarbonate (ABC), 8M urea). Samples were incubated for 30' at 56°C with dithiothreitol (DTT) in a 1:50 DTT-protein ratio for Cysteine bridge reduction and subsequently treated with iodoacetamide (IAA) in a 1:10 IAA to protein ration for Cysteine alkylation. After a 30' incubation step at room temperature in the dark, IAA was quenched with DTT (1:100 DTT to protein ratio) and after dilution of the buffer to 6M urea with 50mM ABC extracts were digested in two steps using LysC (Roche, 2h, 30°C, 1:100 LysC to protein ratio)

and Trypsin Gold (Promega, overnight, 37°C, 1:60 trypsin to protein ratio). After stopping the overnight digest with trifluoric acid (TCA, final conc. 1%), and desalting on Sep-Pak tC18 cartridges (Waters, tC18 3cc Vac Cartridge, 200mg), samples were eluted using acetonitrile (ACN, 70%) and formic acid (FA, 0.1%). For whole cell extract MS measurements, and aliquot of approximately 1µg of protein was used (final ACN conc. ≤ 2%, diluted with 0.1% TFA). Sample storage: snap-freeze in liquid nitrogen, lyophilised, storage at -80°C.

Lyophilised whole cell extracs were dissolved in 100µL TiO_2 loading buffer (0.8M phtalic acid, 80% ACN, 0.1% TFA) and then enriched for phosphopeptides using TiO_2-beads (Titansphere bulk media, 5micron, GL Science)[198,199] that have been equilibrated with 50% methanol (MeOH), H_2O and TiO_2 buffer). After incubation (1h, room temperature) with TiO_2 beads in a 1:2.8 TiO_2 to protein ratio, beads were washed in 3x2 steps, starting with loading buffer, then 80% ACN / 0.1% TFA, and finally with 1% ACN / 0.1% TFA and bound phosphopeptides were eluted using 0.3M ammonium hydroxide. After acidification (pH 2.5) using 10% TFA, desalting, MS measuremenat of an aliquot (1% of eluted post-TiO_2 sample) and sample storage was performed as described earlier. Fractionation of post-TiO_2 samples was performed offline using strong cation exchange chromatography (SCX)[200], with fractions being taken every minute after the flowthrough (~minutes 0-10) and pooled into 12 samples according to phosphopeptide content (see Master's thesis of Natalie Romanov for detailed analysis of phosphopeptide content). For the quantitative analysis of all MS experiments, samples were separated on an reversed-phase high-performance liquid chromatography (rp-HPLC) column (Ultimate 3000 RSLC nano-flow, Thermo Fisher) coupled to a Linear Trap Quadropole Orbitrap Velos (collision-induced dissociation mode), or a Q Exactive HF Orbitrap (higher-energy collisional dissociation mode) mass spectrometer (Thermo Fisher) with an electrospray ionisation interface (nanospray flex ion source, Proxeon Biosystems) between rp-HPLC and MS (data-dependent mode). Settings chosen for rp-HPLC and MS acquisition as well as parameters chosen for the Proteome Discoverer 1.3 and 1.4 analysis are described in are described in Reiter, Anrather *et al.* and Romanov *et al.* (Appendix X.1), and available online in the

Proteomics Identifications (PRIDE) database in datasets PXD004294 to PXD004300. Forward and reverse decoy searches were performed with an FDR of ≤ 1% for peptides and proteins. Affinity-purified proteins were analysed as described previously[155].

VIII.5. MaxQuant analysis and computational processing of SILAC ratios

For raw MS data analysis, default parameters of the quantification software MaxQuant (version 1.5.2.8)[149,150] were used, with the following exceptions: As database to be searched for matching MS2 spectra, the Saccharomyces Genome Database (SGD) all-ORF protein database FASTA file (version February 2011) was used and combined with the MaxQuant common laboratory contaminants database. Maximum number of missed cleavages (enzyme specificity “Trypsin/P”) was set to 2, leucine and isoleucine were treated as one virtual amino acid (activated “I=L” setting). N-terminal acetylation, Deamidation, Oxidation of Methionine, and Phosphorylation on Serine, Threonine and Tyrosin (in the case of post-TiO_2/fractionated samples) were set as variable modifications, whereas carbamidomethylathion of Cysteine was set as fixed modification. ‘Mulitplicity’ of 2 for the SILAC quantification and heavy labels (‘Arg6’, ‘Lys6’) were specified, ‘Requantify’ was activated. In the course of computational processing (Python, version 2.7, scripts by David Hollenstein) of MaxQuant results, SILAC ratios were log2-transformed after extraction from the MaxQuant evidence table (column ‘Ratio H/L’) and corrected in regard to the amount of heavy and light labelled cells present in the sample (visible by the distribution of heavy and light labelled non-phosphopeptides). Heavy labelled arginine-to-proline conversion had been minimised by excess addition of ^{12}C -Proline, any residual signal loss was compensated as follows: Non-phosphopeptides that don’t contain Proline were used as a reference to calculate normalisation factors for every replicate and experiment by substracting the average log2-ratio of the reference set from the log2-ratio of every phosphopeptide and non-phosphopeptide individually. To correct for Proline conversion, the average log2 ratio of non-phosphopeptides containing a single proline was defined as

conversion factor. This factor was multiplied by the number of prolines contained in the peptide sequence and substracted from the log2 ratio individually as well. Phosphopeptides were filtered for probability of correct phosphorylation site assignment higher than 70% and grouped by phosphorylated residues. Thereby, phosphorylation site entries with an average log 2 ratio of all respective phosphopeptide entries in the evidence table were created.

VIII.6. GO enrichment analysis and semantic clustering

For GO-term enrichment, sets of proteins were analysed by online Functional Annotation Enrichment Tool DAVID. Level 4 GO-terms of biological processes were extracted, numbers of proteins per GO-term and fold change of enrichment against the background of the full *S. cerevisae* proteome was extracted and during post-processing either analysed in their entirety (for small protein sets with less than 30 entries) or subjected to a fold change cut-off of $p \leq 0.05$ to filter for significantly enriched processes. GO-terms were then clustered using the online tool REVIGO as follows: all GO terms depicted in Fig. 14 and Fig. 20 were combined with their respectively highest fold change obtained by either one of the analysed protein sets. This value was passed to REVIGO as semantic relevance score for each GO-term, using the 'higher is better' option, to ensure retention of the most relevant GO-term semantics (for example: 'actin cortical patch assembly' with a maximum fold change in any analysed protein set of 14.6 has a higher relevance than 'actin cytoskeleton organisation' with a maximum fold change in any analysed protein set of 3.6). The GO-term database size was set to *S. cerevisiae,* the 'allowed similarity' parameter for the SimRel algorithm was set to 0.7 (medium compression).

VIII.7. Growth assay, serial dilution droplet tests and scoring system

Growth assays, serial dilution droplet tests and scoring system were developed and performed exactly as described in Romanov et al (Appendix X.1).

VIII.8. Protein extracts: SDS-PAGE and Western blot conditions

For detection of Kss1- and Hog1-phosphorylation, whole cell extracts in urea lysis buffer (8M urea, 0.3M NaCl, 50mMTris/HCl pH 8, 50mM Na_2HPO_4/NaH_2PO_4 pH 6.8, 0.5% Nonident P40) were mixed 1:1 with 2X Laemmli buffer (1M Tris-HCl pH 6.8, 10% SDS, 10% Glycerol, 1M DTT) and loaded on 12% SDS-PAGE gels (1.5 mm). Proteins were separated for 1-2h (30mA/gel, unlimited Volts) and then transferred electrophoretically on nitrocellulose membranes (pore diameter: 0.2µm) at 4°C for either 4h (350mA/~50cm²) or overnight (500mA/~200cm²). Membranes were subjected to 5' of Ponceau staining (Ponceau S solution, SigmaAldrich, 1mg/ml in 1% TCA) and washed with H_2O to assess transfer efficiency and reproducibility. Membranes were then blocked with 5% skim milk in 1X phosphate-buffered saline (Na_2HPO_4/NaH_2PO_4, pH = 7.4), containing 0.05% Tween20 (PBS-T) for 1h or overnight, and incubated with primary antibody diluted 1:3000 in 1% skim milk in PBS-T. For analysis, membranes were incubated with either rabbit-raised anti-Phospho-p42/44 (Cell Signaling, Antibody #4370) for Kss1-phosphorylation or rabbit-raised anti-Phospho-p38 (Cell Signaling, Antibody #9215) for Hog1-phosphorylation for 1h at 4°C. After three consecutive 10' washing steps with PBS-T, membranes were incubated with secondary anti-rabbit antibody (Jackson Immunoresearch Laboratories Inc Peroxidase-conjugated AffiniPure goat-raised anti-rabbit IgG #111-035-008), again washed 3 times with PBS-T and developed at different exposures on Fuji RX-N X-ray film after being subjected to SuperSignal™ West Pico PLUS Chemiluminescent Substrate (Thermo Scientific).

VIII.9. Tables

Name	Description	Reference
pCK900	Integrative mycHKMT tag, LEU2	Brezowich et al. 2015 (99)
pCK902	Integrative TEV–protA–H3HA tag, URA3	Brezowich et al. 2015 (99)
pGA2260	Integrative His3MX6 (equivalent to pFA6aHis3MX)	Knop et el. 1999 (154)

Table VI.9.i: Plasmids used in this thesis

Name	Background	Genotype	Reference
WR209	W303, Mat a	*lys1::kanMX arg4::kanMX CAN1 leu2-3,112 trp1-1 ura3-1 ade2-1 his3-11,15*	Reiter et al. (119)
WR210	W303, Mat α	*lys1::kanMX arg4::kanMX CAN1 leu2-3,112 trp1-1 ura3-1 ade2-1 his3-11,15*	Reiter et al. (119)
WR557	W303, Mat a	*HOG1as lys1::kanMX arg4::kanMX CAN1 leu2-3,112 trp1-1 ura3-1 ade2-1 his3-11,23*	Romanov et al. (56)
WR564	W303, Mat α	*HOG1as lys1::kanMX arg4::kanMX CAN1 leu2-3,112 trp1-1 ura3-1 ade2-1 his3-11,23*	Romanov et al. (56)
MJ043	W303, Mat a	*kss1::HIS3 HOG1as lys1::kanMX arg4::kanMX CAN1 leu2-3,112 trp1-1 ura3-1 ade2-1 his3-11,23*	Romanov et al. (56)
MJ243	W303, Mat a	*rck2::HIS3 lys1::kanMX arg4::kanMX CAN1 leu2-3,112 trp1-1 ura3-1 ade2-1 his3-11,23*	Romanov et al. (56)
WR1242	S288c, Mat a	*HOG1-TEV-ProteinA-Histone3-HA-URA3 his3Δ1 leu2Δ0 met15Δ0 ura3Δ0*	Romanov et al. (56)
WR1249	S288c, Mat α	*HOG1-TEV-ProteinA-Histone3-HA-URA3 his3Δ1 leu2Δ0 lys1Δ0 ura3Δ0*	Romanov et al. (56)
WR1288	S288c, Mat a	*NUP2-myc-HKMT-LEU2 HOG1-TEV-ProteinA-Histone3-HA-URA3 his3Δ1 leu2Δ0 met15Δ0 ura3Δ0*	Romanov et al. (56)
WR1627	S288c, Mat a	*NUP2-myc-HKMT-LEU2 HOG1-TEV-ProteinA-Histone3-HA-URA3 his3Δ1 leu2Δ0 met15Δ0 ura3Δ0*	Romanov et al. (56)
MJ050	W303 Mat a	*akl1::HIS3 leu2-3,112 trp1-1 ura3-1 ade2-1 his3-11,23*	Romanov et al. (56)
MJ052	W303 Mat a	*ent3::HIS3 leu2-3,112 trp1-1 ura3-1 ade2-1 his3-11,23*	Romanov et al. (56)
MJ054	W303 Mat a	*nth1::HIS3 leu2-3,112 trp1-1 ura3-1 ade2-1 his3-11,23*	Romanov et al. (56)
MJ067	W303 Mat a	*art5::HIS3 leu2-3,112 trp1-1 ura3-1 ade2-1 his3-11,23*	Romanov et al. (56)
MJ069	W303 Mat a	*ask10::HIS3 leu2-3,112 trp1-1 ura3-1 ade2-1 his3-11,23*	Romanov et al. (56)
MJ071	W303 Mat a	*hal5::HIS3 leu2-3,112 trp1-1 ura3-1 ade2-1 his3-11,23*	Romanov et al. (56)
MJ073	W303 Mat a	*ptk2::HIS3 leu2-3,112 trp1-1 ura3-1 ade2-1 his3-11,23*	Romanov et al. (56)
MJ075	W303 Mat a	*reg1::HIS3 leu2-3,112 trp1-1 ura3-1 ade2-1 his3-11,23*	Romanov et al. (56)
MJ077	W303 Mat a	*sfl1::HIS3 leu2-3,112 trp1-1 ura3-1 ade2-1 his3-11,23*	Romanov et al. (56)
MJ079	W303 Mat a	*spt20::HIS3 leu2-3,112 trp1-1 ura3-1 ade2-1 his3-11,23*	Romanov et al. (56)
MJ081	W303 Mat a	*tod6::HIS3 leu2-3,112 trp1-1 ura3-1 ade2-1 his3-11,23*	Romanov et al. (56)
MJ083	W303 Mat a	*tsl1::HIS3 leu2-3,112 trp1-1 ura3-1 ade2-1 his3-11,23*	Romanov et al. (56)
MJ085	W303 Mat a	*vps9::HIS3 leu2-3,112 trp1-1 ura3-1 ade2-1 his3-11,23*	Romanov et al. (56)
MJ093	W303 Mat a	*are2::HIS3 leu2-3,112 trp1-1 ura3-1 ade2-1 his3-11,23*	Romanov et al. (56)
MJ095	W303 Mat a	*boi1::HIS3 leu2-3,112 trp1-1 ura3-1 ade2-1 his3-11,23*	Romanov et al. (56)
MJ097	W303 Mat a	*bul1::HIS3 leu2-3,112 trp1-1 ura3-1 ade2-1 his3-11,23*	Romanov et al. (56)
MJ099	W303 Mat a	*gip3::HIS3 leu2-3,112 trp1-1 ura3-1 ade2-1 his3-11,23*	Romanov et al. (56)
MJ101	W303 Mat a	*hot1::HIS3 leu2-3,112 trp1-1 ura3-1 ade2-1 his3-11,23*	Romanov et al. (56)
MJ103	W303 Mat a	*ppz1::HIS3 leu2-3,112 trp1-1 ura3-1 ade2-1 his3-11,23*	Romanov et al. (56)
MJ105	W303 Mat a	*ppz2::HIS3 leu2-3,112 trp1-1 ura3-1 ade2-1 his3-11,23*	Romanov et al. (56)
MJ107	W303 Mat a	*sko1::HIS3 leu2-3,112 trp1-1 ura3-1 ade2-1 his3-11,23*	Romanov et al. (56)
MJ109	W303 Mat a	*ylr257w::HIS3 leu2-3,112 trp1-1 ura3-1 ade2-1 his3-11,23*	Romanov et al. (56)
MJ111	W303 Mat a	*ylm081w::HIS3 leu2-3,112 trp1-1 ura3-1 ade2-1 his3-11,23*	Romanov et al. (56)
MJ115	W303 Mat a	*aim21::HIS3 leu2-3,112 trp1-1 ura3-1 ade2-1 his3-11,23*	Romanov et al. (56)
MJ117	W303 Mat a	*get2::HIS3 leu2-3,112 trp1-1 ura3-1 ade2-1 his3-11,23*	Romanov et al. (56)
MJ119	W303 Mat a	*rck2::HIS3 leu2-3,112 trp1-1 ura3-1 ade2-1 his3-11,23*	Romanov et al. (56)
MJ121	W303 Mat a	*rgc1::HIS3 leu2-3,112 trp1-1 ura3-1 ade2-1 his3-11,23*	Romanov et al. (56)
MJ123	W303 Mat a	*rod1::HIS3 leu2-3,112 trp1-1 ura3-1 ade2-1 his3-11,23*	Romanov et al. (56)
MJ125	W303 Mat a	*skg6::HIS3 leu2-3,112 trp1-1 ura3-1 ade2-1 his3-11,23*	Romanov et al. (56)
MJ127	W303 Mat a	*ssk2::HIS3 leu2-3,112 trp1-1 ura3-1 ade2-1 his3-11,23*	Romanov et al. (56)
MJ132	W303 Mat a	*bck1::HIS3 leu2-3,112 trp1-1 ura3-1 ade2-1 his3-11,23*	Romanov et al. (56)
MJ134	W303 Mat a	*bck2::HIS3 leu2-3,112 trp1-1 ura3-1 ade2-1 his3-11,23*	Romanov et al. (56)
MJ136	W303 Mat a	*chs5::HIS3 leu2-3,112 trp1-1 ura3-1 ade2-1 his3-11,23*	Romanov et al. (56)
MJ138	W303 Mat a	*nup2::HIS3 leu2-3,112 trp1-1 ura3-1 ade2-1 his3-11,23*	Romanov et al. (56)
MJ140	W303 Mat a	*tif4632::HIS3 leu2-3,112 trp1-1 ura3-1 ade2-1 his3-11,23*	Romanov et al. (56)
MJ142	W303 Mat a	*ymr124w::HIS3 leu2-3,112 trp1-1 ura3-1 ade2-1 his3-11,23*	Romanov et al. (56)
MJ187	W303 Mat a	*dot6::HIS3 leu2-3,112 trp1-1 ura3-1 ade2-1 his3-11,23*	Romanov et al. (56)
MJ189	W303 Mat a	*ede1::HIS3 leu2-3,112 trp1-1 ura3-1 ade2-1 his3-11,23*	Romanov et al. (56)
MJ191	W303 Mat a	*gal11::HIS3 leu2-3,112 trp1-1 ura3-1 ade2-1 his3-11,23*	Romanov et al. (56)
MJ193	W303 Mat a	*nha1::HIS3 leu2-3,112 trp1-1 ura3-1 ade2-1 his3-11,23*	Romanov et al. (56)
MJ197	W303 Mat a	*rim15::HIS3 leu2-3,112 trp1-1 ura3-1 ade2-1 his3-11,23*	Romanov et al. (56)
MJ199	W303 Mat a	*rph1::HIS3 leu2-3,112 trp1-1 ura3-1 ade2-1 his3-11,23*	Romanov et al. (56)
MJ200	W303 Mat a	*vas1::HIS3 leu2-3,112 trp1-1 ura3-1 ade2-1 his3-11,23*	Romanov et al. (56)
MJ202	W303 Mat a	*vps53::HIS3 leu2-3,112 trp1-1 ura3-1 ade2-1 his3-11,23*	Romanov et al. (56)

Table VI.9.ii: Yeast Strains used in this thesis

IX. References

1. Garcia, J. dos S., Dalmolin, Â. C., França, M. G. C. & Mangabeira, P. A. O. Different salt concentrations induce alterations both in photosynthetic parameters and salt gland activity in leaves of the mangrove Avicennia schaueriana. *Ecotoxicol. Environ. Saf.* **141,** 70–74 (2017).
2. Cornick, S., Tawiah, A. & Chadee, K. Roles and regulation of the mucus barrier in the gut. *Tissue barriers* **3,** e982426 (2015).
3. Charles Edward Marshall. *Microbiology: A Text-Book of Microorganisms, General and Applied, p. 420*. (1912).
4. Gervais, P. & Beney, L. Osmotic mass transfer in the yeast Saccharomyces cerevisiae. *Cell. Mol. Biol. (Noisy-le-grand).* **47,** 831–9 (2001).
5. Schaber, J. & Klipp, E. Short-term volume and turgor regulation in yeast. *Essays Biochem.* **45,** 147–59 (2008).
6. Hohmann, S. Osmotic stress signaling and osmoadaptation in yeasts. *Microbiol. Mol. Biol. Rev.* **66,** 300–72 (2002).
7. Saito, H. & Posas, F. Response to Hyperosmotic Stress. *Genetics* **192,** 289–318 (2012).
8. Brewster, J. L., de Valoir, T., Dwyer, N. D., Winter, E. & Gustin, M. C. An osmosensing signal transduction pathway in yeast. *Science* **259,** 1760–3 (1993).
9. Brewster, J. L. & Gustin, M. C. Hog1: 20 years of discovery and impact. *Sci. Signal.* **7,** re7-re7 (2014).
10. Chen, Z. *et al.* MAP kinases. *Chem. Rev.* **101,** 2449–76 (2001).
11. Ray, L. B. & Sturgill, T. W. Characterization of insulin-stimulated microtubule-associated protein kinase. Rapid isolation and stabilization of a novel serine/threonine kinase from 3T3-L1 cells. *J. Biol. Chem.* **263,** 12721–7 (1988).
12. Widmann, C., Gibson, S., Jarpe, M. B. & Johnson, G. L. Mitogen-activated protein kinase: conservation of a three-kinase module from yeast to human. *Physiol. Rev.* **79,** 143–80 (1999).
13. Chen, R. E. & Thorner, J. Function and regulation in MAPK signaling pathways: lessons learned from the yeast Saccharomyces cerevisiae. *Biochim. Biophys. Acta* **1773,** 1311–40 (2007).
14. Cargnello, M. & Roux, P. P. Activation and function of the MAPKs and their substrates, the MAPK-activated protein kinases. *Microbiol. Mol. Biol. Rev.* **75,** 50–83 (2011).
15. Davenport, K. R., Sohaskey, M., Kamada, Y., Levin, D. E. & Gustin, M. C. A second osmosensing signal transduction pathway in yeast. Hypotonic shock activates the PKC1 protein kinase-regulated cell integrity pathway. *J. Biol. Chem.* **270,** 30157–61 (1995).
16. Martín, H., Rodríguez-Pachón, J. M., Ruiz, C., Nombela, C. & Molina, M. Regulatory mechanisms for modulation of signaling through the cell integrity Slt2-mediated pathway in Saccharomyces cerevisiae. *J. Biol. Chem.* **275,** 1511–9 (2000).
17. Krisak, L. *et al.* SMK1, a developmentally regulated MAP kinase, is required for spore wall assembly in Saccharomyces cerevisiae. *Genes Dev.* **8,** 2151–61 (1994).
18. Chu, S. *et al.* The transcriptional program of sporulation in budding yeast. *Science* **282,** 699–705 (1998).
19. Courchesne, W. E., Kunisawa, R. & Thorner, J. A putative protein kinase overcomes pheromone-induced arrest of cell cycling in S. cerevisiae. *Cell* **58,** 1107–19 (1989).
20. Elion, E. A., Grisafi, P. L. & Fink, G. R. FUS3 encodes a cdc2+/CDC28-related kinase required for the transition from mitosis into conjugation. *Cell* **60,** 649–64 (1990).
21. Cook, J. G., Bardwell, L., Kron, S. J. & Thorner, J. Two novel targets of the MAP kinase Kss1 are negative regulators of invasive growth in the yeast Saccharomyces cerevisiae. *Genes Dev.* **10,** 2831–48 (1996).
22. Tedford, K., Kim, S., Sa, D., Stevens, K. & Tyers, M. Regulation of the mating pheromone and invasive growth responses in yeast by two MAP kinase substrates. *Curr. Biol.* **7,** 228–38 (1997).
23. Han, J., Lee, J. D., Bibbs, L. & Ulevitch, R. J. A MAP kinase targeted by endotoxin and hyperosmolarity in mammalian cells. *Science* **265,** 808–11 (1994).
24. Sheikh-Hamad, D. & Gustin, M. C. MAP kinases and the adaptive response to hypertonicity: functional preservation from yeast to mammals. *Am. J. Physiol. Renal Physiol.* **287,** F1102-10 (2004).
25. ZARUBIN, T. & HAN, J. Activation and signaling of the p38 MAP kinase pathway. *Cell Res.* **15,** 11–18 (2005).
26. Cuadrado, A. & Nebreda, A. R. Mechanisms and functions of p38 MAPK signalling. *Biochem. J.* **429,** 403–417 (2010).
27. Posas, F. *et al.* Yeast HOG1 MAP kinase cascade is regulated by a multistep phosphorelay mechanism in the SLN1-YPD1-SSK1 'two-component' osmosensor. *Cell* **86,** 865–875 (1996).
28. Reiser, V., Raitt, D. C. & Saito, H. Yeast osmosensor Sln1 and plant cytokinin receptor Cre1 respond to changes in turgor pressure. *J. Cell Biol.* **161,** 1035–1040 (2003).
29. Hao, N., Zeng, Y., Elston, T. C. & Dohlman, H. G. Control of MAPK specificity by feedback phosphorylation of shared adaptor protein Ste50. *J. Biol. Chem.* **283,** 33798–802 (2008).
30. Yamamoto, K., Tatebayashi, K., Tanaka, K. & Saito, H. Dynamic Control of Yeast MAP Kinase Network by Induced Association and Dissociation between the Ste50 Scaffold and the Opy2 Membrane Anchor. *Mol. Cell* **40,** 87–98 (2010).
31. Posas, F. & Saito, H. Osmotic activation of the HOG MAPK pathway via Ste11p MAPKKK: scaffold role of Pbs2p MAPKK. *Science* **276,** 1702–5 (1997).
32. Mansour, S. J. *et al.* Mitogen-activated protein (MAP) kinase phosphorylation of MAP kinase kinase: determination of phosphorylation sites by mass spectrometry and site-directed mutagenesis. *J. Biochem.* **116,** 304–14 (1994).
33. Maeda, T., Takekawa, M. & Saito, H. Activation of yeast PBS2 MAPKK by MAPKKKs or by binding of an SH3-containing osmosensor. *Science* **269,** 554–8 (1995).
34. Ferrigno, P., Posas, F., Koepp, D., Saito, H. & Silver, P. A. Regulated nucleo/cytoplasmic exchange of HOG1 MAPK requires the importin beta homologs NMD5 and XPO1. *EMBO J.* **17,** 5606–5614 (1998).
35. Tatebayashi, K., Takekawa, M. & Saito, H. A docking site determining specificity of Pbs2 MAPKK for Ssk2/Ssk22 MAPKKKs in the yeast HOG pathway. *EMBO J.* **22,** 3624–3634 (2003).
36. Hao, N. *et al.* A Systems-Biology Analysis of Feedback Inhibition in the Sho1 Osmotic-Stress-Response Pathway. *Curr. Biol.* **17,** 659–667 (2007).
37. Rep, M., Krantz, M., Thevelein, J. M. & Hohmann, S. The transcriptional response of Saccharomyces cerevisiae to osmotic shock. Hot1p and Msn2p/Msn4p are required for the induction of subsets of high osmolarity glycerol pathway-

dependent genes. *J. Biol. Chem.* **275,** 8290–8300 (2000).
38. Warmka, J., Hanneman, J., Lee, J., Amin, D. & Ota, I. Ptc1, a Type 2C Ser/Thr Phosphatase, Inactivates the HOG Pathway by Dephosphorylating the Mitogen-Activated Protein Kinase Hog1. *Mol. Cell. Biol.* **21,** 51–60 (2001).
39. Wurgler-Murphy, S. M., Maeda, T., Witten, E. A. & Saito, H. Regulation of the Saccharomyces cerevisiae HOG1 mitogen-activated protein kinase by the PTP2 and PTP3 protein tyrosine phosphatases. *Mol. Cell. Biol.* **17,** 1289–97 (1997).
40. Mattison, C. P. & Ota, I. M. Two protein tyrosine phosphatases, Ptp2 and Ptp3, modulate the subcellular localization of the Hog1 MAP kinase in yeast. *Genes Dev.* **14,** 1229–35 (2000).
41. Ferreira, C. A Member of the Sugar Transporter Family, Stl1p Is the Glycerol/H+ Symporter in Saccharomyces cerevisiae. *Mol. Biol. Cell* **16,** 2068–2076 (2005).
42. Lee, J. *et al.* MAPK Hog1 closes the S. cerevisiae glycerol channel Fps1 by phosphorylating and displacing its positive regulators. *Genes Dev.* **27,** 2590–601 (2013).
43. Albertyn, J., Hohmann, S., Thevelein, J. M. & Prior, B. A. GPD1, which encodes glycerol-3-phosphate dehydrogenase, is essential for growth under osmotic stress in Saccharomyces cerevisiae, and its expression is regulated by the high-osmolarity glycerol response pathway. *Mol. Cell. Biol.* **14,** 4135–44 (1994).
44. Pahlman, A. K., Granath, K., Ansell, R., Hohmann, S. & Adler, L. The yeast glycerol 3-phosphatases Gpp1p and Gpp2p are required for glycerol biosynthesis and differentially involved in the cellular responses to osmotic, anaerobic, and oxidative stress. *J. Biol. Chem.* **276,** 3555–63 (2001).
45. Escoté, X., Zapater, M., Clotet, J. & Posas, F. Hog1 mediates cell-cycle arrest in G1 phase by the dual targeting of Sic1. *Nat. Cell Biol.* **6,** 997–1002 (2004).
46. Regot, S. *et al.* The Hog1 stress-activated protein kinase targets nucleoporins to control mrna export upon stress. *J. Biol. Chem.* **288,** 17384–17398 (2013).
47. Alepuz, P. M., Jovanovic, A., Reiser, V. & Ammerer, G. Stress-induced map kinase Hog1 is part of transcription activation complexes. *Mol. Cell* **7,** 767–77 (2001).
48. Rep, M. *et al.* Osmotic stress-induced gene expression in Saccharomyces cerevisiae requires Msn1p and the novel nuclear factor Hot1p. *Mol. Cell. Biol.* **19,** 5474–5485 (1999).
49. Alepuz, P. M., De Nadal, E., Zapater, M., Ammerer, G. & Posas, F. Osmostress-induced transcription by Hot1 depends on a Hog1-mediated recruitment of the RNA Pol II. *EMBO J.* **22,** 2433–2442 (2003).
50. Martínez-Pastor, M. T. *et al.* The Saccharomyces cerevisiae zinc finger proteins Msn2p and Msn4p are required for transcriptional induction through the stress response element (STRE). *EMBO J.* **15,** 2227–35 (1996).
51. Nehlin, J. O., Carlberg, M. & Ronne, H. Yeast SKO1 gene encodes a bZIP protein that binds to the CRE motif and acts as a repressor of transcription. *Nucleic Acids Res.* **20,** 5271–8 (1992).
52. Proft, M. *et al.* Regulation of the Sko1 transcriptional repressor by the Hog1 MAP kinase in response to osmotic stress. *EMBO J.* **20,** 1123–1133 (2001).
53. Proft, M. & Struhl, K. Hog1 kinase converts the Sko1-Cyc8-Tup1 repressor complex into an activator that recruits SAGA and SWI/SNF in response to osmotic stress. *Mol. Cell* **9,** 1307–17 (2002).
54. de Nadal, E., Casadomé, L. & Posas, F. Targeting the MEF2-like transcription factor Smp1 by the stress-activated Hog1 mitogen-activated protein kinase. *Mol. Cell. Biol.* **23,** 229–37 (2003).
55. Cairns, B. R. *et al.* RSC, an essential, abundant chromatin-remodeling complex. *Cell* **87,** 1249–1260 (1996).
56. Mas, G. *et al.* Recruitment of a chromatin remodelling complex by the Hog1 MAP kinase to stress genes. *EMBO J.* **28,** 326–336 (2009).
57. Melcher, M. L. & Thorner, J. Identification and characterization of the CLK1 gene product, a novel CaM kinase-like protein kinase from the yeast Saccharomyces cerevisiae. *J. Biol. Chem.* **271,** 29958–68 (1996).
58. Bilsland-Marchesan, E., Ariño, J., Saito, H., Sunnerhagen, P. & Posas, F. Rck2 kinase is a substrate for the osmotic stress-activated mitogen-activated protein kinase Hog1. *Mol. Cell. Biol.* **20,** 3887–3895 (2000).
59. Teige, M., Scheikl, E., Reiser, V., Ruis, H. & Ammerer, G. Rck2, a member of the calmodulin-protein kinase family, links protein synthesis to high osmolarity MAP kinase signaling in budding yeast. *Proc. Natl. Acad. Sci.* **98,** 5625–5630 (2001).
60. Babazadeh, R., Furukawa, T., Hohmann, S. & Furukawa, K. Rewiring yeast osmostress signalling through the MAPK network reveals essential and non-essential roles of Hog1 in osmoadaptation. *Sci. Rep.* **4,** 4697 (2014).
61. Brauer, M. J. *et al.* Coordination of Growth Rate, Cell Cycle, Stress Response, and Metabolic Activity in Yeast. *Mol. Biol. Cell* **19,** 352–367 (2008).
62. Gasch, A. P. *et al.* Genomic expression programs in the response of yeast cells to environmental changes. *Mol. Biol. Cell* **11,** 4241–57 (2000).
63. Morano, K. a., Grant, C. M. & Moye-Rowley, W. S. The Response to Heat Shock and Oxidative Stress in Saccharomyces cerevisiae. *Genetics* **190,** 1157–1195 (2012).
64. Westfall, P. J., Patterson, J. C., Chen, R. E. & Thorner, J. Stress resistance and signal fidelity independent of nuclear MAPK function. *Proc. Natl. Acad. Sci.* **105,** 12212–12217 (2008).
65. Luyten, K. *et al.* Fps1, a yeast member of the MIP family of channel proteins, is a facilitator for glycerol uptake and efflux and is inactive under osmotic stress. *EMBO J.* **14,** 1360–71 (1995).
66. Tamás, M. J. *et al.* Fps1p controls the accumulation and release of the compatible solute glycerol in yeast osmoregulation. *Mol. Microbiol.* **31,** 1087–104 (1999).
67. Soufi, B. *et al.* Global analysis of the yeast osmotic stress response by quantitative proteomics. *Mol. Biosyst.* **5,** 1337 (2009).
68. Kanshin, E., Bergeron-Sandoval, L.-P., Isik, S. S., Thibault, P. & Michnick, S. W. A Cell-Signaling Network Temporally Resolves Specific versus Promiscuous Phosphorylation. *Cell Rep.* **10,** 1202–1214 (2015).
69. Romanov, N. *et al.* Identifying protein kinase–specific effectors of the osmostress response in yeast. *Sci. Signal.* **10,** (2017).
70. Knighton, D. R. *et al.* Crystal structure of the catalytic subunit of cyclic adenosine monophosphate-dependent protein kinase. *Science* **253,** 407–14 (1991).
71. Knighton, D. R. *et al.* Structure of a peptide inhibitor bound to the catalytic subunit of cyclic adenosine monophosphate-dependent protein kinase. *Science (80-.).* **253,** 414–420 (1991).
72. Pearson, R. B. & Kemp, B. E. Protein kinase phosphorylation site sequences and consensus specificity motifs:

tabulations. *Methods Enzymol.* **200,** 62–81 (1991).
73. Songyang, Z. *et al.* Use of an oriented peptide library to determine the optimal substrates of protein kinases. *Curr. Biol.* **4,** 973–982 (1994).
74. Amanchy, R. *et al.* A curated compendium of phosphorylation motifs. *Nat. Biotechnol.* **25,** 285–286 (2007).
75. Mok, J. *et al.* Deciphering protein kinase specificity through large-scale analysis of yeast phosphorylation site motifs. *Sci. Signal.* **3,** ra12 (2010).
76. Nigg, E. A. Mitotic kinases as regulators of cell division and its checkpoints. *Nat. Rev. Mol. Cell Biol.* **2,** 21–32 (2001).
77. Ubersax, J. A. & Ferrell Jr, J. E. Mechanisms of specificity in protein phosphorylation. *Nat. Rev. Mol. Cell Biol.* **8,** 530–541 (2007).
78. Holt, L. J. *et al.* Global Analysis of Cdk1 Substrate Phosphorylation Sites Provides Insights into Evolution. *Science (80-.).* **325,** 1682–1686 (2009).
79. Rust, H. L. & Thompson, P. R. Kinase consensus sequences: a breeding ground for crosstalk. *ACS Chem. Biol.* **6,** 881–92 (2011).
80. Caffrey, D. R., O'Neill, L. A. & Shields, D. C. The evolution of the MAP kinase pathways: coduplication of interacting proteins leads to new signaling cascades. *J Mol Evol* **49,** 567–582 (1999).
81. Harrison, J. C., Zyla, T. R., Bardes, E. S. G. & Lew, D. J. Stress-specific Activation Mechanisms for the 'Cell Integrity' MAPK Pathway. *J. Biol. Chem.* **279,** 2616–2622 (2004).
82. Levin, D. E. Cell Wall Integrity Signaling in Saccharomyces cerevisiae. *Microbiol. Mol. Biol. Rev*. **69,** 262–291 (2005).
83. Roberts, R. L. & Fink, G. R. Elements of a single map kinase cascade in Saccharomyces cerevisiae mediate two developmental programs in the same cell type: Mating and invasive growth. *Genes Dev.* **8,** 2974–2985 (1994).
84. Leberer, E. *et al.* Functional characterization of the Cdc42p binding domain of yeast Ste20p protein kinase. *EMBO J.* **16,** 83–97 (1997).
85. Moskow, J. J., Gladfelter, a S., Lamson, R. E., Pryciak, P. M. & Lew, D. J. Role of Cdc42p in pheromone-stimulated signal transduction in Saccharomyces cerevisiae. *Mol. Cell. Biol.* **20,** 7559–71 (2000).
86. Flatauer, L. J., Zadeh, S. F. & Bardwell, L. Mitogen-Activated Protein Kinases with Distinct Requirements for Ste5 Scaffolding Influence Signaling Specificity in Saccharomyces cerevisiae. *Mol. Cell. Biol.* **25,** 1793–1803 (2005).
87. Bhattacharyya, R. P. *et al.* The Ste5 Scaffold Allosterically Modulates Signaling Output of the Yeast Mating Pathway. *Science (80-.).* **311,** 822–826 (2006).
88. Hao, N. *et al.* Regulation of Cell Signaling Dynamics by the Protein Kinase-Scaffold Ste5. *Mol. Cell* **30,** 649–656 (2008).
89. Good, M., Tang, G., Singleton, J., Reményi, A. & Lim, W. A. The Ste5 Scaffold Directs Mating Signaling by Catalytically Unlocking the Fus3 MAP Kinase for Activation. *Cell* **136,** 1085–1097 (2009).
90. Pelet, S. Nuclear relocation of Kss1 contributes to the specificity of the mating response. *Sci. Rep.* **7,** (2017).
91. Errede, B. & Ammerer, G. STE12, a protein involved in cell-type-specific transcription and signal transduction in yeast, is part of protein-DNA complexes. *Genes Dev.* **3,** 1349–61 (1989).
92. Kusari, A. B., Molina, D. M., Sabbagh, W., Lau, C. S. & Bardwell, L. A conserved protein interaction network involving the yeast MAP kinases Fus3 and Kss1. *J. Cell Biol.* **164,** 267–277 (2004).
93. Wang, Y., Abu Irqeba, A., Ayalew, M. & Suntay, K. Sumoylation of Transcription Factor Tec1 Regulates Signaling of Mitogen-Activated Protein Kinase Pathways in Yeast. *PLoS One* **4,** e7456 (2009).
94. Brückner, S. *et al.* Differential regulation of Tec1 by Fus3 and Kss1 confers signaling specificity in yeast development. *Curr. Genet.* **46,** 331–342 (2004).
95. Chou, S., Huang, L. & Liu, H. Fus3-regulated Tec1 degradation through SCFCdc4 determines MAPK signaling specificity during mating in yeast. *Cell* **119,** 981–990 (2004).
96. Bao, M. Z., Schwartz, M. A., Cantin, G. T., Yates, J. R. & Madhani, H. D. Pheromone-Dependent Destruction of the Tec1 Transcription Factor Is Required for MAP Kinase Signaling Specificity in Yeast. *Cell* **119,** 991–1000 (2004).
97. O'Rourke, S. M. & Herskowitz, I. The Hog1 MAPK prevents cross talk between the HOG and pheromone response MAPK pathways in Saccharomyces cerevisiae. *Genes Dev.* **12,** 2874–2886 (1998).
98. Davenport, K. D., Williams, K. E., Ullmann, B. D. & Gustin, M. C. Activation of the Saccharomyces cerevisiae filamentation/invasion pathway by osmotic stress in high-osmolarity glycogen pathway mutants. *Genetics* **153,** 1091–1103 (1999).
99. Shock, T. R., Thompson, J., Yates, J. R. & Madhani, H. D. Hog1 mitogen-activated protein kinase (MAPK) interrupts signal transduction between the Kss1 MAPK and the Tec1 transcription factor to maintain pathway specificity. *Eukaryot. Cell* **8,** 606–616 (2009).
100. Sabbagh, W., Flatauer, L. J., Bardwell, A. J. & Bardwell, L. Specificity of MAP kinase signaling in yeast differentiation involves transient versus sustained MAPK activation. *Mol. Cell* **8,** 683–91 (2001).
101. Dale, S., Wilson, W. A., Edelman, A. M. & Hardie, D. G. Similar substrate recognition motifs for mammalian AMP-activated protein kinase, higher plant HMG-CoA reductase kinase-A, yeast SNF1, and mammalian calmodulin-dependent protein kinase I. *FEBS Lett.* **361,** 191–5 (1995).
102. Wang, Z., Wilson, W. a, Fujino, M. a & Roach, P. J. Antagonistic controls of autophagy and glycogen accumulation by Snf1p, the yeast homolog of AMP-activated protein kinase, and the cyclin-dependent kinase Pho85p. *Mol. Cell. Biol.* **21,** 5742–52 (2001).
103. Gruhler, A. *et al.* Quantitative Phosphoproteomics Applied to the Yeast Pheromone Signaling Pathway. *Mol. Cell. Proteomics* **4,** 310–327 (2005).
104. Albuquerque, C. P. *et al.* A Multidimensional Chromatography Technology for In-depth Phosphoproteome Analysis. *Mol. Cell. Proteomics* **7,** 1389–1396 (2008).
105. Breitkreutz, A. *et al.* A Global Protein Kinase and Phosphatase Interaction Network in Yeast. *Science (80-.).* **328,** 1043–1046 (2010).
106. Bodenmiller, B. *et al.* Phosphoproteomic Analysis Reveals Interconnected System-Wide Responses to Perturbations of Kinases and Phosphatases in Yeast. *Sci. Signal.* **3,** rs4-rs4 (2010).
107. Mascaraque, V. *et al.* Phosphoproteomic analysis of protein kinase C signaling in Saccharomyces cerevisiae reveals Slt2 mitogen-activated protein kinase (MAPK)-dependent phosphorylation of eisosome core components. *Mol. Cell. Proteomics* **12,** 557–74 (2013).
108. Muir, A., Roelants, F. M., Timmons, G., Leskoske, K. L. & Thorner, J. Down-regulation of TORC2-Ypk1 signaling

promotes MAPK-independent survival under hyperosmotic stress. *Elife* **4,** (2015).
109. Roelants, F. M., Breslow, D. K., Muir, A., Weissman, J. S. & Thorner, J. Protein kinase Ypk1 phosphorylates regulatory proteins Orm1 and Orm2 to control sphingolipid homeostasis in Saccharomyces cerevisiae. *Proc. Natl. Acad. Sci.* **108,** 19222–19227 (2011).
110. Sun, Y. *et al.* Orm protein phosphoregulation mediates transient sphingolipid biosynthesis response to heat stress via the Pkh-Ypk and Cdc55-PP2A pathways. *Mol. Biol. Cell* **23,** 2388–2398 (2012).
111. Muir, A., Ramachandran, S., Roelants, F. M., Timmons, G. & Thorner, J. TORC2-dependent protein kinase Ypk1 phosphorylates ceramide synthase to stimulate synthesis of complex sphingolipids. *Elife* **3,** (2014).
112. De Hoffmann, E. Tandem mass spectrometry: A primer. *Journal of Mass Spectrometry* **31,** 129–137 (1996).
113. Petrovic, M. & Barceló, D. Liquid chromatography-tandem mass spectrometry. *Analytical and Bioanalytical Chemistry* **405,** 5857–5858 (2013).
114. Zhang, Z. Prediction of low-energy collision-induced dissociation spectra of peptides. *Anal. Chem.* **76,** 3908–3922 (2004).
115. Mitchell Wells, J. & McLuckey, S. A. Collision-induced dissociation (CID) of peptides and proteins. *Methods Enzymol.* **402,** 148–185 (2005).
116. Olsen, J. V. *et al.* Higher-energy C-trap dissociation for peptide modification analysis. *Nat. Methods* **4,** 709–712 (2007).
117. Sainani, K. L. The Problem of Multiple Testing. *PM&R* **1,** 1098–1103 (2009).
118. Elias, J. E. & Gygi, S. P. Target-decoy search strategy for increased confidence in large-scale protein identifications by mass spectrometry. *Nat. Methods* **4,** 207–214 (2007).
119. Bern, M. W. & Kil, Y. J. Two-dimensional target decoy strategy for shotgun proteomics. *J. Proteome Res.* **10,** 5296–5301 (2011).
120. Aggarwal, S. & Yadav, A. K. in 119–128 (2016). doi:10.1007/978-1-4939-3106-4_7
121. Solari, F. A., Dell'Aica, M., Sickmann, A. & Zahedi, R. P. Why phosphoproteomics is still a challenge. *Mol. BioSyst.* **11,** 1487–1493 (2015).
122. Winter, D., Seidler, J., Ziv, Y., Shiloh, Y. & Lehmann, W. D. Citrate Boosts the Performance of Phosphopeptide Analysis by UPLC-ESI-MS/MS. *J. Proteome Res.* **8,** 418–424 (2009).
123. Liu, S. *et al.* Formation of phosphopeptide-metal ion complexes in liquid chromatography/electrospray mass spectrometry and their influence on phosphopeptide detection. *Rapid Commun. Mass Spectrom.* **19,** 2747–56 (2005).
124. Choi, H., Lee, H. & Park, Z.-Y. Detection of multiphosphorylated peptides in LC-MS/MS analysis under low pH conditions. *Anal. Chem.* **80,** 3007–15 (2008).
125. Steen, H., Jebanathirajah, J. A., Rush, J., Morrice, N. & Kirschner, M. W. Phosphorylation Analysis by Mass Spectrometry. *Mol. Cell. Proteomics* **5,** 172–181 (2006).
126. Dickhut, C., Feldmann, I., Lambert, J. & Zahedi, R. P. Impact of Digestion Conditions on Phosphoproteomics. *J. Proteome Res.* **13,** 2761–2770 (2014).
127. Ong, S.-E. *et al.* Stable isotope labeling by amino acids in cell culture, SILAC, as a simple and accurate approach to expression proteomics. *Mol. Cell. Proteomics* **1,** 376–386 (2002).
128. Klein, M. *et al.* Design, synthesis and characterization of a highly effective inhibitor for analog-sensitive (as) kinases. *PLoS One* **6,** (2011).
129. Zuzuarregui, A. *et al.* M-Track: detecting short-lived protein-protein interactions in vivo. *Nat. Methods* **9,** 594–6 (2012).
130. Brezovich, A., Schuschnig, M., Ammerer, G. & Kraft, C. An in vivo detection system for transient and low abundant protein interactions and their kinetics in budding yeast. *Yeast* (2015). doi:10.1002/yea.3063
131. Schwartz, D. & Gygi, S. P. An iterative statistical approach to the identification of protein phosphorylation motifs from large-scale data sets. *Nat. Biotechnol.* **23,** 1391–1398 (2005).
132. Chou, M. F. & Schwartz, D. Biological Sequence Motif Discovery Using motif-x. *Curr. Protoc. Bioinformatics* **Chapter 13,** Unit13.15 (2011).
133. Pascual-Ahuir, A. & Proft, M. The Sch9 kinase is a chromatin-associated transcriptional activator of osmostress-responsive genes. *EMBO J.* **26,** 3098–3108 (2007).
134. Liu, K., Zhang, X., Lester, R. L. & Dickson, R. C. The sphingoid long chain base phytosphingosine activates AGC-type protein kinases in Saccharomyces cerevisiae including Ypk1, Ypk2, and Sch9. *J. Biol. Chem.* **280,** 22679–22687 (2005).
135. Ptacek, J. *et al.* Global analysis of protein phosphorylation in yeast. *Nature* **438,** 679–84 (2005).
136. Sharifpoor, S. *et al.* Functional wiring of the yeast kinome revealed by global analysis of genetic network motifs. *Genome Res.* **22,** 791–801 (2012).
137. Huang, D. W., Sherman, B. T. & Lempicki, R. A. Bioinformatics enrichment tools: Paths toward the comprehensive functional analysis of large gene lists. *Nucleic Acids Res.* **37,** 1–13 (2009).
138. Huang, D. W., Sherman, B. T. & Lempicki, R. A. Systematic and integrative analysis of large gene lists using DAVID bioinformatics resources. *Nat. Protoc.* **4,** 44–57 (2009).
139. Supek, F., Bošnjak, M., Škunca, N. & Šmuc, T. Revigo summarizes and visualizes long lists of gene ontology terms. *PLoS One* **6,** (2011).
140. Michaillat, L. & Mayer, A. Identification of Genes Affecting Vacuole Membrane Fragmentation in Saccharomyces cerevisiae. *PLoS One* **8,** (2013).
141. Burd, C. G., Mustol, P. a, Schu, P. V & Emr, S. D. A yeast protein related to a mammalian Ras-binding protein, Vps9p, is required for localization of vacuolar proteins. *Mol. Cell. Biol.* **16,** 2369–2377 (1996).
142. Fröhlich, F. *et al.* The GARP complex is required for cellular sphingolipid homeostasis. *Elife* **4,** (2015).
143. Dudley, A. M., Janse, D. M., Tanay, A., Shamir, R. & Church, G. M. A global view of pleiotropy and phenotypically derived gene function in yeast. *Mol. Syst. Biol.* **1,** E1–E11 (2005).
144. Yoshikawa, K. *et al.* Comprehensive phenotypic analysis for identification of genes affecting growth under ethanol stress in Saccharomyces cerevisiae. *FEMS Yeast Res.* **9,** 32–44 (2009).
145. Martin, H. *et al.* Differential genetic interactions of yeast stress response MAPK pathways. *Mol. Syst. Biol.* **11,** 800 (2015).
146. Gonzalez, R. *et al.* New genes involved in osmotic stress tolerance in saccharomyces cerevisiae. *Front. Microbiol.* **7,** (2016).
147. Eng, J. K., Mccormack, A. L. & Yates, J. R. An Approach to Correlate Tandem Mass Spectral Data of Peptides with

Amino Acid Sequences in a Protein Database. *Am. Soc. Mass Spectrom.* **5,** 976–989 (1994).
148. Perkins, D. N., Pappin, D. J., Creasy, D. M. & Cottrell, J. S. Probability-based protein identification by searching sequence databases using mass spectrometry data. *Electrophoresis* **20,** 3551–67 (1999).
149. Cox, J. & Mann, M. MaxQuant enables high peptide identification rates, individualized p.p.b.-range mass accuracies and proteome-wide protein quantification. *Nat. Biotechnol.* **26,** 1367–1372 (2008).
150. Tyanova, S. *et al.* Visualization of LC-MS/MS proteomics data in MaxQuant. *Proteomics* **15,** 1453–1456 (2015).
151. Swaney, D. L. *et al.* Global analysis of phosphorylation and ubiquitylation cross-talk in protein degradation. *Nat. Methods* **10,** 676–82 (2013).
152. Bodenmiller, B. *et al.* Phosphoproteomic Analysis Reveals Interconnected System-Wide Responses to Perturbations of Kinases and Phosphatases in Yeast. *Sci. Signal.* **3,** rs4-rs4 (2010).
153. Yamamoto, K., Tatebayashi, K., Tanaka, K. & Saito, H. Dynamic Control of Yeast MAP Kinase Network by Induced Association and Dissociation between the Ste50 Scaffold and the Opy2 Membrane Anchor. *Mol. Cell* **40,** 87–98 (2010).
154. Hao, N., Zeng, Y., Elston, T. C. & Dohlman, H. G. Control of MAPK Specificity by Feedback Phosphorylation of Shared Adaptor Protein Ste50. *J. Biol. Chem.* **283,** 33798–33802 (2008).
155. Reiter, W. *et al.* Validation of regulated protein phosphorylation events in yeast by quantitative mass spectrometry analysis of purified proteins. *Proteomics* **12,** 3030–43 (2012).
156. Kanshin, E., Bergeron-Sandoval, L.-P., Isik, S. S., Thibault, P. & Michnick, S. W. A cell-signaling network temporally resolves specific versus promiscuous phosphorylation. *Cell Rep.* **101. Kansh,** 1202–14 (2015).
157. Hruby, A. *et al.* A constraint network of interactions: protein-protein interaction analysis of the yeast type II phosphatase Ptc1p and its adaptor protein Nbp2p. *J. Cell Sci.* **124,** 1603–1603 (2011).
158. Sun, Y. *et al.* Orm protein phosphoregulation mediates transient sphingolipid biosynthesis response to heat stress via the Pkh-Ypk and Cdc55-PP2A pathways. *Mol. Biol. Cell* **23,** 2388–2398 (2012).
159. Partow, S., Siewers, V., Bjørn, S., Nielsen, J. & Maury, J. Characterization of different promoters for designing a new expression vector in Saccharomyces cerevisiae. *Yeast* **27,** 955–964 (2010).
160. Alepuz, P. M., de Nadal, E., Zapater, M., Ammerer, G. & Posas, F. Osmostress-induced transcription by Hot1 depends on a Hog1-mediated recruitment of the RNA Pol II. *EMBO J.* **22,** 2433–42 (2003).
161. Teige, M., Scheikl, E., Reiser, V., Ruis, H. & Ammerer, G. Rck2, a member of the calmodulin-protein kinase family, links protein synthesis to high osmolarity MAP kinase signaling in budding yeast. *Proc. Natl. Acad. Sci.* **98,** 5625–5630 (2001).
162. Ruiz-Roig, C., Noriega, N., Duch, A., Posas, F. & de Nadal, E. The Hog1 SAPK controls the Rtg1/Rtg3 transcriptional complex activity by multiple regulatory mechanisms. *Mol. Biol. Cell* **23,** 4286–4296 (2012).
163. Sharifian, H. *et al.* Parallel feedback loops control the basal activity of the HOG MAPK signaling cascade. *Integr. Biol.* **7,** 412–422 (2015).
164. García-Rodríguez, L. J., Valle, R., Durán, Á. & Roncero, C. Cell integrity signaling activation in response to hyperosmotic shock in yeast. *FEBS Lett.* **579,** 6186–6190 (2005).
165. Kim, K. Y., Truman, A. W., Caesar, S., Schlenstedt, G. & Levin, D. E. Yeast Mpk1 Cell Wall Integrity Mitogen-activated Protein Kinase Regulates Nucleocytoplasmic Shuttling of the Swi6 Transcriptional Regulator. *Mol. Biol. Cell* **21,** 1609–1619 (2010).
166. Alonso-Rodríguez, E., Fernández-Piñar, P., Sacristán-Reviriego, A., Molina, M. & Martín, H. An analog-sensitive version of the protein kinase Slt2 allows identification of novel targets of the yeast cell wall integrity pathway. *J. Biol. Chem.* **291,** 5461–5472 (2016).
167. Jung, U. S., Sobering, A. K., Romeo, M. J. & Levin, D. E. Regulation of the yeast Rlm1 transcription factor by the Mpk1 cell wall integrity MAP kinase. *Mol. Microbiol.* **46,** 781–789 (2002).
168. Watanabe, Y., Takaesu, G., Hagiwara, M., Irie, K. & Matsumoto, K. Characterization of a serum response factor-like protein in Saccharomyces cerevisiae, Rlm1, which has transcriptional activity regulated by the Mpk1 (Slt2) mitogen-activated protein kinase pathway. *Mol. Cell. Biol.* **17,** 2615–23 (1997).
169. Reiter, W. *et al.* Yeast protein phosphatase 2A-Cdc55 regulates the transcriptional response to hyperosmolarity stress by regulating Msn2 and Msn4 chromatin recruitment. *Mol. Cell. Biol.* **33,** 1057–72 (2013).
170. Breitkreutz, A. *et al.* A Global Protein Kinase and Phosphatase Interaction Network in Yeast. *Science (80-.).* **328,** 1043–1046 (2010).
171. Albuquerque, C. P. *et al.* A Multidimensional Chromatography Technology for In-depth Phosphoproteome Analysis. *Mol. Cell. Proteomics* **7,** 1389–1396 (2008).
172. Gruhler, A. *et al.* Quantitative phosphoproteomics applied to the yeast pheromone signaling pathway. *Mol. Cell. Proteomics* **4,** 310–27 (2005).
173. Ferrer-Dalmau, J., Randez-Gil, F., Marquina, M., Prieto, J. A. & Casamayor, A. Protein kinase Snf1 is involved in the proper regulation of the unfolded protein response in *Saccharomyces cerevisiae*. *Biochem. J.* **468,** 33–47 (2015).
174. Mizuno, T., Masuda, Y. & Irie, K. The Saccharomyces cerevisiae AMPK, Snf1, Negatively Regulates the Hog1 MAPK Pathway in ER Stress Response. *PLoS Genet.* **11,** (2015).
175. Lussier, M. *et al.* Large scale identification of genes involved in cell surface biosynthesis and architecture in Saccharomyces cerevisiae. *Genetics* **147,** 435–50 (1997).
176. Bilsland-Marchesan, E., Ariño, J., Saito, H., Sunnerhagen, P. & Posas, F. Rck2 kinase is a substrate for the osmotic stress-activated mitogen-activated protein kinase Hog1. *Mol. Cell. Biol.* **20,** 3887–95 (2000).
177. Dickhut, C., Feldmann, I., Lambert, J. & Zahedi, R. P. Impact of digestion conditions on phosphoproteomics. *J. Proteome Res.* **13,** 2761–70 (2014).
178. Tabb, D. L. *et al.* Repeatability and reproducibility in proteomic identifications by liquid chromatography-tandem mass spectrometry. *J. Proteome Res.* **9,** 761–76 (2010).
179. Nelson, B. *et al.* RAM: A Conserved Signaling Network That Regulates Ace2p Transcriptional Activity and Polarized Morphogenesis. *Mol. Biol. Cell* **14,** 3782–3803 (2003).
180. Vossen, J. H. *et al.* The protein kinase Kic1 affects 1,6-β-glucan levels in the cell wall of Saccharomyces cerevisiae. *Microbiology* **148,** 4035–4048 (2002).
181. Ren, P., Malik, A. & Zeng, F. Identification of YPL014W (Cip1) as a novel negative regulator of cyclin-dependent kinase in *Saccharomyces cerevisiae*. *Genes to Cells* **21,** 543–552 (2016).
182. Chang, Y.-L. *et al.* Yeast Cip1 is activated by environmental stress to inhibit Cdk1–G1 cyclins via Mcm1 and Msn2/4.

Nat. Commun. **8,** 56 (2017).
183. Ewald, J. C., Kuehne, A., Zamboni, N. & Skotheim, J. M. The Yeast Cyclin-Dependent Kinase Routes Carbon Fluxes to Fuel Cell Cycle Progression. *Mol. Cell* **62,** 532–545 (2016).
184. Kono, K., Al-Zain, A., Schroeder, L., Nakanishi, M. & Ikui, A. E. Plasma membrane/cell wall perturbation activates a novel cell cycle checkpoint during G1 in *Saccharomyces cerevisiae*. *Proc. Natl. Acad. Sci.* **113,** 6910–6915 (2016).
185. Breslow, D. K. *et al.* Orm family proteins mediate sphingolipid homeostasis. *Nature* **463,** 1048–1053 (2010).
186. Han, S., Lone, M. A., Schneiter, R. & Chang, A. Orm1 and Orm2 are conserved endoplasmic reticulum membrane proteins regulating lipid homeostasis and protein quality control. *Proc. Natl. Acad. Sci.* **107,** 5851–5856 (2010).
187. Liu, M., Huang, C., Polu, S. R., Schneiter, R. & Chang, A. Regulation of sphingolipid synthesis through Orm1 and Orm2 in yeast. *J. Cell Sci.* **125,** 2428–2435 (2012).
188. Roelants, F. M., Torrance, P. D., Bezman, N. & Thorner, J. Pkh1 and Pkh2 Differentially Phosphorylate and Activate Ypk1 and Ykr2 and Define Protein Kinase Modules Required for Maintenance of Cell Wall Integrity. *Mol. Biol. Cell* **13,** 3005–3028 (2002).
189. Gururaj, C., Federman, R., Chang, A. & Chang, A. Orm Proteins Integrate Multiple Signals to Maintain Sphingolipid Homeostasis. *J. Biol. Chem.* **288,** 20453–20463 (2013).
190. Voordeckers, K. *et al.* Yeast 3-Phosphoinositide-dependent Protein Kinase-1 (PDK1) Orthologs Pkh1–3 Differentially Regulate Phosphorylation of Protein Kinase A (PKA) and the Protein Kinase B (PKB)/S6K Ortholog Sch9. *J. Biol. Chem.* **286,** 22017–22027 (2011).
191. Pohlers, S. *et al.* Lipid Signaling via Pkh1/2 Regulates Fungal CO_2 Sensing through the Kinase Sch9. *MBio* **8,** e02211-16 (2017).
192. Takeda, E. *et al.* Vacuole-mediated selective regulation of TORC1-Sch9 signaling following oxidative stress. *Mol. Biol. Cell* mbc.E17-09-0553 (2017). doi:10.1091/mbc.E17-09-0553
193. deHart, A. K. A., Schnell, J. D., Allen, D. A. & Hicke, L. The conserved Pkh–Ypk kinase cascade is required for endocytosis in yeast. *J. Cell Biol.* **156,** 241–248 (2002).
194. Janke, C. *et al.* A versatile toolbox for PCR-based tagging of yeast genes: New fluorescent proteins, more markers and promoter substitution cassettes. *Yeast* **21,** 947–962 (2004).
195. Knop, M. *et al.* Epitope tagging of yeast genes using a PCR-based strategy: more tags and improved practical routines. *Yeast* **15,** 963–972 (1999).
196. Wach, A., Brachat, A., Pöhlmann, R. & Philippsen, P. New heterologous modules for classical or PCR-based gene disruptions in Saccharomyces cerevisiae. *Yeast* **10,** 1793–1808 (1994).
197. Behera, A. K., Kumar, M., Lockey, R. F. & Mohapatra, S. S. 2'-5' Oligoadenylate synthetase plays a critical role in interferon-gamma inhibition of respiratory syncytial virus infection of human epithelial cells. *J. Biol. Chem.* **277,** 25601–25608 (2002).
198. Mazanek, M. *et al.* Titanium dioxide as a chemo-affinity solid phase in offline phosphopeptide chromatography prior to HPLC-MS/MS analysis. *Nat. Protoc.* **2,** 1059–1069 (2007).
199. Thingholm, T. E., Jørgensen, T. J. D., Jensen, O. N. & Larsen, M. R. Highly selective enrichment of phosphorylated peptides using titanium dioxide. *Nat. Protoc.* **1,** 1929–1935 (2006).
200. Roitinger, E. *et al.* Quantitative Phosphoproteomics of the Ataxia Telangiectasia-Mutated (ATM) and Ataxia Telangiectasia-Mutated and Rad3-related (ATR) Dependent DNA Damage Response in *Arabidopsis thaliana*. *Mol. Cell. Proteomics* **14,** 556–571 (2015).

X. Appendix

X.1. Romanov et al.

SCIENCE SIGNALING | RESEARCH RESOURCE

CELL BIOLOGY

Identifying protein kinase–specific effectors of the osmostress response in yeast

Natalie Romanov,[1]* David Maria Hollenstein,[1†] Marion Janschitz,[1†] Gustav Ammerer,[1] Dorothea Anrather,[2] Wolfgang Reiter[1‡]

The budding yeast *Saccharomyces cerevisiae* reacts to increased external osmolarity by modifying many cellular processes. Adaptive signaling relies primarily on the high-osmolarity glycerol (HOG) pathway, which is closely related to the mammalian p38 mitogen-activated protein kinase (MAPK) pathway in core architecture. To identify target proteins of the MAPK Hog1, we designed a mass spectrometry–based high-throughput experiment to measure the impact of Hog1 activation or inhibition on the *S. cerevisiae* phosphoproteome. In addition, we analyzed how deletion of *RCK2*, which encodes a known effector protein kinase target of Hog1, modulated osmotic stress–induced phosphorylation. Our results not only provide an overview of the diversity of cellular functions that are directly and indirectly affected by the activity of the HOG pathway but also enabled an assessment of the Hog1-independent events that occur under osmotic stress conditions. We extended the number of putative Hog1 direct targets by analyzing the modulation of motifs consisting of serine or threonine followed by a proline (S/T-P motif) and subsequently validated these with an in vivo interaction assay. Rck2 appears to act as a central hub for many Hog1-mediated secondary phosphorylation events. This study clarifies many of the direct and indirect effects of HOG signaling and its stress-adaptive functions.

INTRODUCTION

Adaptive responses to fluctuations in extracellular parameters are generally controlled by complex signal transduction systems that transmit information on environmental cues to various effector molecules. These regulatory systems often constitute highly intertwined kinase and phosphatase networks rather than one single well-defined signal transduction pathway. To add further complexity, individual kinases and phosphatases can show different response kinetics depending on the stimulus, resulting in primary and complementary responses. Several high-throughput mass spectrometry (MS) shotgun studies have been undertaken to globally record cellular responses with the aim of determining the individual contribution of kinases to a given phosphoproteomic state (*1*–*6*). However, the collective frequency of phosphorylation and dephosphorylation events hampers the identification of specific kinase-substrate interactions (*1*, *7*).

The hyperosmotic stress response of the budding yeast *Saccharomyces cerevisiae* is a paradigm for such responses and has been well characterized using mRNA microarrays and MS-based approaches (*4*, *6*, *8*–*10*). Upon exposure to high osmolarity, yeast cells experience rapid water loss and shrinkage. Reprogramming of gene expression patterns, a temporary cell cycle arrest, and, ultimately, an increase in the intracellular concentration of the compatible osmolyte glycerol are the cornerstones of this response (*11*). In addition, osmostress effects on glycolysis and cytoskeletal and mitotic spindle dynamics have been proposed (*4*, *6*).

One of the main signaling cascades involved in the osmostress response is the high-osmolarity glycerol (HOG) mitogen-activated protein kinase (MAPK) pathway (*12*–*14*), which is highly conserved across the fungal kingdom and homologous to the mammalian p38 stress-activated protein kinase (SAPK) pathway. Its central module essentially consists of the MAPK Hog1, the MAPK kinase (MAPKK) Pbs2, and the three MAPKK kinases (MAPKKK) Ssk2, Ssk22, and Ste11. Upon activation by extracellular hyperosmolarity, the MAPK undergoes dual phosphorylation at residues Thr^{174} and Tyr^{176}. This dual phosphorylation correlates with Hog1 kinase activity, which peaks at 5 min after stress induction and returns to the original state within 20 to 30 min (*11*). The activated MAPK coordinates the osmostress response by phosphorylating motifs consisting of serine or threonine followed by a proline (S/T-P motifs) on several target proteins. Ultimately, the cascade leads to the activation of downstream kinases, such as Rck2 (*15*), which has been associated primarily with translation.

Despite the fact that many direct and indirect targets of Hog1 have already been described, several aspects of the hyperosmotic stress response are still not completely understood (*11*), including which cellular functions are directly controlled and which are indirectly controlled by Hog1. Kanshin *et al.* and Soufi *et al.* describe the scale and dynamics of the hyperosmotic stress response on a phosphoproteomic scale and find the response to be complex, involving many kinases and phosphatases (*4*, *6*). Motif searches using sequences flanking dynamic phosphorylation sites reveal the involvement of basophilic protein kinase A (PKA) and p21-activating kinases (PAKs), proline-directed kinases [MAPKs and cyclin-dependent kinases (CDKs)], and others (*4*, *6*). Although these data sets provide an excellent overview of osmostress-induced changes in the yeast proteome, the lack of experiments where Hog1 is specifically deactivated hampers efforts to unambiguously define substrates of this MAPK. Moreover, identification of dynamically phosphorylated sites does not allow unequivocal assignment of phosphorylated targets to one specific kinase, which we demonstrated for S/T-P sites of Pan1, a protein involved in early endocytosis (*7*). To extract kinase-substrate interactions in a system-wide manner, it is therefore necessary to use experimental means to resolve kinase dependencies of distinct phosphorylation sites.

Here, we addressed this problem using a dual MS shotgun approach based on stable isotope labeling with amino acids in cell culture (SILAC) (*16*, *17*) with the aim of identifying substrates of Hog1. Integration of the MS data sets revealed more than 25 previously unidentified putative substrates and numerous indirect targets of Hog1. Identified target proteins were further validated by their ability to directly

[1]Department for Biochemistry, Max F. Perutz Laboratories, University of Vienna, Dr. Bohr-Gasse 9, A-1030 Vienna, Austria. [2]Mass Spectrometry Facility, Max F. Perutz Laboratories, Dr. Bohr-Gasse 9, A-1030 Vienna, Austria.
*Present address: Structural and Computational Biology Unit, European Molecular Biology Laboratory, Meyerhofstrasse 1, 69117 Heidelberg, Germany.
†These authors contributed equally to this work.
‡Corresponding author. Email: wolfgang.l.reiter@univie.ac.at

interact with Hog1 in vivo using a protein-protein proximity assay (*18*). In addition, we demonstrated the role of the kinase Rck2 as a master regulator of secondary responses downstream of Hog1.

RESULTS

Experimental setup to identify Hog1 targets

In yeast, extracellular hyperosmolarity activates the MAPK Hog1, which regulates various cellular processes important for stress adaptation and survival (*11*). Large-scale MS studies sought to predict specific Hog1-substrate interactions either by measuring osmostress induction or by using a *hog1*Δ strain (*1*, *4*, *6*). However, the overwhelming complexity of secondary effects impedes the discovery of specific substrates. We hypothesized that only the integration of both layers of information (induction and inactivation of Hog1, ideally by using a Hog1-specific inhibitor) would allow unambiguous assignment of phosphorylation events to Hog1 activity. Hence, to identify previously undescribed substrates of Hog1, we designed a two-step experimental setup using a quantitative proteomics strategy based on SILAC MS labeling (Fig. 1A). As the first step, we measured global changes in the phosphorylation pattern of the yeast proteome 5 min after exposure to increased extracellular salt concentrations, hereafter referred to as setup stress response (SR). As the second step, we conducted a series of quantitative MS shotgun experiments using a strain of yeast bearing a point mutation in the endogenous *Hog1* locus (*Hog1as*) that renders the encoded protein sensitive to inhibition by the adenosine 5′-triphosphate (ATP) analog 1-isopropyl-3-(phenylethynyl)-1*H*-pyrazolo[3,4-*d*]pyrimidin-4-amine, also called SPP86 (*19*). After application of the inhibitor, cells were subsequently exposed to hyperosmotic stress treatment for 0, 5, or 10 min, designated as setups I + 0′S, I + 5′S, and I + 10′S, respectively (Fig. 1A). Phosphorylated S/T-P motifs displaying more than a twofold increase in abundance in setup SR and sensitivity to inhibitor treatment in setups I + 0′S, I + 5′S, or I + 10′S were considered putative Hog1 substrates (Fig. 1B).

Identification of stress-induced changes in the *S. cerevisiae* phosphorylome

From our analysis of 283 liquid chromatography (LC)–tandem MS runs, we identified 39,055 peptides with a false-positive rate below 1% for both peptides and proteins (table S1). On average, we achieved a ~40% overlap for peptides between setups, allowing a systematic integrative analysis of the data sets (Fig. 2A). To facilitate phosphorylation site analysis, we integrated all SILAC peptide ratios corresponding to a specific phosphorylation site. In this way, we quantified 8055 phosphorylation sites in setup SR, 23% of which showed more than a twofold change in abundance (corresponding to 735 proteins), confirming the broadness of the hyperosmotic SR in yeast. Seventy-seven percent of phosphorylation sites were static (≤2-fold change in abundance).

To test whether our setup SR adequately reflected the anticipated response of cells challenged with hyperosmolarity, we looked at well-known phosphorylation events of osmostress signaling (Fig. 2B). First and foremost, we found phosphorylations at two key residues of Hog1 (Thr^{174} and Tyr^{176}) to be increased by about 70-fold, suggesting stress activation of the MAPK. In agreement with this, we also observed a more than 10-fold increase in phosphorylation at the regulatory amino acid residues of the MAPKK Pbs2 (Ser^{514} and Thr^{518}). In addition, several well-established Hog1 target sites showed increased phosphorylation, namely, Ser^{379} and Ser^{520} of the Ca^{2+}- or calmodulin-dependent protein kinase (CaMK)–like kinase Rck2 (~50- and ~20-fold, respectively) (*15*), Ser^{153} of transcription factor Hot1 (~4-fold) (*20*), Thr^{774} and Ser^{975} of Rgc1 (~10-fold), and Thr^{808} of Rgc2, also known as Ask10 (~3-fold). Rgc1 and Rgc2 are regulators of the aquaglyceroporin Fps1 (*21*), which mediates the export of glycerol. We also confirmed a decrease in Ser^{185} phosphorylation of Fps1, which has been proposed to activate docking of Hog1 to this channel (*4*, *21*). Comparing setup SR with similar approaches (*4*) yielded a positive correlation ($R = 0.53$) for most of the dynamic phosphorylation sites (fig. S1, A and B). We thus recovered generally accepted hallmarks of the SR and demonstrate full activation of Hog1 as well as data consistency with previous studies. We provide a detailed list of the integrated results of all shotgun experiments (table S2).

Hog1-specific and general responses to hyperosmotic stress

A previously unaddressed aspect of the HOG response concerns how many changes in the global phosphorylation pattern are mediated by Hog1 in a direct or indirect manner. To tackle this question, we compared the corresponding SILAC ratios of data sets SR to I + 5′S and I +10′S (Fig. 2, B to D). The distribution of SILAC fold changes, shown along the *x* axis, represents phosphorylation changes in response to hyperosmotic stress. The dispersion along the *y* axis indicates susceptibility to inhibitor treatment and therefore the degree of Hog1 dependency. By setting conservative ratio cutoffs (twofold) along both axes, we defined eight data fields containing sites with distinct properties that can be characterized individually (Fig. 2D). Field 1 includes phosphorylation sites that increase in abundance in response to high osmolarity but remain unchanged if Hog1 is specifically inhibited. Therefore, the phosphorylation status of these sites is directly or indirectly dependent on Hog1 activity. Field 2 includes phosphorylation sites that do not change in response to osmostress but are susceptible to inhibition of Hog1. Field 3 contains sites that decrease in abundance in response to stress and are also less abundant upon inhibitor treatment, and so forth. Finally, field 8 includes all phosphorylation sites that increase in abundance in response to high osmolarity in a Hog1-independent manner. Although we observed a shift of data points toward higher values along the *x* axis, suggesting an increase of phosphorylation events during stress in general, the distribution along the *y* axis did not show any particular skewing. We expected changes along the *y* axis to be minor given that the response was limited to inhibition of a very specific pathway. In total, 9% of phosphorylation sites covered in setup I + 5′S (10% of setup I + 10′S) were positively or negatively affected by inhibition of Hog1.

We evaluated the functional properties of the set of proteins clustering in field 1 (Fig. 2E) and found enrichment for proteins involved in transport of solutes, endocytosis, and signal transduction, which is in line with previous reports (*7*, *9*, *11*, *15*, *21*–*23*). In addition, gene ontology (GO) terms related to the regulation of catalytic activity and diverse metabolic processes were also overrepresented, emphasizing the previously suggested role of Hog1 in metabolic fine-tuning (*11*). Although previously attributed to HOG signaling (*4*), actin- and cytoskeleton-related processes were enriched within the Hog1-independent set of proteins (field 8).

We next tested for overrepresentation of peptide motifs surrounding dynamic phosphorylation sites using MotifX (Fig. 2F and fig. S1C) (*24*, *25*) and first focused on phosphorylation at sites with prolines at position P + 1 (S/T-P motifs), which is indicative of targeting by proline-directed kinases such as MAPKs and CDKs. Surprisingly, phosphorylation of most S/T-P motifs was independent of Hog1 (field 8), suggesting that multiple proline-directed kinases are active during the SR (Fig. 2, D and F, and fig. S1, D to F). Only a minor fraction of S/T-P motifs were located in field 1, the group of phosphorylation sites that increase in

abundance in response to high osmolarity but remain unchanged if Hog1 is specifically inhibited. Twelve proteins contained multiple S/T-P motifs, some of which were phosphorylated dependently of Hog1 and some of which were phosphorylated independently of Hog1 [in total, 542 proteins harbored sites from more than one field (table S3)] and might therefore represent hubs where multiple signaling cues are integrated (*7*). Inhibitor susceptibility of some S/T-P motifs might have been masked due to pathway cross-talk from Kss1, the MAPK of the filamentous growth pathway (*26*), which could result in a relocation of Hog1 substrates to field 8. To determine whether the data were biased by Kss1 cross-talk, we determined stress-induced changes in the phosphorylome in cells in which both Hog1 and Kss1 were inactivated (fig. S2, A and B). A comparison of this data set with setup SR revealed a linear correlation (R = 0.61) for almost the entire overlapping set (>90%) of Hog1-independent S/T-P motifs (63% of S/T-P motifs of field 8 were covered), indicating that these sites were not affected by Kss1 cross-talk (fig. S2A). Hog1-dependent sites, on the other hand, did not show linear correlation except for Ser^{45} of Get2, which is probably targeted by both these MAPKs (fig. S2B). Furthermore, phosphorylation at Kss1 key residues Thr^{183} and Tyr^{185} was not altered by *as*-inhibitor treatment (fig. S2C and table S2), and its 4-fold increase in setup SR was negligible when compared to Hog1 (~70-fold) or Kss1 activity in a *hog1*Δ strain background (fig. S2D).

We therefore conclude that most of the stress-induced phosphorylation dynamics of S/T-P motifs are in fact phosphorylated not by Hog1 and Kss1 but by another proline-directed kinase (or kinases) and that the direct impact of Hog1 on the global phosphorylation pattern is probably smaller than anticipated.

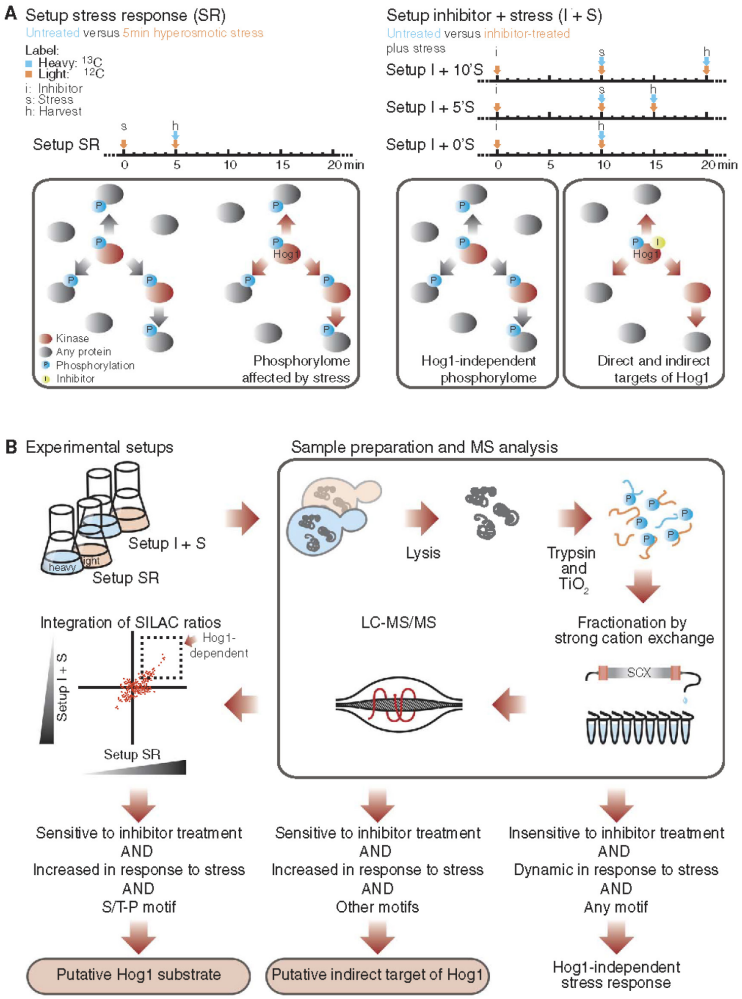

Fig. 1. A two-step quantitative proteomics strategy to identify substrates of the MAPK Hog1 in yeast expressing an ATP analog–sensitive form of Hog1 (Hog1as). (**A**) Timing diagram (top) and schematic illustration (bottom) of the two experimental setups. In setup SR (left), global changes in the yeast phosphorylome in response to hyperosmotic stress were determined; n = 6 biological replicates. In setups I + 0′S, I + 5′S, and I + 10′S (right), Hog1as was inactivated by the addition of *as*-inhibitor, an ATP analog, followed by hyperosmotic stress treatment for 0, 5, or 10 min, respectively; n = 2 biological replicates for each of the three experimental setups. Stress-activated kinases are indicated in red, and phosphorylation events are indicated in blue. The yellow dot indicates the *as*-inhibitor. (**B**) Schematic illustration of the applied workflow. Phosphorylation events displaying a greater than twofold increase or decrease in abundance between the SR and I + S setups were considered significant changes. The phosphorylated S/T-P motifs that increased in abundance in response to stress and showed sensitivity to inhibitor treatment were considered putative substrates of Hog1. SCX, strong cation exchange.

Identification of putative Hog1 substrates

The 36 S/T-P motifs in field 1 correspond to a total of 32 proteins that might represent direct targets of Hog1 (Table 1A and fig. S2E). To prevent the omission of targets due to incorrectly assigned phosphorylation sites, which included established hallmarks for Hog1 activity, such as Rck2 (Thr^{379} and Ser^{520}) (*15*), Hot1 (Thr^{153}) (*20*), Rgc1 (Ser^{975} and Thr^{774}), and Rgc2 (Thr^{808}) (*21*), as putative direct substrates of Hog1. In addition, we found previously undescribed phosphorylation sites in

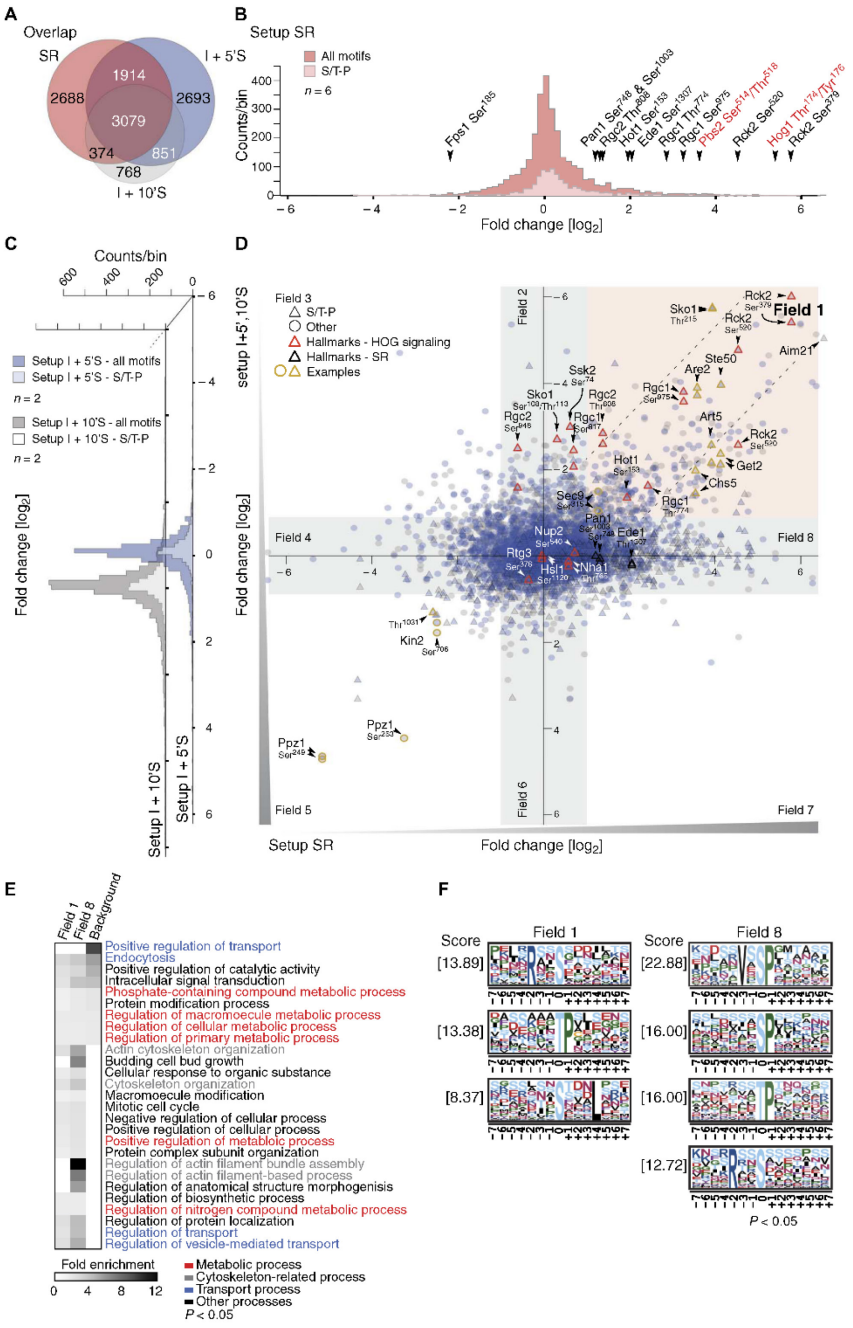

Fig. 2. Effects of hyperosmotic stress and Hog1 inhibition on the *S. cerevisiae* phosphorylome. (**A**) Venn diagram showing the overlap of unique phosphorylation sites between setups SR ($n = 6$), I + 5′S ($n = 2$), and I + 10′S ($n = 2$). (**B**) Histogram of SILAC ratios of quantified sites in setup SR. Light pink bins indicate the distribution of S/T-P motifs, and dark pink bins indicate other motifs. Ratios are $\log_2$-transformed. Hallmarks of osmostress and HOG signaling are highlighted with arrowheads; key residues of the MAPK Hog1 and the MAPKK Pbs2 are indicated in red. (**C**) Distribution of SILAC ratios of quantified sites in setups I + 5′S (blue bins) and I + 10′S (gray bins). S/T-P motifs, light blue and light gray bins, respectively; other motifs, dark blue and dark gray bins, respectively. Ratios are $\log_2$-transformed. (**D**) Scatter plot overlaying SILAC ratios of setups SR, I + 5′S, and I + 10′S. *x* axis, setup SR; *y* axis, setups I + 5′S (blue) and I + 10′S (gray), respectively; S/T-P motifs, triangles; other motifs, circles. Red outlines indicate hallmarks of HOG signaling; yellow outlines indicate examples discussed in the main text. Ratios are $\log_2$-transformed. (**E**) Heatmap of overrepresented GO terms in the individual fields defined in (D). Fold enrichment of biological processes; $P < 0.05$. Background, *S. cerevisiae* proteome. (**F**) Overrepresented motifs in the individual fields were detected with MotifX; $P < 0.05$ (see also fig. S1C).

well-established Hog1 targets, such as the transcription factor Sko1 (Thr^{215}) (*27*) and the adapter protein Ste50 (Thr^{244}) (*22*, *23*).

Next, we aimed to extract leads for additional putative Hog1 targets from our data sets, focusing on S/T-P motifs that showed susceptibility to inhibitor treatment but were not covered in setup SR. This group of sites was compared with published data from Kanshin *et al.* (*4*) and browsed for increased phosphorylation in the early response to hyperosmotic stress. We found three phosphorylation sites that fit these criteria: Ser^{790} of the Golgi-associated retrograde protein Vps53 (*28*), which has not previously been associated with the HOG pathway, Ser^{54} and Ser^{57} of the MAPKKK Ssk2 (*9*), and Ser^{227} of the retrograde and target of rapamycin pathway transcription factor Rtg3 (Table 1B) (*29*).

In a second approach to examine the data set for potential targets, we grouped S/T-P motifs that get phosphorylated in setup SR but were not covered in at least one of the inhibitor data sets. Again, we compared this group with the data set of Kanshin *et al.*, who hypothesized that conserved and putatively functional kinase-substrate interactions in the HOG response occur more rapidly than promiscuous interactions (*4*). This way, we were able to extract three additional candidates, namely, the trehalose synthase Tsl1 (Ser^{147} and Ser^{161}), the PAK-Ste20 family protein kinase Kic1 (Thr^{625}), and the uncharacterized protein Ynl115c (Ser^{244}) (Table 1B). Of these four phosphorylation sites, Ser^{161} of Tsl1 showed the largest increase in stress-induced phosphorylation (~17-fold) and therefore strongly qualified for being a bona fide target of Hog1. Because trehalose functions as an osmolyte and protects the plasma membrane in *Escherichia coli* (*30*), one could assume that it might exert a similar function in yeast in response to hyperosmotic stress (*31*, *32*). Given the potential link to the HOG pathway, which had not yet been investigated, we performed some further in-depth analysis of the Tsl1 phosphorylation pattern in response to stress and Hog1 inhibition using a validation strategy based on tandem affinity purification using a histidine-biotin tag (HTB) (*7*). We confirmed Hog1 dependency for phosphorylation of two S/T-P motifs of Tsl1: Ser^{135} and Ser^{147} (fig. S3).

Finally, we also considered S/T-P motifs as potentially interesting if they were identified in at least two of the inhibitor setups, even if no other information on stress dependency was available. Four phosphorylation sites fulfilled these criteria: Ser^{176} of Are2 (*33*), Ser^{602} of Rod1 (*34*), Ser^{477} of Ecm25 (*35*), and Thr^{67} of Ppz1 (*36*). Of this group, Ecm25 and Ppz1 were not identified by any other selection criteria described above (Table 1B). To complete our search, we browsed the data from setups I + 5′S and I + 10′S for quantifications relying solely on one peptide identification and found *as*-inhibitor–susceptible S/T-P motifs from 22 proteins that were quantified only in a single LC-MS run (table S4). It must be emphasized, however, that SILAC ratios based on a single identification must be considered as highly uncertain. This group contained some interesting candidates, for example, the transcription factor Smp1, the protein kinase Ste50, and the F-Bar protein Syp1, all of which have been previously connected to HOG signaling (*4*, *22*, *23*, *37*). The group also included protein kinases such as Akl1, Kin1, Rim15, and Ste20 (*38*–*41*).

In summary, our MS shotgun approach revealed a total of 40 putative target proteins of the MAPK Hog1: 32 from field 1, 6 based on the integration of our data with previously published data sets, and 2 additional candidates that were selected based on coinciding ratios in two of the inhibitor data sets. In total, this set contains 32 putative Hog1-substrate interactions that have not been described previously (Table 1).

Identification of Hog1-dependent secondary targets

Because Hog1 activity influences the activity of other kinases, we also expected indirect effects of HOG signaling to be prominent in Field 1. Indeed, 82.4% of the phosphopeptides in field 1 were phosphorylated at non–S/T-P motif sequences. We considered this group to represent putative indirect targets of Hog1 (table S5 and fig. S4A) and attempted to assign kinase dependencies for some of these phosphorylation sites. To do so, we initially searched for overrepresented peptide motifs and found R-X-X-S and S-X-X-X-L motifs to be significantly enriched (Fig. 2F). Motifs with an arginine at the P−3 position (R-X-X-S motifs) suggest the involvement of basophilic kinases, such as the members of the protein kinase A, G, and C (AGC) and CaMK group, or of the casein kinase I family (*42*). Additional hydrophobic residues at the P+4 position (S-X-X-X-L motif) further suggest the involvement of a particular subfamily of the CaMK group (*43*, *44*). HOG signaling has previously been connected to CaMK-like kinases (*15*, *45*, *46*). For example, it is well known that CaMK Rck2 is a target of the HOG pathway (*15*, *47*), and its key residues are fully phosphorylated within 60 s of stress induction (fig. S1B) (*4*). Hence, it seemed likely that Rck2-mediated phosphorylation events also accumulated in field 1. To systematically capture these, we performed an MS shotgun experiment using a strain lacking *RCK2* (setup *rck2*Δ). We found the Rck2-dependent phosphoproteome to be complex, including positive or negative changes in 13.46% of quantified phosphorylation sites. At least 316 sites, including 108 basophilic kinase motifs, corresponding to 219 proteins, were less phosphorylated in the *rck2*Δ strain than in wild-type cells in response to hyperosmotic stress (Fig. 3A and table S2). Rck2 seems to phosphorylate a large portion of the candidate indirect targets of Hog1 because most of the non–S/T-P motifs of field 1 were affected by *RCK2* deletion, whereas the impact of *RCK2* deletion on S/T-P motifs of field 1 was negligible (Fig. 3B and fig. S4, B to D). In total, we allocated 57 indirectly affected targets and an additional 48 stress- or inhibitor-responsive phosphorylation sites to Rck2 activity (table S2). Hence, we propose Rck2 as a major effector kinase of HOG signaling, influencing various cellular processes during osmostress.

Among the affected proteins, we found several suggested interactors of Rck2 (*48*–*50*) and 25 protein kinases from different families, including prominent basophilic kinases such as Gin4, Hsl1, Kcc4, Sch9, and Snf1 (Fig. 3C and table S2). These kinases most likely contribute to secondary responses within the HOG-Rck2 network, thus complicating the interpretation of kinase-substrate interactions. Such an example would be the regulation of the potassium transporter Trk1 (*36*, *51*, *52*) by the kinase Hal5 and the phosphatases Ppz1 and Ppz2, which have not previously been connected to HOG signaling. We found phosphorylation of Ser^{63} of Hal5 to be dependent on Rck2 (table S2), whereas Ppz1 and Ppz2 would, based on the MS data, possibly constitute direct targets of Hog1 (Table 1). These regulatory events might explain changes in the phosphorylation pattern of Trk1 because we found Ser^{412} and Ser^{414}, which are not present in S/T-P motifs, to increase in abundance in a stress- and HOG-dependent manner. Ser^{414} additionally showed susceptibility to deletion of *RCK2*, supporting a regulatory role for Rck2 in potassium transport (table S2).

To unravel further network hubs within the HOG-Rck2 network, we applied NetworKIN (*53*, *54*), an algorithm designed to predict kinase-substrate interactions (Fig. 3C). The enrichment for both R-X-X-S and S-X-X-X-L motifs points toward a particular family of kinases of the CaMK group that may act downstream of Hog1 and Rck2 (*42*, *44*, *55*). NetworKIN analysis showed that proteins with these motifs are likely targeted by Kin1, Kin2, Hsl1, Snf1, or Gin4 (Fig. 3C and fig. S5). However, key residues of the activation loops of these kinases either were

Table 1. Putative direct targets of Hog1. (**A**) Candidates extracted from field 1 that contain phosphorylated S/T-P and S/T-S/T-P motifs. SILAC ratios increasing ≥2-fold are highlighted in blue, and those increasing ≤0.5-fold are highlighted in yellow. Phosphoaccepting residues of S/T-P motifs are indicated in bold. "Up" indicates that phosphorylation of these sites was also reported to increase in response to osmostress by Kanshin *et al.* (*4*). (**B**) Candidates extracted by indirect evidence (see main text). SR n.a., not assigned in setup SR; I + S n.a., not assigned in inhibitor setups.

	Protein name	PhosphoSite	Field assignment	Setup SR	Setup I + 0′S	Setup I + 5′S	Setup I + 10′S	Setup *rck2*Δ	Motif	Kanshin *et al.* (*4*)	Known substrate	Reference
A	Aim21	**476**(S)	Field 1	93.37			0.03	0.01	PKA or STP	Up	No	
	Are2	**175**(S)	Field 1	12.03		0.08	0.07	0.07	STP		No	
	Art5	**158**(S)	Field 1	15.15	1.21	0.17	0.22	0.20	CaMK or STP	Up	No	
	Bck1	**765**(T)	Field 1	7,54		0.44		0.73	STP		No	
	Bck2	**258**(S)	Field 1	22.67		0.50			STP or SL		No	
	Boi1	**647**(T)	Field 1	7.55	1.08	0.48	0.51		STP		No	
	Bul1	107(T),**111**(T)	Field 1	25.96		0.67	0.37	0.17	PKA or STP		No	
	Chs5	**373**(T)	Field 1	11.70	0.95	0.36	0.25	0.91	STP		No	
	Ent3	**320**(T)	Field 1	11.14		0.38		1.18	STP		No	
	Epo1	**209**(S)	Field 1	9.49		0.21			STP		No	
	Erg11	**458**(S)	Field 1	4.88	0.95	0.46	0.40	0.93	STP		No	
	Ett1	33(S),**34**(T)	Field 1	2.19	0.46				STP		No	
	Gal11	**750**(T)	Field 1	5.08		0.47	0.65	1.75	STP		No	
	Get2	**45**(S)	Field 1	17.56		0.23	0.19	0.58	STP		No	
	Gip3	260(S),**264**(T)	Field 1	2.06		0.47			STP		No	
	Hal5	**63**(S),66(S)	Field 1	2.29		0.12			STP		No	
	Hot1	**153**(S)	Field 1	3.88	0.77	0.39		1.02	STP	Static	Yes	*20*
	Ppz2	**310**(S)	Field 1	3.35	1.26	0.48		0.79	STP		No	
	Rck2	**350**(T)	Field 1	5.48	0.67	0.20			STP		Yes	*15*
	Rck2	**379**(T)	Field 1	55.24		0.02	0.02		STP	Up	Yes	*15*
	Rck2	**520**(S)	Field 1	23.36		0.04	0.17		STP	Up	Yes	*15*
	Reg1	**898**(S)	Field 1	3.18		0.05		1.09	STP		No	
	Rgc1	**774**(T)	Field 1	5.42		0.32		0.56	STP		Yes	*21*
	Rgc1	**975**(S)	Field 1	9.67		0.07	0.08		STP	Up	Yes	*21*
	Rgc2/Ask10	**808**(T)	Field 1	2.62	1.06	0.14	0.16	1.06	STP	Up	Yes	*21*
	Rod1	**602**(S),608(S)	Field 1	2.17		0.37			STP or SL		No	
	Sfl1	**556**(S)	Field 1	7.43		1.00	0.35		STP		No	
	Sko1	**215**(T)	Field 1	15.40	0.97	0.02	0.02	1.00	STP	Up	Yes	*69*
	Spt20	**516**(T)	Field 1	7.04	0.88	0.56	0.45	0.88	STP	Static	No	
	Ste50	**244**(T)	Field 1	17.64		0.06		0.91	STP		Yes	*22, 23*
	Tif4632	**196**(T)	Field 1	2.34	0.38	0.29		0.74	STP	Up	No	
	Tod6	**152**(T)	Field 1	24.46		0.42			STP		No	
	Vas1	**294**(S)	Field 1	2.74		0.56	0.40	1.25	STP		No	

continued on next page

	Protein name	PhosphoSite	Field assignment	Setup SR	Setup I + 0′S	Setup I + 5′S	Setup I + 10′S	Setup *rck2Δ*	Motif	Kanshin *et al.* (*4*)	Known substrate	Reference
	Vps9	**375**(S)	Field 1	3.95	0.80	0.37	0.26	0.76	STP	Up	No	
	Ylr257W	**8**(T)	Field 1	2.49	0.81	0.61	0.50	0.64	CaMK or STP		No	
	Ylr257W	**7**(S)	Field 1	2.53	0.95		0.50		STP or SL		No	
B	Rtg3	**227**(S)	SR n.a.		0.94	0.46	0.70	0.87	STP	Up	Yes	*29*
	Ssk2	**54**(S),**57**(S)	SR n.a.			0.22			CaMK or STP	Up	Yes	*9*
	Vps53	**790**(S)	SR n.a.			0.15	0.17	0.07	CaMK or STP	Up	No	
	Kic1	**625**(T)	I + S n.a.	6.82					STP	Up	No	
	Tsl1	**147**(S)	I + S n.a.	4.16				0.36	CaMK or STP	Up	No	
	Tsl1	**161**(S)	I + S n.a.	16.97					CaMK or STP	Up	No	
	Ynl115C	**244**(S)	I + S n.a.	4.11					STP	Up	No	
	Ecm25	463(T),**477**(S)	SR n.a.			0.18	0.18		STP		No	
	Ppz1	49(S),**67**(T)	SR n.a.			0.36	0.31		STP		No	

not identified in our MS experiments or did not reveal HOG-Rck2–dependent activation, as in the case of Snf1, for example (table S2). Hence, we considered an alternative approach and hypothesized that, as previously suggested, functional phosphorylation sites would be more likely to be conserved than promiscuous sites (*4*). We therefore performed sequence alignments for the members of the individual kinase families and mapped affected phosphorylation sites obtained from our MS shotgun data sets. Thereby, we identified a conserved cluster of multiple phosphorylation sites, including an S/T-P motif, at the C-terminal regulatory domain of Kin1 and Kin2 (Fig. 3D) (*39*, *56*, *57*). Although the cluster could not be clearly assigned as a Hog1 or Rck2 substrate, the overall phosphorylation pattern hinted at dependency on HOG signaling. Furthermore, among the NetworKIN-predicted downstream targets of Kin1 or Kin2, we found Ser^{351} of Sec9, which is an in vitro substrate of these kinases (Fig. 3D) (*57*). This observation suggested that the kinases might become activated in response to hyperosmotic stress and puts forward the hypothesis that Kin1 and Kin2 are activated in a manner that depends on HOG signaling.

Validation of Hog1-substrate interactions

To confirm whether the newly identified putative target proteins (Table 1) directly interact with Hog1, we performed the so-called M-track protein-protein proximity assay (*18*, *58*), which is designed to capture transient interactions, such as those between kinases and their substrates. To do so, we tagged each of the candidate proteins with an active enzymatic domain from the SUV39 histone lysine methyltransferase [HKMT-myc (*58*)]. Hog1 was fused with the prey sequence protA-H3 (*58*), which is a tobacco etch virus (TEV) protease–cleavable histone H3 tag fused to protein A and hemagglutinin (HA) tags that becomes permanently methylated upon coming into close proximity with the candidate protein bearing the HKMT-myc moiety (Fig. 4A). Each tagged candidate was co-expressed with Hog1-protA-H3 in yeast cells, and the cells were subjected to various treatments. The proximity signal was detected by Western blotting using an antibody directed against triple-methylated lysine 9 of histone H3 (me3K9H3) (Fig. 4B). We created functional HKMT-myc tag fusions for 35 of the 40 candidates described above (Table 1). Our analysis further included the following bait proteins and controls: (i) the kinases Akl1 and Rim15 (*38*, *41*), the transcription factor Tda9 (*59*), and membrane protein Skg6 (*60*) from table S4; (ii) trehalase Nth1 (*61*), because we discovered a possible link between Hog1 signaling and trehalose metabolism, further supported by an S/T-P–containing peptide that was affected under stress conditions (table S2 and fig. S6); (iii) the potassium transporter Trk1, because three regulators of this transporter were identified as putative Hog1 substrates; (iv) three known targets of Hog1, the osmosensor Sho1 (*62*), the Na^+ and H^+ antiporter Nha1 (*63*), and the nucleoporin Nup2 (*64*); (v) paralogs of three factors, Boi2, Bul2, and Dot6; and, finally, (vi) field 8–annotated proteins Mlf3, Nob1, Vts1, and Yol019w and nuclear proteins Bud13, Cac2, and Lin1 as background controls. Background signal intensity was defined using a yeast strain expressing only Hog1-protA-H3.

We first analyzed whole-cell lysates (WCLs) in response to increased NaCl or sorbitol concentrations. Sorbitol treatment also activates Hog1 (*65*) but does not exert the same potentially toxic effects as sodium; thus, Hog1-substrate interactions captured under this condition additionally confirm the validity of our approach. To saturate proximity signals, we exposed cells for 40 min to the corresponding stimulus. Nineteen of our candidates showed induction of the proximity signal after stress treatment, whereas the negative control (Hog1-protA-H3 alone) did not. Field 8–annotated proteins did not indicate proximity to Hog1 (Fig. 4C). Most of the strong proximity signals were observed with sorbitol-treated samples (Fig. 4, C and D, and fig. S7). Some of the candidate factors (for example, Erg11) showed high proximity signals even in the unstressed state, suggesting an interaction with Hog1 under isosmotic conditions. Finally, we also recovered candidate factors that were selected by less-stringent search criteria, such as, for example, Kin1 and Kin2 or Tsl1 and Nth1 (Fig. 4D).

However, because of the high variance in the signal intensities, the sensitivity of the applied statistical methods on the accumulated data

was not optimal. To reduce variance and improve the signal-to-noise ratio, we performed additional M-track assays using a tag cleavage-enrichment system (*58*) and analyzed only the response to sorbitol (Fig. 4E). To identify significantly increased proximity signals, we applied Welch's *t* test to compare signals to the negative control (Hog1-protA-H3 alone). Thirty-five (74.5%) of the 47 kinase-substrate interactions we tested showed proximity signal intensities significantly above background intensity (based on a q value of <0.05). Within this group of proximity signals, 28 (including 24 proteins that have not previously been associated with Hog1) showed a q value of <0.01, implying a direct interaction with Hog1 after stress induction (Fig. 4E). This group of proteins included well-established hallmarks of HOG signaling, such as Hot1, Nup2, Sko1, Rgc1, Sho1, and Ste50. Among the group of candidates with moderate proximity signals ($q > 0.01$ and $q < 0.05$), we found three proteins containing both Hog1-dependent (S/T-P motifs) and Rck2-dependent sites: Boi1, Gip3, and Rod1. This group also contained Akl1 and Bul1, both of which contain phosphorylation sites that were stress- and inhibitor-responsive as well as Rck2-dependent (fig. S4D and table S2). This observation might indicate that either these sites are phosphorylated by both Hog1 and Rck2 or the corresponding proteins contain both Hog1-dependent and Rck2-dependent sites. In summary, our independent validation showed that most of the putative targets identified in our MS shotgun experiments interact with the MAPK.

Testing for osmosensitive phenotypes of the putative direct targets of Hog1

We next tested the newly identified Hog1 targets for potential functional relevance in osmostress adaptation and survival by performing growth assays. To capture short-term stress effects, we compared the growth rates of hyperosmotically challenged and unstressed deletion mutants for each of these proteins relative to those of wild-type and *hog1*Δ controls. Eleven of the tested deletion mutants showed osmosensitive growth outside the fluctuation margin of the wild type, and four of these had not previously been associated with osmosensitivity, namely, *reg1*Δ, *rod1*Δ, *vps9*Δ, and *ylr275w*Δ (Fig. 5, A and B).

We determined the effects of long-term stress on growth with serial dilution droplet tests on complete medium (YPD) plates containing one of the following stressors: 0.5 M NaCl, 0.8 M NaCl, 1.2 M NaCl, 0.8 M KCl, 1.2 M KCl, or 1.2 M sorbitol. *hog1*Δ cells were most sensitive to osmotic shock, whereas wild-type and all the deletion mutants showed lower sensitivity to osmotic stress. Six of the tested candidates, including Rck2, were highly osmosensitive, indicating that they play an essential role in the response to increased extracellular osmolarity (Fig. 5C). Two additional deletion strains, *spt20*Δ and *vps53*Δ, showed weak sensitivity to osmotic stress (fig. S8). Because these proteins are associated with processes other than increasing the intracellular concentration of osmolytes, we assume that Hog1 might affect additional functional modules in a posttranslational manner. Results from growth curve analysis and serial dilution droplet tests for different conditions (NaCl, sorbitol, and KCl) are summarized in Fig. 5D.

Signaling network revealing yet undiscovered functions of the MAPK Hog1

Our approach allowed the identification of several previously unidentified target proteins of Hog1; however, the total number is too small for a statistically solid GO enrichment analysis. Seven of the protein candidates fall into the functional GO category of transcription and translation, four into the category of endocytosis, three into vesicle-related processes, and four into stress and starvation signaling (Fig. 6). For a better overview, we created a protein network based on known protein-protein

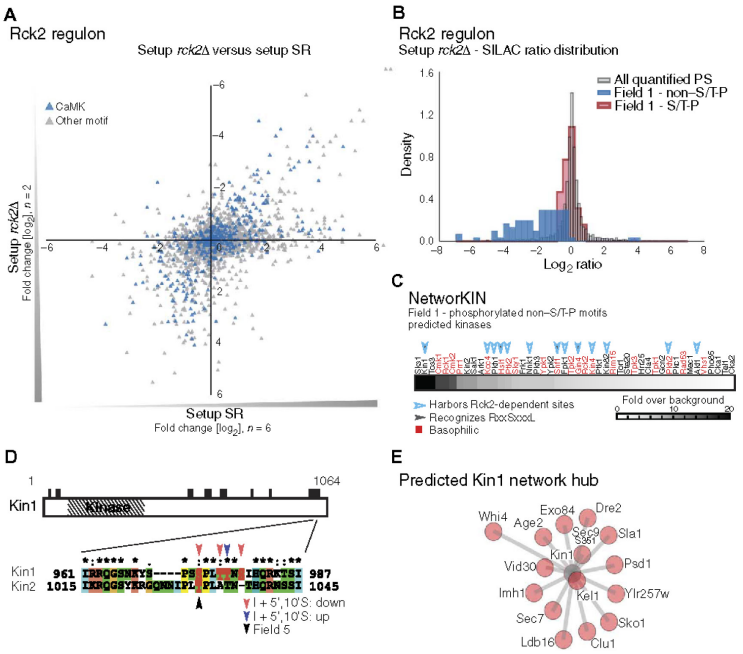

Fig. 3. The kinase Rck2 is a major effector of HOG signaling. (**A**) Scatter plot comparing distribution of quantified phosphorylation sites between setup *rck2*Δ [SILAC ratio, *rck2*Δ (light)/wild-type (heavy), both treated with NaCl; $n = 2$] and setup SR ($n = 6$). (**B**) Histogram showing the distribution of SILAC ratios of quantified sites in setup *rck2*Δ. Red, field 1 S/T-P motifs; blue, results for field 1 non–S/T-P motifs; gray, all quantified phosphorylation sites (PS). (**C**) Prediction of kinases involved in the regulation of the indirect targets of Hog1. Basophilic kinases are indicated in red. Filled arrowheads, kinases recognizing S-X-X-X-L motifs; open arrowheads, kinases containing Rck2-dependent phosphorylation sites. (**D**) Diagram showing phosphorylated residues (black bars) of the kinase Kin1. Inset illustrates the conserved S/T-P motifs in Kin1 and Kin2, which include an *as*-inhibitor–sensitive serine [Ser^{973} in Kin1 (black arrowhead)]. Phosphorylation at highlighted residues was either decreased (red arrowheads) or increased (blue arrowhead) upon inhibitor treatment or associated with field 5 (black arrowhead). (**E**) Predicted interactions between Kin1 (gray) and substrates (red) based on NetworKIN analysis. The relative length of each edge was calculated according to NetworKIN scores: the closer to the kinase, the higher the score.

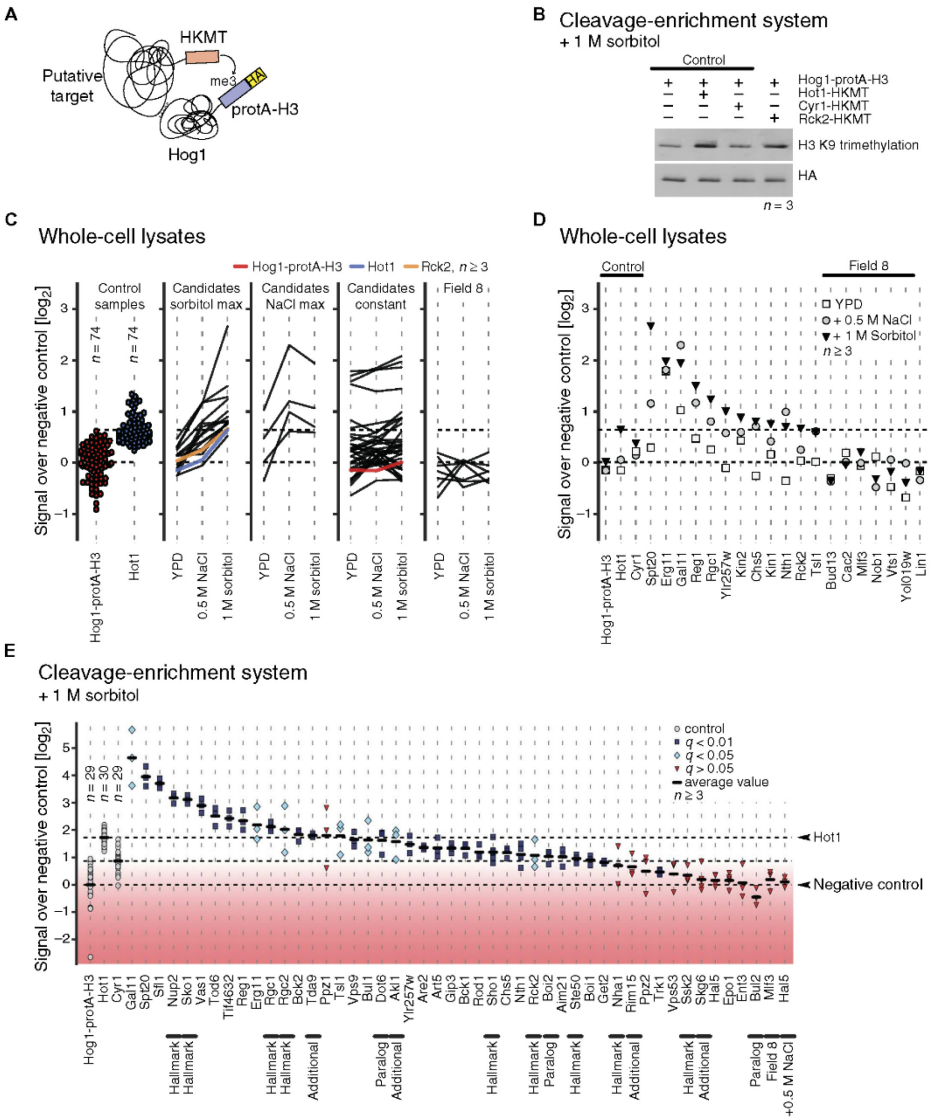

Fig. 4. Validation of kinase-substrate interactions. (**A**) Cartoon illustrating the M-track protein-protein proximity assay. Hog1 is tagged with protA-H3 (prey), which gets permanently methylated when it is in close proximity to a putative target protein that is fused to an active domain of a histone lysine methyltransferase (HKMT), posing as bait. (**B**) Representative Western blot showing M-track results obtained for Rck2 using cleavage enrichment system. $n \geq 3$ replicates per sample. (**C**) M-track proximity signals in whole-cell extracts, comparing unstressed conditions to conditions of increased NaCl or sorbitol. Each line corresponds to one protein. $n \geq 3$ replicates per sample per condition. From left to right: loading controls, candidate proteins with maximum induction under sorbitol treatment, candidate proteins with maximum induction under NaCl treatment, candidate proteins that were not induced by sorbitol or NaCl, proteins derived from field 8. Ratios are $\log_2$-transformed. (**D**) Detailed proximity signals for tested targets described in the main text. $n \geq 3$ replicates per sample. Ratios are $\log_2$-transformed. (**E**) Quantification of proximity signals. $n \geq 3$ replicates per sample. Black lines indicate average proximity signal. Proximity signals that differ significantly from background are marked in light blue diamonds ($q < 0.05$ and $q > 0.01$) and dark blue squares ($q < 0.01$). The red gradient indicates low confidence based on q values. One-tailed Welch's t test was applied, and P values were corrected for multiple testing by the Benjamini-Hochberg procedure. Hallmarks of HOG signaling are noted, and proteins that were chosen for validation based on less-stringent criteria are marked as "additional."

interactions from the STRING (Search Tool for the Retrieval of Interacting Genes/Proteins) database (*66*–*68*) using a list of 47 known and newly identified targets of Hog1 as input. Many of the cellular functions and pathways known to be directly affected by Hog1 signaling were captured, including cell cycle, signaling, nuclear pore complex, endocytosis, and glycerol channels plus their regulators. Moreover, the network included other molecular functions that have not been previously associated with HOG signaling, such as the Exomer and GET complexes, both of which are involved in vesicular transport to the Golgi; trehalose and ergosterol metabolism; and the SAGA, Mediator, and Rpd3 complex (Fig. 6). In summary, our analysis emphasizes that the Hog1-mediated response to hyperosmotic stress affects a broader set of functional units than previously anticipated.

DISCUSSION

The study presented here provides a comprehensive MS shotgun analysis designed to monitor the impact of Hog1 activity on the phosphoproteome of *S. cerevisiae*. To ensure specificity of the screening, we integrated two experimental setups that monitor changes in phosphorylation patterns upon both exposure to hyperosmotic stress and inactivation of Hog1. Using a protein-protein proximity assay, we further validated the candidates that we predicted to interact directly with Hog1 as substrates (*18*). In addition, we evaluated contributions made by the effector kinase Rck2. Our approach thus generated a comprehensive view of the Hog1 network, revealing at least 25 previously unidentified substrates and a broad set of indirect target proteins that extend our understanding of the HOG signaling system (Table 1).

Evaluating known hallmarks of the Hog1 response

Signaling through Hog1 has been previously associated with various cellular processes required for the adaptation to hyperosmotic stress, such as the regulation of intracellular glycerol concentration, gene expression, and cell cycle arrest. As a proof of principle for our experimental strategy, we expected to detect phosphosites of established Hog1 substrates that are involved in these processes, which was true for Hot1 (*20*), Rck2 (*15*), Rgc1, Rgc2 (*21*), Rtg3 (*29*), Sko1 (*69*), Ssk2 (*9*), and Ste50 (Fig. 2C and Table 1) (*22*, *23*).

However, because of the inherent incompleteness of MS shotgun data sets, not all described hallmarks of Hog1 signaling were covered. We did not identify or quantify the relevant phosphorylation sites of the osmosensor Sho1 (*62*), the CDK inhibitor Sic1 (*70*), or some other proteins previously implicated in Hog1 responses (*37*, *71*–*73*). Notably, some known Hog1 target sites (*29*, *45*, *63*, *64*) were influenced by neither stress nor inhibitor treatment (Fig. 2 and table S2), which agrees with previous observations (*4*, *6*). Given that Hog1 dependency of many of these sites has been established using in vitro kinase assays (*29*, *45*, *63*, *64*), it is questionable whether they are genuine in vivo substrates of Hog1. Alternatively, such observations could be explained by promiscuous modifications due to a related kinase(s) such as Kss1. We addressed this possibility and provided evidence of Kss1 effectively having only a minor impact on our data (fig. S2). Another possible explanation could be that these sites are already saturated for phosphorylation by basal Hog1 activity. If the duration of inhibitor treatment is shorter than the turnover kinetics of phosphorylation, a decrease of phosphorylation events at these sites would not have been readily detected in our experiments.

Other well-established Hog1 target sites showed more clear patterns of phosphorylation that were dependent on Hog1 but independent of osmotic stress (field 2)—for example, Ser^{108} and Thr^{113} of Sko1 and Ser^{74} of Ssk2 (Fig. 2D and table S2). These S/T-P motifs are probably already modified to saturation by Hog1 under isosmotic conditions or undergo rapid dephosphorylation. These observations make it apparent that approaches to measure the turnover rates at individual sites are needed in the future to address such speculations.

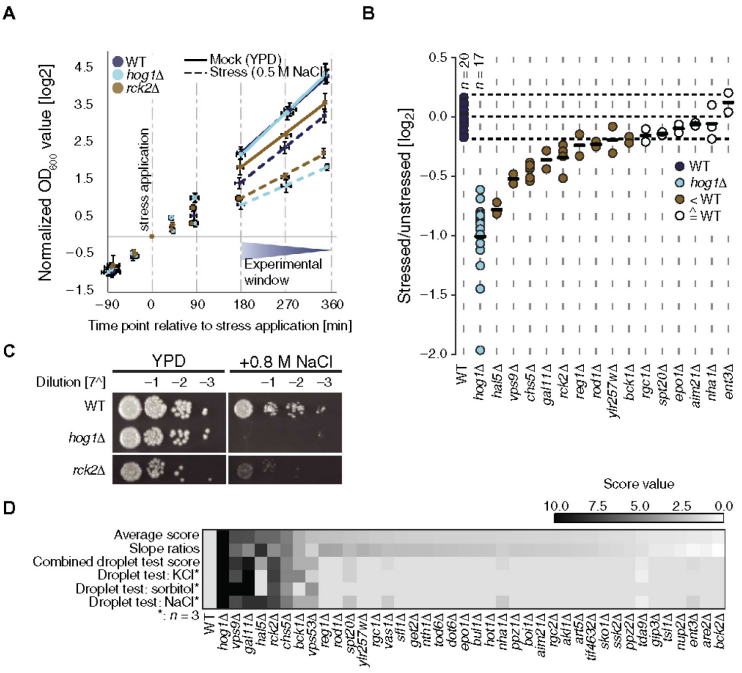

Fig. 5. Characterization of osmosensitive phenotypes. (**A**) Log_2-transformed growth curves of wild-type (WT), *hog1Δ*, and *rck2Δ* cells in the absence of hyperosmotic stress and after induction of hyperosmotic stress. OD_{600}, optical density at 600 nm. (**B**) Stressed/unstressed (mock) ratios of log-transformed growth curve slopes depicted in (A); $n \geq 2$ replicates per sample. (**C**) Serial dilution droplet test of the individual deletion mutants on YPD plates on YPD + 0.8 M NaCl. (**D**) Heatmap illustrating scaled scores from growth curve analysis (slope ratios) and dilution droplet tests under different conditions. Rows are sorted according to combined average score (0 to 10).

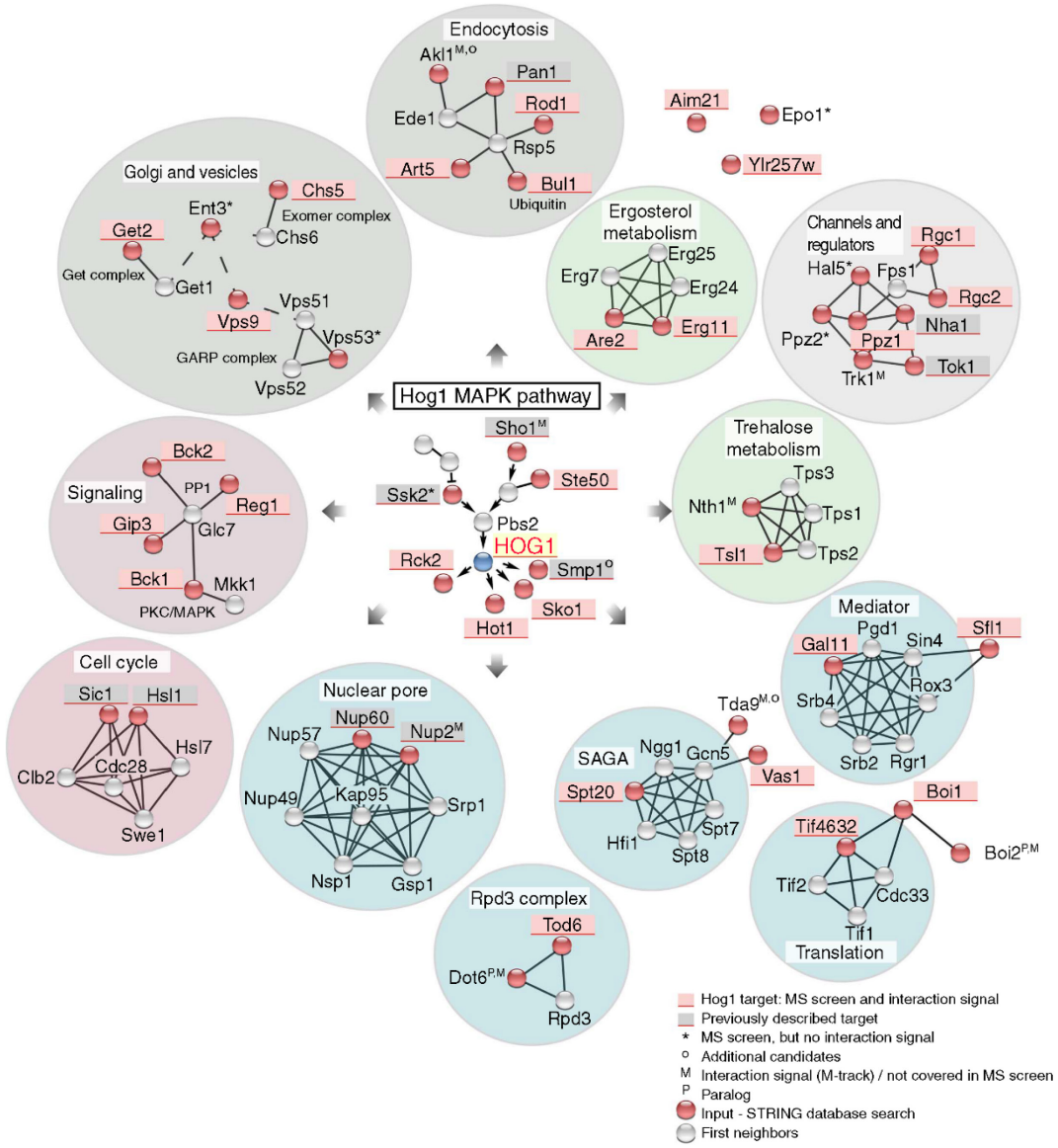

Fig. 6. Hog1 network based on STRING. Putative Hog1 target proteins from field 1 that also showed proximity to Hog1 are shaded in red. Previously described Hog1 substrates not covered in our MS data or lacking a proximity signal to Hog1 are shaded in gray. Red circles indicate protein targets derived from the shotgun screen, with gray circles indicating their first neighbor according to STRING. Periphery: Shaded circles enclosing groups of proteins highlight functional groups, such as metabolism (green) and gene expression regulation (blue).

Hog1-dependent phosphorylation events connected to osmoadaptation

Our analysis provides insights into some open questions regarding the influence of Hog1 on the cellular metabolism (Fig. 6) (*11*), such as the previously underestimated interconnection of Hog1 signaling and trehalose metabolism and ergosterol biosynthesis. Although hyperosmotic stress tolerance in yeast has been primarily linked to glycerol production (*13*), it is also correlated with accumulation of trehalose (*31, 32*). This disaccharide is produced by the trehalose 6-phosphate synthase/phosphatase complex, which is composed of the catalytic subunit Tps1, the phosphatase Tps2, and the regulatory subunit Tsl1. When it is dispensable, trehalose is degraded by the neutral trehalases Nth1 and Nth2. In addition to being a candidate substrate of Hog1, Nth1 is also targeted by PKA (*74–77*), and we recovered a phosphorylation event at Ser^{83} of Nth1, which lies in a predicted PKA target motif. The phosphorylation of this site decreased in response to stress (table S2), which is in line with previous observations on PKA-targeted motifs that are transiently affected under hyperosmotic stress conditions (*78*). We also recovered a phosphorylation event at Nth1 Ser^{66} (fig. S6), which is targeted by Cdk1 to coordinate the cell cycle with central carbon metabolism (*79, 80*). Notably, a peptide including unphosphorylated Ser^{66} decreased fivefold upon hyperosmotic stress (table S2), suggesting stress dependency of Nth1 as well. This observation, along with our detection of a significant Hog1-Nth1 proximity signal (Fig. 4E), leads us to propose that Nth1 is a direct target of Hog1, coinciding with an increase in Nth1 activity during recovery from stress (*61*). Moreover, we demonstrated Hog1-dependent changes in the phosphorylation pattern of Tsl1 (fig. S3) and prove proximity to Hog1 as well (Fig. 4E). Tps3, a known paralog of Tsl1 (*81*), was not recovered as a Hog1 target in our analysis. Although the function of trehalose during cell stress is not fully understood and trehalose is usually connected to heat stress (*31, 77, 82*), it is a widespread assumption that trehalose is somehow involved in protecting and preserving membrane structure (*83*). Similarly, sterols, which are essential components of the eukaryotic plasma membrane that affect the fluidity and permeability of the membrane, have been implicated in osmostress adaptation in yeast, and transcription of *ERG* genes is negatively regulated by Hog1 (*84*). Here, we provide evidence that Erg11, a lanosterol 14-α-demethylase, is directly targeted by Hog1, suggesting a transcription-independent and thereby faster mechanism for controlling ergosterol biosynthesis. These observations could thus provide novel insights into the mechanisms of plasma membrane protection during hyperosmotic stress.

Besides plasma membrane–related processes, several proteins related to vesicular transport as part of the endocytosis, exocytosis, and retrograde transport machineries were recovered as Hog1 substrates in our analysis. Our findings regarding the serine-threonine kinase Akl1 as a potential Hog1 target (*38, 85*) agree with previous associations of the actin cytoskeleton regulatory complex member Pan1 with Hog1 (*7*). Both Akl1 and Pan1 are key constituents of the early endocytic machinery (*86–90*) that could be affected by Hog1-mediated phosphorylation. Regarding exocytosis, we identified Chs5, a scaffold protein of the exomer (*91–93*) complex, as a potential Hog1 substrate. Finally, Hog1-dependent phosphorylations of downstream kinases and phosphatases suggest the involvement of yet other signaling pathways, such as protein kinase C [Bck1 (*94, 95*)] and protein phosphatase 1 [Reg1 and Gip3 (*96*)] signaling.

To explore additional putative Hog1-substrate interactions, we also took into account fold changes of peptide variants containing potential target sites but carrying phosphogroups at different positions, as well as their respective unphosphorylated variants. If alternative, or even unphosphorylated, peptide variants showed dependency on Hog1, the corresponding protein might be somehow affected by Hog1 signaling. The corresponding peptides could then harbor phosphorylation sites that, although not necessarily covered in our MS experiment, might be affected by Hog1 (for example, see Ppz1 in Fig. 2C, field 5). These considerations pointed toward Kin1 and Kin2 (*39, 56, 57*) because their detected phosphopeptides resided in field 5. The overall behavior of these sites suggested a Hog1-dependent phosphorylation at a conserved S/T-P motif at the C terminus (Fig. 3D). Using the M-track assay, we confirmed proximity of these proteins to Hog1 in response to sorbitol treatment (Fig. 4D). Both of these kinases belong to the Snf1 family of the CaMK group, which require structural rearrangements to unmask the kinase domain for activation. By analogy to Rck2 (*15*), Hog1 might affect exposure of the activation loop by phosphorylating C-terminal sites of these kinases. The only substrate of these kinases suggested so far, Ser^{351} of the t-SNARE protein Sec9 (*57*), was found among the group of proteins that we identified as indirect targets of Hog1.

The high number of indirectly affected targets of Hog1 we identified extends the diversity of putative cellular functions of Hog1. In a first attempt to dissect this signaling system into distinct kinase-target cascades, we focused on the proteins indirectly targeted by Hog1 through the CaMK Rck2, which reside in field 1. We found the Rck2 network to be surprisingly complex, encompassing a large number of proteins of diverse cellular functions. The impact of *rck2*Δ under stress conditions on the sites of field 1 was vast when compared to the set directly modified by Hog1. Rck2 seems to constitute a central hub of an underlying phosphorylation network because phosphorylation sites of at least 16 kinases were affected by *rck2*Δ. Some proteins also seemed to integrate Hog1 and Rck2 signaling, either by having separate Hog1 and Rck2 phosphorylation sites or by having a phosphorylation site that could be targeted by either kinase. We conclude that the indirect targets of Hog1 are, to a large extent, controlled by Rck2 and therefore propose Rck2 as a major effector kinase of Hog1 signaling. Correspondingly, growth of a *RCK2* deletion mutant was severely diminished in response to various hyperosmotic stress conditions. It will be interesting to see how future studies unravel the complexity of the Rck2 network, perhaps by applying a similar experimental strategy, as presented here.

Hog1 substrates exerting diverse cellular functions

Babazadeh *et al.* found that rewiring osmostress signaling through the Kss1 MAPK network reconstitutes osmoadaptation in *hog1*Δ cells (*97*). This reconstitution approach revealed that osmostress-induced upregulation of intracellular glycerol concentration is sufficient for successful osmoadaptation. The authors further anticipated that the number of MAPK functions essential for the response might be smaller than estimated from knockout approaches and genome-wide analyses. However, if increasing intracellular glycerol concentration is sufficient for survival of and adaptation to hyperosmotic stress, it remains unclear why Hog1 would—directly and indirectly—affect such a variety of different cellular functions.

We challenged this hypothesis by analyzing growth phenotypes of deletion mutants of the identified candidate proteins and, for some, observed growth effects of differing severity from one another in response to hyperosmotic stress treatment. Although we cannot fully exclude that those targets could be bystander substrates that do not severely affect growth under hyperosmotic stress, the observed differences on growth under stress conditions indicate that some of the Hog1-modified processes might have more or less impact on overall cell physiology and

growth rate. Proteins that appear to have only a subtle effect on cellular fitness during stress might be of more relevance when cells become exposed to continuous fluctuations in extracellular osmolarity or exhibit a cumulative phenotype when combined. It is intriguing to speculate that under constant fluctuation of environmental conditions, such minor adjustments of phosphorylation patterns are important for competitive fitness.

MATERIALS AND METHODS

Yeast strain and plasmid construction

Yeast strains and plasmids are listed in tables S6 and S7. Yeast strains WR557 (W303-1A SILAC *Hog1as*, Mat a) and WR564 (W303-1A SILAC *Hog1as*, Mat α) were obtained from a cross of WR210 with WR549 (*7*). Endogenous tagging (HTBeaq) and deletion mutations (*kss1*Δ and *rck2*Δ) were obtained by methods described in (*7*, *98*–*100*). Yeast strains used in M-track assays were generated as described in (*58*) using a strain library available from Life Technologies [http://clones.thermofisher.com/; (*101*)].

Growth conditions

Yeast cells were grown shaking (200 rpm) at 30°C in synthetic medium (0.17% yeast nitrogen base, 0.5% ammonium sulfate, 2% glucose, and amino acids as required) or rich medium (YPD; 1% yeast extract, 2% peptone, and 2% glucose) for at least seven generations until mid-log phase (OD_{600} ~1). For MS shotgun experiments (summarized in table S8), cells were subsequently treated, according to the experimental setup, with either 0.5 M NaCl for 5 min (setups SR and *rck2*Δ) or addition of the *as*-inhibitor {1-isopropyl-3-(phenylethynyl)-1*H*-pyrazolo[3,4-*d*]pyrimidin-4-amine}; a gift from M. Grøtli at the University of Gothenburg] at a final concentration of 5 μM for 10 min (setup I + 0'S) with subsequent salt treatment (0.5 M NaCl) for 5 or 10 min (setups HKi, I + 5'S, I + 10'S, respectively). For HTB purifications, stress and (if applied) inhibitor treatment were similar to setups SR and I + 5'S. Conditions for growth and proximity assays are described below.

SILAC labeling

SILAC labeling was performed as described previously (*3*, *7*, *17*). For the experiments involving the analog-sensitive inhibitor targeted at the Hog1 kinase, a yeast strain containing the *Hog1as* allele was used. With the addition of the inhibitor to the cell culture (final concentration, 5 μm) for 10 min, we ensure full inactivation of the Hog1 kinase. The inhibitor is designed to block the vicinity of the kinase that is usually reserved for ATP binding (ATP pocket) (*19*). Details on the experimental setups are provided in table S8.

Purification and MS analysis

MS shotgun experiments were performed as described previously (*7*). Briefly, cells were harvested by filtration and proteins were extracted using TRIzol (Invitrogen) (*7*). Tryptic digests were subjected to TiO_2 enrichment (*102*, *103*). Phosphopeptides were fractionated offline by strong cation exchange chromatography and analyzed on a reversed-phase nano–high-performance LC-MS system coupled with an electrospray ionization interface (Proxeon Biosystems). MS analysis was performed using a Linear Trap Quadropole Orbitrap Velos (collision-induced dissociation mode) or a Q Exactive (higher-energy collisional dissociation mode) mass spectrometer (Thermo Fisher Scientific). Data analysis was performed using the SEQUEST algorithm (Proteome Discoverer 1.3 and 1.4). Parameter settings are described in the corresponding data sets in PRIDE (see submissions PXD004294 to PXD004300) (*104*). We performed both forward and reverse (decoy) searches and calculated protein and peptide false discovery rate (FDR) <1%. MS analysis of affinity-purified proteins was performed as described previously (*7*).

Computational analysis of (phospho)peptide ratios

Normalization of data was performed as follows: Correction factors for the experiments were calculated as the geometric mean of the light-to-heavy (L/H) ratios for all unphosphorylated peptides that contained either zero, one, two, etc., prolines (necessary correction for the signal loss due to arginine-proline conversion). The ratios measured for the phosphopeptides were divided by the correction factor.

To facilitate interpretation of phosphorylation sites, we grouped peptides together where the same residues are phosphorylated, regardless of potential missed cleavages or additional modifications such as oxidation (corresponding to a so-called "phosphorylation site group"). The eventual ratio for the phosphorylation site group is an average over all peptide ratios available in the group. Note that this kind of grouping could not be performed for the unphosphorylated peptide counterparts; however, we calculated the average and median of ratios corresponding to peptides of each protein, thereby estimating the impact experimental conditions had on the overall protein ratio.

For the analysis of the resulting peptide spectrum matches (PSMs) (FDR calculation, normalization of ratios, and extraction of quantified phosphorylation sites), we used in-house Python scripts (Python Software Foundation, Python Language Reference, version 2.7; www.python.org). The scripts include a library of functions for extracting forward and reverse PSMs and the search summary for .msf files, allowing easier and much faster handling of the data. All scripts and functions are available on demand.

GO enrichment analysis

GO enrichment analyses were performed (http://geneontology.org/page/go-enrichment-analysis) using the PANTHER classification system (*105*). Gene ontologies from the category "biological process" (GO level 5) were extracted (corrected *P* value of fold enrichments <0.05); note that GO levels for each term have been downloaded from SUPERFAMILY (http://supfam.cs.bris.ac.uk/SUPERFAMILY/) for proteins of each field designated in Fig. 2.

Kinase prediction analyses

We used the MotifX algorithm (*24*, *25*) to identify overrepresented linear motifs within our set of dynamic phosphorylation sites. Each field was analyzed separately. The following settings were applied: minimum occurrences, 10; background, *Saccharomyces* Genome Database proteome. A binomial test was used to identify statistically enriched motifs, using a *P* value of 0.05 as a significance cutoff. Furthermore, we applied the NetworKIN algorithm (*54*) with default settings for kinase predictions for the dynamic phosphorylation sites. We determined the relative frequency for each kinase in individual fields and divided the resulting values by kinase frequencies that occur in the group of static phosphorylation sites (cutoff for graph set at 0.3). Thereby, we get an interpretable relative enrichment of kinases over a background represented by static phosphorylation sites.

Protein network analysis

Protein-protein interaction network for all putative targets of Hog1 was created using STRING database (version 10.0) (*66*). All factors listed in Fig. 4F were used as search entries, with first neighbors automatically included in the network by the STRING database. All interaction

predictions were based on physical, genetic, and text mining evidence types with the minimal confidence score of >0.7 (high), and a total of 40 white nodes and 0 interactors were allowed. We used the integrated MCL clustering algorithm according to STRING clustering instructions; clustering level was set to 3.

Growth tests

W303-1A wild-type and deletion mutant strains were grown until mid-log phase, shifted to an OD_{600} of 0.025 to 0.05, split, grown for one to two generations, and then treated with either 0.5 M NaCl (final concentration) or the corresponding volume of YPD (mock). OD_{600} was monitored for a minimum of four generations after stress treatment. Slopes were obtained from log-transformed growth curves between generations 2 and 4 after stress application (for the experimental window, see Fig. 5A), and a stressed (added 0.5 M NaCl) versus unstressed (mock) slope ratio was calculated for every replicate (at least two per strain and condition; $n = 17$ for *hog1Δ* and $n = 20$ for wild type). Slope ratios were $\log_2$-transformed (Fig. 5B).

Protein-protein proximity assay (M-track)

M-track protein-protein proximity assays were performed as described previously (*18*, *58*). Cells were grown until mid-log phase, treated with either 0.5 M NaCl or 1 M sorbitol (final concentration) for 40 min, and harvested by filtration. Protein extraction was carried out under nondenaturing conditions by glass bead lysis. Analysis of WCLs was performed as described previously (*58*) using buffer 1 (*106*). Immunoprecipitation and TEV cleavage (cleavage enrichment) of prey proteins were performed as described previously (*58*). Histone H3 Lys 9 trimethylation (me3K9H3) of peptides was visualized by Western blot using an antibody recognizing me3K9H3 [WCL, ab8898 (Abcam); immunoprecipitate, NBP 1-30141 (Novus Biochemicals)]. Loading was controlled using an antibody (12CA5) recognizing HA. WCL loading was additionally controlled using an antibody targeting Pkg2 (Novex). Peak areas of signals were determined using ImageJ. Proximity signals were calculated as follows: Peak areas of me3K9H3 and HA signals were determined using ImageJ, and proximity signals were calculated as the $\log_2$ ratio of me3K9H3 over HA signal of the individual candidates. Different Western blot experiments were normalized by subtracting the average $\log_2$ signal intensity of the control samples Hot1 (positive control), Cyr1 (internal control), and Hog1-protA-H3 (negative control). We used a one-tailed Welch's *t* test to identify the statistically significant candidates. In short, for each candidate gene, the signal intensities of all replicates were compared against all signal intensities of the negative control. *P* values were corrected for multiple testing by the Benjamini-Hochberg procedure with α of 0.01 to generate *q* values. Candidate genes with a mean signal intensity lower than the negative control were considered as not significant. Statistical analysis was performed independently for the whole-cell lysate and cleavage enrichment data sets. Data analysis and figure generation were performed using Python scripts utilizing the libraries NumPy (*107*), matplotlib (*108*), seaborn (*109*), scipy (*107*), and statsmodels (*110*).

Serial dilution droplet test

W303-1A wild-type and deletion mutant strains were grown to mid-log phase. OD_{600} values of cultures were equalized to 0.1, and serial dilution steps of 1:7 dilutions were prepared. Droplets of 2.5 µl were transferred onto hyperosmotic stress plates (YPD; +0.5 M NaCl, +0.8 M NaCl, +1.2 M NaCl, +0.8 M KCl, +1.2 M KCl, and +1.2 M sorbitol) and onto a YPD plate with no additives as a control. Plates were incubated at 30°C, and growth was monitored for 4 days.

Scoring system in serial dilution droplet test

Growth was monitored for 1 to 4 days and compared to wild type and *hog1Δ*. Long-term growth effects were assayed using an additive scoring system, endowing a score of 2 for a strong phenotype, a score of 1 for a weak phenotype, and score of 0 in case no phenotype was observed. Scores were further weighted according the molarity of the stressor (multiplied with a weight of three for 0.5 M, two for 0.8 M, and one for 1.2 M), resulting in a maximum score of 40 (applied for *hog1Δ*). Strains with scores corresponding to ≥13.5 (threefold of the wild type) were regarded as highly osmosensitive candidates, and scores between <13 and ≥5 as moderate or weakly sensitive. Mutants with a score similar to wild type (lower than 5) were regarded as insensitive to hyperosmotic stress. Finally, to calculate a final score integrating both droplet test scores and slope ratios, we scaled scores from these assays from 0 to 10 and computed the average score (see Fig. 5D).

SUPPLEMENTARY MATERIALS

www.sciencesignaling.org/cgi/content/full/10/469/eaag2435/DC1

Fig. S1. Data from the setup SR are consistent with data described in previous studies.
Fig. S2. Effects caused by Kss1 cross-talk are negligible.
Fig. S3. Tsl1 is a target of Hog1.
Fig. S4. Rck2 is the effector kinase of HOG signaling.
Fig. S5. Network hubs of NetworKIN-predicted interactions of kinases possibly involved in the regulation of the indirect targets of Hog1.
Fig. S6. Nth1 might be a target of Hog1.
Fig. S7. M-track whole-cell extract measurements (complete data set).
Fig. S8. Serial dilution droplet test of deletion mutants (complete data set).
Table S1. Peptide list over each separate replicate experiment.
Table S2. Summary of quantified phosphorylation sites over all MS experiments
Table S3. Number of peptides in different fields per protein.
Table S4. Inhibitor-susceptible S/T-P motifs (not assigned in setup SR) covered in only one of the setups.
Table S5. Putative indirect targets of Hog1.
Table S6. Strains used in this study.
Table S7. Plasmids used in this study.
Table S8. Details of the individual experimental setups.
References (*111*, *112*)

REFERENCES AND NOTES

1. B. Bodenmiller, S. Wanka, C. Kraft, J. Urban, D. Campbell, P. G. Pedrioli, B. Gerrits, P. Picotti, H. Lam, O. Vitek, M.-Y. Brusniak, B. Roschitzki, C. Zhang, K. M. Shokat, R. Schlapbach, A. Colman-Lerner, G. P. Nolan, A. I. Nesvizhskii, M. Peter, R. Loewith, C. von Mering, R. Aebersold, Phosphoproteomic analysis reveals interconnected system-wide responses to perturbations of kinases and phosphatases in yeast. *Sci. Signal* **3**, rs4 (2010).
2. A. Breitkreutz, H. Choi, J. R. Sharom, L. Boucher, V. Neduva, B. Larsen, Z. Y. Lin, B.-J. Breitkreutz, C. Stark, G. Liu, J. Ahn, D. Dewar-Darch, T. Reguly, X. Tang, R. Almeida, Z. S. Qin, T. Pawson, A.-C. Gingras, A. I. Nesvizhskii, M. Tyers, A global protein kinase and phosphatase interaction network in yeast. *Science* **328**, 1043–1046 (2010).
3. A. Gruhler, J. V. Olsen, S. Mohammed, P. Mortensen, N. J. Færgeman, M. Mann, O. N. Jensen, Quantitative phosphoproteomics applied to the yeast pheromone signaling pathway. *Mol. Cell. Proteomics* **4**, 310–327 (2005).
4. E. Kanshin, L.-P. Bergeron-Sandoval, S. S. Isik, P. Thibault, S. W. Michnick, A cell-signaling network temporally resolves specific versus promiscuous phosphorylation. *Cell Rep.* **10**, 1202–1214 (2015).
5. V. Mascaraque, M. L. Hernaez, M. Jiménez-Sánchez, R. Hansen, C. Gil, H. Martin, V. J. Cid, M. Molina, Phosphoproteomic analysis of protein kinase C signaling in *Saccharomyces cerevisiae* reveals Slt2 mitogen-activated protein kinase (MAPK)-dependent phosphorylation of eisosome core components. *Mol. Cell. Proteomics* **12**, 557–574 (2013).
6. B. Soufi, C. D. Kelstrup, G. Stoehr, F. Fröhlich, T. C. Walther, J. V. Olsen, Global analysis of the yeast osmotic stress response by quantitative proteomics. *Mol. Biosyst.* **5**, 1337–1346 (2009).
7. W. Reiter, D. Anrather, I. Dohnal, P. Pichler, J. Veis, M. Grøtli, F. Posas, G. Ammerer, Validation of regulated protein phosphorylation events in yeast by quantitative mass spectrometry analysis of purified proteins. *Proteomics* **12**, 3030–3043 (2012).

8. D. Chasman, Y.-H. Ho, D. B. Berry, C. M. Nemec, M. E. MacGilvray, J. Hose, A. E. Merrill, M. V. Lee, J. L. Will, J. J. Coon, A. Z. Ansari, M. Craven, A. P. Gasch, Pathway connectivity and signaling coordination in the yeast stress-activated signaling network. *Mol. Syst. Biol.* **10**, 759 (2014).
9. H. Sharifian, F. Lampert, K. Stojanovski, S. Regot, S. Vaga, R. Buser, S. S. Lee, H. Koeppl, F. Posas, S. Pelet, M. Peter, Parallel feedback loops control the basal activity of the HOG MAPK signaling cascade. *Integr. Biol. (Camb.)* **7**, 412–422 (2015).
10. S. Vaga, M. Bernardo-Faura, T. Cokelaer, A. Maiolica, C. A. Barnes, L. C. Gillet, B. Hegemann, F. van Drogen, H. Sharifian, E. Klipp, M. Peter, J. Saez-Rodriguez, R. Aebersold, Phosphoproteomic analyses reveal novel cross-modulation mechanisms between two signaling pathways in yeast. *Mol. Syst. Biol.* **10**, 767 (2014).
11. H. Saito, F. Posas, Response to hyperosmotic stress. *Genetics* **192**, 289–318 (2012).
12. E. de Nadal, G. Ammerer, F. Posas, Controlling gene expression in response to stress. *Nat. Rev. Genet.* **12**, 833–845 (2011).
13. S. Hohmann, Osmotic stress signaling and osmoadaptation in yeasts. *Microbiol. Mol. Biol. Rev.* **66**, 300–372 (2002).
14. F. Posas, J. R. Chambers, J. A. Heyman, J. P. Hoeffler, E. de Nadal, J. Ariño, The transcriptional response of yeast to saline stress. *J. Biol. Chem.* **275**, 17249–17255 (2000).
15. M. Teige, E. Scheikl, V. Reiser, H. Ruis, G. Ammerer, Rck2, a member of the calmodulin-protein kinase family, links protein synthesis to high osmolarity MAP kinase signaling in budding yeast. *Proc. Natl. Acad. Sci. U.S.A.* **98**, 5625–5630 (2001).
16. S. B. Ficarro, M. L. McCleland, P. T. Stukenberg, D. J. Burke, M. M. Ross, J. Shabanowitz, D. F. Hunt, F. M. White, Phosphoproteome analysis by mass spectrometry and its application to *Saccharomyces cerevisiae*. *Nat. Biotechnol.* **20**, 301–305 (2002).
17. S.-E. Ong, B. Blagoev, I. Kratchmarova, D. B. Kristensen, H. Steen, A. Pandey, M. Mann, Stable isotope labeling by amino acids in cell culture, SILAC, as a simple and accurate approach to expression proteomics. *Mol. Cell. Proteomics* **1**, 376–386 (2002).
18. A. Zuzuarregui, T. Kupka, B. Bhatt, I. Dohnal, I. Mudrak, C. Friedmann, S. Schüchner, I. E. Frohner, G. Ammerer, E. Ogris, M-Track: Detecting short-lived protein-protein interactions in vivo. *Nat. Methods* **9**, 594–596 (2012).
19. M. Klein, M. Morillas, A. Vendrell, L. Brive, M. Gebbia, I. M. Wallace, G. Glaever, C. Nislow, F. Posas, M. Grøtli, Design, synthesis and characterization of a highly effective inhibitor for analog-sensitive (*as*) kinases. *PLOS ONE* **6**, e20789 (2011).
20. P. M. Alepuz, E. de Nadal, M. Zapater, G. Ammerer, F. Posas, Osmostress-induced transcription by Hot1 depends on a Hog1-mediated recruitment of the RNA Pol II. *EMBO J.* **22**, 2433–2442 (2003).
21. J. Lee, W. Reiter, I. Dohnal, C. Gregori, S. Beese-Sims, K. Kuchler, G. Ammerer, D. E. Levin, MAPK Hog1 closes the *S. cerevisiae* glycerol channel Fps1 by phosphorylating and displacing its positive regulators. *Genes Dev.* **27**, 2590–2601 (2013).
22. N. Hao, Y. Zeng, T. C. Elston, H. G. Dohlman, Control of MAPK specificity by feedback phosphorylation of shared adaptor protein Ste50. *J. Biol. Chem.* **283**, 33798–33802 (2008).
23. K. Yamamoto, K. Tatebayashi, K. Tanaka, H. Saito, Dynamic control of yeast MAP kinase network by induced association and dissociation between the Ste50 scaffold and the Opy2 membrane anchor. *Mol. Cell* **40**, 87–98 (2010).
24. M. F. Chou, D. Schwartz, Biological sequence motif discovery using *motif-x*. *Curr. Protoc. Bioinformatics* **Chapter 13**, Unit 13.15-24 (2011).
25. D. Schwartz, S. P. Gygi, An iterative statistical approach to the identification of protein phosphorylation motifs from large-scale data sets. *Nat. Biotechnol.* **23**, 1391–1398 (2005).
26. S. M. O'Rourke, I. Herskowitz, The Hog1 MAPK prevents cross talk between the HOG and pheromone response MAPK pathways in *Saccharomyces cerevisiae*. *Genes Dev.* **12**, 2874–2886 (1998).
27. M. Proft, A. Pascual-Ahuir, E. de Nadal, J. Arino, R. Serrano, F. Posas, Regulation of the Sko1 transcriptional repressor by the Hog1 MAP kinase in response to osmotic stress. *EMBO J.* **20**, 1123–1133 (2001).
28. E. Conibear, T. H. Stevens, Vps52p, Vps53p, and Vps54p form a novel multisubunit complex required for protein sorting at the yeast late Golgi. *Mol. Biol. Cell* **11**, 305–323 (2000).
29. C. Ruiz-Roig, N. Noriega, A. Duch, F. Posas, E. de Nadal, The Hog1 SAPK controls the Rtg1/Rtg3 transcriptional complex activity by multiple regulatory mechanisms. *Mol. Biol. Cell* **23**, 4286–4296 (2012).
30. H. Zähringer, J. M. Thevelein, S. Nwaka, Induction of neutral trehalase Nth1 by heat and osmotic stress is controlled by STRE elements and Msn2/Msn4 transcription factors: Variations of PKA effect during stress and growth. *Mol. Microbiol.* **35**, 397–406 (2000).
31. M. J. Neves, J. François, On the mechanism by which a heat shock induces trehalose accumulation in *Saccharomyces cerevisiae*. *Biochem. J.* **288**, 859–864 (1992).
32. J. L. Parrou, M.-A. Teste, J. François, Effects of various types of stress on the metabolism of reserve carbohydrates in *Saccharomyces cerevisiae*: Genetic evidence for a stress-induced recycling of glycogen and trehalose. *Microbiology* **143**, 1891–1900 (1997).
33. D. Zweytick, E. Leitner, S. D. Kohlwein, C. Yu, J. Rothblatt, G. Daum, Contribution of Are1p and Are2p to steryl ester synthesis in the yeast *Saccharomyces cerevisiae*. *Eur. J. Biochem.* **267**, 1075–1082 (2000).
34. M. Becuwe, N. Vieira, D. Lara, J. Gomes-Rezende, C. Soares-Cunha, M. Casal, R. Haguenauer-Tsapis, O. Vincent, S. Paiva, S. Léon, A molecular switch on an arrestin-like protein relays glucose signaling to transporter endocytosis. *J. Cell Biol.* **196**, 247–259 (2012).
35. M. Lussier, A.-M. White, J. Sheraton, T. di Paolo, J. Treadwell, S. B. Southard, C. I. Horenstein, J. Chen-Weiner, A. F. J. Ram, J. C. Kapteyn, T. W. Roemer, D. H. Vo, D. C. Bondoc, J. Hall, W. W. Zhong, A.-M. Sdicu, J. Davies, F. M. Klis, P. W. Robbins, H. Bussey, Large scale identification of genes involved in cell surface biosynthesis and architecture in *Saccharomyces cerevisiae*. *Genetics* **147**, 435–450 (1997).
36. L. Yenush, J. M. Mulet, J. Ariño, R. Serrano, The Ppz protein phosphatases are key regulators of K^+ and pH homeostasis: Implications for salt tolerance, cell wall integrity and cell cycle progression. *EMBO J.* **21**, 920–929 (2002).
37. E. de Nadal, L. Casadomé, F. Posas, Targeting the MEF2-like transcription factor Smp1 by the stress-activated Hog1 mitogen-activated protein kinase. *Mol. Cell. Biol.* **23**, 229–237 (2003).
38. M. J. T. V. Cope, S. Yang, C. Shang, D. G. Drubin, Novel protein kinases Ark1p and Prk1p associate with and regulate the cortical actin cytoskeleton in budding yeast. *J. Cell Biol.* **144**, 1203–1218 (1999).
39. A. Lamb, M. Tibbetts, C. I. Hammond, The product of the *KIN1* locus in *Saccharomyces cerevisiae* is a serine/threonine-specific protein kinase. *Yeast* **7**, 219–228 (1991).
40. E. Leberer, D. Dignard, D. Harcus, D. Y. Thomas, M. Whiteway, The protein kinase homologue Ste20p is required to link the yeast pheromone response G-protein βγ subunits to downstream signalling components. *EMBO J.* **11**, 4815–4824 (1992).
41. S. Vidan, A. P. Mitchell, Stimulation of yeast meiotic gene expression by the glucose-repressible protein kinase Rim15p. *Mol. Cell. Biol.* **17**, 2688–2697 (1997).
42. T. Hunter, G. D. Plowman, The protein kinases of budding yeast: Six score and more. *Trends Biochem. Sci.* **22**, 18–22 (1997).
43. S. Dale, W. A. Wilson, A. M. Edelman, D. G. Hardie, Similar substrate recognition motifs for mammalian AMP-activated protein kinase, higher plant HMG-CoA reductase kinase-A, yeast SNF1, and mammalian calmodulin-dependent protein kinase I. *FEBS Lett.* **361**, 191–195 (1995).
44. J. Mok, P. M. Kim, H. Y. Lam, S. Piccirillo, X. Zhou, G. R. Jeschke, D. L. Sheridan, S. A. Parker, V. Desai, M. Jwa, E. Cameroni, H. Niu, M. Good, A. Remenyi, J. L. Ma, Y.-J. Sheu, H. E. Sassi, R. Sopko, C. S. Chan, C. De Virgilio, N. M. Hollingsworth, W. A. Lim, D. F. Stern, B. Stillman, B. J. Andrews, M. B. Gerstein, M. Snyder, B. E. Turk, Deciphering protein kinase specificity through large-scale analysis of yeast phosphorylation site motifs. *Sci. Signal* **3**, ra12 (2010).
45. J. Clotet, X. Escote, M. À. Adrover, G. Yaakov, E. Garí, M. Aldea, E. de Nadal, F. Posas, Phosphorylation of Hsl1 by Hog1 leads to a G_2 arrest essential for cell survival at high osmolarity. *EMBO J.* **25**, 2338–2346 (2006).
46. T. Mizuno, Y. Masuda, K. Irie, The *Saccharomyces cerevisiae* AMPK, Snf1, negatively regulates the Hog1 MAPK pathway in ER stress response. *PLOS Genet.* **11**, e1005491 (2015).
47. E. Bilsland-Marchesan, J. Ariño, H. Saito, P. Sunnerhagen, F. Posas, Rck2 kinase is a substrate for the osmotic stress-activated mitogen-activated protein kinase Hog1. *Mol. Cell. Biol.* **20**, 3887–3895 (2000).
48. J. Ptacek, G. Devgan, G. Michaud, H. Zhu, X. Zhu, J. Fasolo, H. Guo, G. Jona, A. Breitkreutz, R. Sopko, R. R. McCartney, M. C. Schmidt, N. Rachidi, S. J. Lee, A. S. Mah, L. Meng, M. J. R. Stark, D. F. Stern, C. De Virgilio, M. Tyers, B. Andrews, M. Gerstein, B. Schweitzer, P. F. Predki, M. Snyder, Global analysis of protein phosphorylation in yeast. *Nature* **438**, 679–684 (2005).
49. S. Sharifpoor, D. van Dyk, M. Costanzo, A. Baryshnikova, H. Friesen, A. C. Douglas, J.-Y. Youn, B. VanderSluis, C. L. Myers, B. Papp, C. Boone, B. J. Andrews, Functional wiring of the yeast kinome revealed by global analysis of genetic network motifs. *Genome Res.* **22**, 791–801 (2012).
50. Z. Wang, W. A. Wilson, M. A. Fujino, P. J. Roach, Antagonistic controls of autophagy and glycogen accumulation by Snf1p, the yeast homolog of AMP-activated protein kinase, and the cyclin-dependent kinase Pho85p. *Mol. Cell. Biol.* **21**, 5742–5752 (2001).
51. J. M. Mulet, M. P. Leube, S. J. Kron, G. Rios, G. R. Fink, R. Serrano, A novel mechanism of ion homeostasis and salt tolerance in yeast: The Hal4 and Hal5 protein kinases modulate the Trk1-Trk2 potassium transporter. *Mol. Cell. Biol.* **19**, 3328–3337 (1999).
52. L. Yenush, S. Merchan, J. Holmes, R. Serrano, pH-responsive, posttranslational regulation of the Trk1 potassium transporter by the type 1-related Ppz1 phosphatase. *Mol. Cell. Biol.* **25**, 8683–8692 (2005).
53. H. Hom, E. M. Schoof, J. Kim, X. Robin, M. L. Miller, F. Diella, A. Palma, G. Cesareni, L. J. Jensen, R. Linding, KinomeXplorer: An integrated platform for kinome biology studies. *Nat. Methods* **11**, 603–604 (2014).
54. R. Linding, L. J. Jensen, G. J. Ostheimer, M. A. T. M. van Vugt, C. Jorgensen, I. M. Miron, F. Diella, K. Colwill, L. Taylor, K. Elder, P. Metalnikov, V. Nguyen, A. Pasculescu, J. Jin, J. G. Park, L. D. Samson, J. R. Woodgett, R. B. Russell, P. Bork, M. B. Yaffe, T. Pawson, Systematic discovery of in vivo phosphorylation networks. *Cell* **129**, 1415–1426 (2007).

55. F. C. Smith, S. P. Davies, W. A. Wilson, D. Carling, D. G. Hardie, The SNF1 kinase complex from *Saccharomyces cerevisiae* phosphorylates the transcriptional repressor protein Mig1p in vitro at four sites within or near regulatory domain 1. *FEBS Lett.* **453**, 219–223 (1999).
56. M. Donovan, P. Romano, M. Tibbetts, C. I. Hammond, Characterization of the *KIN2* gene product in *Saccharomyces cerevisiae* and comparison between the kinase activities of $p145^{KIN1}$ and $p145^{KIN2}$. *Yeast* **10**, 113–124 (1994).
57. M. Elbert, G. Rossi, P. Brennwald, The yeast Par-1 homologs Kin1 and Kin2 show genetic and physical interactions with components of the exocytic machinery. *Mol. Biol. Cell* **16**, 532–549 (2005).
58. A. Brezovich, M. Schuschnig, G. Ammerer, C. Kraft, An in vivo detection system for transient and low-abundant protein interactions and their kinetics in budding yeast. *Yeast* **32**, 355–365 (2015).
59. C. J. Walkey, Z. Luo, L. L. Madilao, H. J. J. van Vuuren, The fermentation stress response protein Aaf1p/Ynl081Wp regulates acetate production in *Saccharomyces cerevisiae*. *PLOS ONE* **7**, e51551 (2012).
60. N. Tomishige, Y. Noda, H. Adachi, K. Yoda, *SKG6*, a suppressor gene of synthetic lethality of *kex2Δ gas1Δ* mutations, encodes a novel membrane protein showing polarized intracellular localization. *J. Gen. Appl. Microbiol.* **51**, 323–326 (2005).
61. S. Nwaka, H. Holzer, Molecular biology of trehalose and the trehalases in the yeast *Saccharomyces cerevisiae*. *Prog. Nucleic Acid Res. Mol. Biol.* **58**, 197–237 (1997).
62. N. Hao, M. Behar, S. C. Parnell, M. P. Torres, C. H. Borchers, T. C. Elston, H. G. Dohlman, A systems-biology analysis of feedback inhibition in the Sho1 osmotic-stress-response pathway. *Curr. Biol.* **17**, 659–667 (2007).
63. M. Proft, K. Struhl, MAP kinase-mediated stress relief that precedes and regulates the timing of transcriptional induction. *Cell* **118**, 351–361 (2004).
64. S. Regot, E. de Nadal, S. Rodríguez-Navarro, A. González-Novo, J. Pérez-Fernandez, O. Gadal, G. Seisenbacher, G. Ammerer, F. Posas, The Hog1 stress-activated protein kinase targets nucleoporins to control mRNA export upon stress. *J. Biol. Chem.* **288**, 17384–17398 (2013).
65. P. J. Westfall, J. Thorner, Analysis of mitogen-activated protein kinase signaling specificity in response to hyperosmotic stress: Use of an analog-sensitive HOG1 allele. *Eukaryot. Cell* **5**, 1215–1228 (2006).
66. A. Franceschini, D. Szklarczyk, S. Frankild, M. Kuhn, M. Simonovic, A. Roth, J. Lin, P. Minguez, P. Bork, C. von Mering, L. J. Jensen, STRING v9.1: Protein-protein interaction networks, with increased coverage and integration. *Nucleic Acids Res.* **41**, D808–D815 (2013).
67. B. Snel, G. Lehmann, P. Bork, M. A. Huynen, STRING: A web-server to retrieve and display the repeatedly occurring neighbourhood of a gene. *Nucleic Acids Res.* **28**, 3442–3444 (2000).
68. D. Szklarczyk, A. Franceschini, S. Wyder, K. Forslund, D. Heller, J. Huerta-Cepas, M. Simonovic, A. Roth, A. Santos, K. P. Tsafou, M. Kuhn, P. Bork, L. J. Jensen, C. von Mering, STRING v10: Protein–protein interaction networks, integrated over the tree of life. *Nucleic Acids Res.* **43**, D447–D452 (2015).
69. M. Proft, K. Struhl, Hog1 kinase converts the Sko1-Cyc8-Tup1 repressor complex into an activator that recruits SAGA and SWI/SNF in response to osmotic stress. *Mol. Cell* **9**, 1307–1317 (2002).
70. X. Escoté, M. Zapater, J. Clotet, F. Posas, Hog1 mediates cell-cycle arrest in G1 phase by the dual targeting of Sic1. *Nat. Cell Biol.* **6**, 997–1002 (2004).
71. H. Dihazi, R. Kessler, K. Eschrich, High osmolarity glycerol (HOG) pathway-induced phosphorylation and activation of 6-phosphofructo-2-kinase are essential for glycerol accumulation and yeast cell proliferation under hyperosmotic stress. *J. Biol. Chem.* **279**, 23961–23968 (2004).
72. M. Mollapour, P. W. Piper, Hog1 mitogen-activated protein kinase phosphorylation targets the yeast Fps1 aquaglyceroporin for endocytosis, thereby rendering cells resistant to acetic acid. *Mol. Cell. Biol.* **27**, 6446–6456 (2007).
73. M. Thorsen, Y. Di, C. Tangemo, M. Morillas, D. Ahmadpour, C. Van der Does, A. Wagner, E. Johansson, J. Boman, F. Posas, R. Wysocki, M. J. Tamas, The MAPK Hog1p modulates Fps1p-dependent arsenite uptake and tolerance in yeast. *Mol. Biol. Cell* **17**, 4400–4410 (2006).
74. H. App, H. Holzer, Purification and characterization of neutral trehalase from the yeast ABYS1 mutant. *J. Biol. Chem.* **264**, 17583–17588 (1989).
75. M. Kopp, S. Nwaka, H. Holzer, Corrected sequence of the yeast neutral trehalase-encoding gene (NTH1): Biological implications. *Gene* **150**, 403–404 (1994).
76. J. M. Thevelein, M. Beullens, Cyclic AMP and the stimulation of trehalase activity in the yeast *Saccharomyces cerevisiae* by carbon sources, nitrogen sources and inhibitors of protein synthesis. *J. Gen. Microbiol.* **131**, 3199–3209 (1985).
77. H. Zähringer, H. Holzer, S. Nwaka, Stability of neutral trehalase during heat stress in *Saccharomyces cerevisiae* is dependent on the activity of the catalytic subunits of cAMP-dependent protein kinase, Tpk1 and Tpk2. *Eur. J. Biochem.* **255**, 544–551 (1998).
78. W. Reiter, E. Klopf, V. De Wever, D. Anrather, A. Petryshyn, A. Roetzer, G. Niederacher, E. Roitinger, I. Dohnal, W. Gömer, K. Mechtler, C. Brocard, C. Schuller, G. Ammerer, Yeast protein phosphatase 2A-Cdc55 regulates the transcriptional response to hyperosmolarity stress by regulating Msn2 and Msn4 chromatin recruitment. *Mol. Cell. Biol.* **33**, 1057–1072 (2013).
79. J. C. Ewald, A. Kuehne, N. Zamboni, J. M. Skotheim, The yeast cyclin-dependent kinase routes carbon fluxes to fuel cell cycle progression. *Mol. Cell* **62**, 532–545 (2016).
80. G. Zhao, Y. Chen, L. Carey, B. Futcher, Cyclin-dependent kinase co-ordinates carbohydrate metabolism and cell cycle in *S. cerevisiae*. *Mol. Cell* **62**, 546–557 (2016).
81. O. E. Vuorio, N. Kalkkinen, J. Londesborough, Cloning of two related genes encoding the 56-kDa and 123-kDa subunits of trehalose synthase from the yeast *Saccharomyces cerevisiae*. *Eur. J. Biochem.* **216**, 849–861 (1993).
82. S. Diamant, N. Eliahu, D. Rosenthal, P. Goloubinoff, Chemical chaperones regulate molecular chaperones in vitro and in cells under combined salt and heat stresses. *J. Biol. Chem.* **276**, 39586–39591 (2001).
83. L. K. Conlin, H. C. Nelson, The natural osmolyte trehalose is a positive regulator of the heat-induced activity of yeast heat shock transcription factor. *Mol. Cell. Biol.* **27**, 1505–1515 (2007).
84. F. M. Montañés, A. Pascual-Ahuir, M. Proft, Repression of ergosterol biosynthesis is essential for stress resistance and is mediated by the Hog1 MAP kinase and the Mot3 and Rox1 transcription factors. *Mol. Microbiol.* **79**, 1008–1023 (2011).
85. K. R. Henry, K. D'Hondt, J. S. Chang, D. A. Nix, M. J. T. V. Cope, C. S. M. Chan, D. G. Drubin, S. K. Lemmon, The actin-regulating kinase Prk1p negatively regulates Scd5p, a suppressor of clathrin deficiency, in actin organization and endocytosis. *Curr. Biol.* **13**, 1564–1569 (2003).
86. M. C. Duncan, M. J. T. V. Cope, B. L. Goode, B. Wendland, D. G. Drubin, Yeast Eps15-like endocytic protein, Pan1p, activates the Arp2/3 complex. *Nat. Cell Biol.* **3**, 687–690 (2001).
87. H.-Y. Tang, J. Xu, M. Cai, Pan1p, End3p, and S1a1p, three yeast proteins required for normal cortical actin cytoskeleton organization, associate with each other and play essential roles in cell wall morphogenesis. *Mol. Cell. Biol.* **20**, 12–25 (2000).
88. J. Toshima, J. Y. Toshima, M. C. Duncan, M. J. T. V. Cope, Y. Sun, A. C. Martin, S. Anderson, J. R. Yates III, K. Mizuno, D. G. Drubin, Negative regulation of yeast Eps15-like Arp2/3 complex activator, Pan1p, by the Hip1R-related protein, Sla2p, during endocytosis. *Mol. Biol. Cell* **18**, 658–668 (2007).
89. B. Wendland, S. D. Emr, Pan1p, yeast eps15, functions as a multivalent adaptor that coordinates protein–protein interactions essential for endocytosis. *J. Cell Biol.* **141**, 71–84 (1998).
90. B. Wendland, K. E. Steece, S. D. Emr, Yeast epsins contain an essential N-terminal ENTH domain, bind clathrin and are required for endocytosis. *EMBO J.* **18**, 4383–4393 (1999).
91. M. Huranova, G. Muruganandam, M. Weiss, A. Spang, Dynamic assembly of the exomer secretory vesicle cargo adaptor subunits. *EMBO Rep.* **17**, 202–219 (2016).
92. M. Trautwein, C. Schindler, R. Gauss, J. Dengjel, E. Hartmann, A. Spang, Arf1p, Chs5p and the ChAPs are required for export of specialized cargo from the Golgi. *EMBO J.* **25**, 943–954 (2006).
93. C.-W. Wang, S. Hamamoto, L. Orci, R. Schekman, Exomer: A coat complex for transport of select membrane proteins from the trans-Golgi network to the plasma membrane in yeast. *J. Cell Biol.* **174**, 973–983 (2006).
94. K. Irie, M. Takase, K. S. Lee, D. E. Levin, H. Araki, K. Matsumoto, Y. Oshima, *MKK1* and *MKK2*, which encode *Saccharomyces cerevisiae* mitogen-activated protein kinase-kinase homologs, function in the pathway mediated by protein kinase C. *Mol. Cell. Biol.* **13**, 3076–3083 (1993).
95. K. S. Lee, D. E. Levin, Dominant mutations in a gene encoding a putative protein kinase (*BCK1*) bypass the requirement for a *Saccharomyces cerevisiae* protein kinase C homolog. *Mol. Cell. Biol.* **12**, 172–182 (1992).
96. B. A. Pinsky, C. V. Kotwaliwale, S. Y. Tatsutani, C. A. Breed, S. Biggins, Glc7/protein phosphatase 1 regulatory subunits can oppose the Ipl1/aurora protein kinase by redistributing Glc7. *Mol. Cell. Biol.* **26**, 2648–2660 (2006).
97. R. Babazadeh, T. Furukawa, S. Hohmann, K. Furukawa, Rewiring yeast osmostress signalling through the MAPK network reveals essential and non-essential roles of Hog1 in osmoadaptation. *Sci. Rep.* **4**, 4697 (2014).
98. C. Janke, M. M. Magiera, N. Rathfelder, C. Taxis, S. Reber, H. Maekawa, A. Moreno-Borchart, G. Doenges, E. Schwob, E. Schiebel, M. Knop, A versatile toolbox for PCR-based tagging of yeast genes: New fluorescent proteins, more markers and promoter substitution cassettes. *Yeast* **21**, 947–962 (2004).
99. M. Knop, K. Siegers, G. Pereira, W. Zachariae, B. Winsor, K. Nasmyth, E. Schiebel, Epitope tagging of yeast genes using a PCR-based strategy: More tags and improved practical routines. *Yeast* **15**, 963–972 (1999).
100. A. Wach, A. Brachat, R. Pöhlmann, P. Philippsen, New heterologous modules for classical or PCR-based gene disruptions in *Saccharomyces cerevisiae*. *Yeast* **10**, 1793–1808 (1994).
101. W.-K. Huh, J. V. Falvo, L. C. Gerke, A. S. Carroll, R. W. Howson, J. S. Weissman, E. K. O'Shea, Global analysis of protein localization in budding yeast. *Nature* **425**, 686–691 (2003).
102. M. Mazanek, G. Mituloviæ, F. Herzog, C. Stingl, J. R. Hutchins, J.-M. Peters, K. Mechtler, Titanium dioxide as a chemo-affinity solid phase in offline phosphopeptide chromatography prior to HPLC-MS/MS analysis. *Nat. Protoc.* **2**, 1059–1069 (2007).

103. T. E. Thingholm, T. J. Jørgensen, O. N. Jensen, M. R. Larsen, Highly selective enrichment of phosphorylated peptides using titanium dioxide. *Nat. Protoc.* **1**, 1929–1935 (2006).
104. J. A. Vizcaíno, R. G. Côté, A. Csordas, J. A. Dianes, A. Fabregat, J. M. Foster, J. Griss, E. Alpi, M. Birim, J. Contell, G. O'Kelly, A. Schoenegger, D. Ovelleiro, Y. Pérez-Riverol, F. Reisinger, D. Ríos, R. Wang, H. Hermjakob, The Proteomics Identifications (PRIDE) database and associated tools: Status in 2013. *Nucleic Acids Res.* **41**, D1063–D1069 (2013).
105. H. Mi, A. Muruganujan, J. T. Casagrande, P. D. Thomas, Large-scale gene function analysis with the PANTHER classification system. *Nat. Protoc.* **8**, 1551–1566 (2013).
106. C. Tagwerker, K. Flick, M. Cui, C. Guerrero, Y. Dou, B. Auer, P. Baldi, L. Huang, P. Kaiser, A tandem affinity tag for two-step purification under fully denaturing conditions: Application in ubiquitin profiling and protein complex identification combined with in vivo cross-linking. *Mol. Cell. Proteomics* **5**, 737–748 (2006).
107. S. van der Walt, S. C. Colbert, G. Varoquaux, The NumPy array: A structure for efficient numerical computation. *Comput. Sci. Eng.* **13**, 22–30 (2011).
108. J. D. Hunter, Matplotlib: A 2D Graphics Environment. *Comput. Sci. Eng.* **9**, 90–95 (2007).
109. M. Waskom, C. Evans, J. Warmenhoven, T. Yarkoni, K. K. Meyer, L. Rocher, P. Hobson, Y. Halchenko, M. Koskinen, seaborn: v0.6.0. *Zenodo*, 10.5281/zenodo.19108 (2015).
110. S. Seabold, J. Perktold, Statsmodels: Econometric and statistical modeling with Python, paper presented at the Proceedings of the 9th Python in Science Conference, Austin, TX, 28 June to 3 July 2010.
111. Y. T. Chong, J. L. Y. Koh, H. Friesen, S. K. Duffy, M. J. Cox, A. Moses, J. Moffat, C. Boone, B. J. Andrews, Yeast proteome dynamics from single cell imaging and automated analysis. *Cell* **161**, 1413–1424 (2015).
112. A. Mitchell, H.-Y. Chang, L. Daugherty, M. Fraser, S. Hunter, R. Lopez, C. McAnulla, C. McMenamin, G. Nuka, S. Pesseat, A. Sangrador-Vegas, M. Scheremetjew, C. Rato, S.-Y. Yong, A. Bateman, M. Punta, T. K. Attwood, C. J. A. Sigrist, N. Redaschi, C. Rivoire, I. Xenarios, D. Kahn, D. Guyot, P. Bork, I. Letunic, J. Gough, M. Oates, D. Haft, H. Huang, D. A. Natale, C. H. Wu, C. Orengo, I. Sillitoe, H. Mi, P. D. Thomas, R. D. Finn, The InterPro protein families database: The classification resource after 15 years. *Nucleic Acids Res.* **43**, D213–D221 (2015).

Acknowledgments: We thank J. Augustine for the comments; M. Hartl and V. Unterwurzacher for the help with MS analyses; J. Augustine, M. Grøtli, A. Brezovich, and C. Kraft for providing the reagents; and B. Klaus and M. Rogon for the advice on statistical and network analysis. **Funding:** This work was supported by grants from the Seventh EU framework project (UNICELLSYS) and the Austrian Science Fund (project F34) and by the foundation "Verein zur Förderung der Genomforschung." **Author contributions:** G.A. and W.R. designed the project. N.R., D.M.H., M.J., D.A., and W.R. performed the experiments and analyzed the data. W.R. wrote the manuscript. All authors commented and edited the text. **Competing interests:** The authors declare that they have no competing interests. **Data and materials availability:** The MS proteomics data have been deposited to the ProteomeXchange Consortium through the PRIDE partner repository (*104*) with the data set identifiers PXD004294 to PXD004300. The plasmids require a material transfer agreement from the American Association for the Advancement of Science, United States.

Submitted 10 June 2016
Accepted 31 January 2017
Published 7 March 2017
10.1126/scisignal.aag2435

Citation: N. Romanov, D. M. Hollenstein, M. Janschitz, G. Ammerer, D. Anrather, W. Reiter, Identifying protein kinase–specific effectors of the osmostress response in yeast. *Sci. Signal.* **10**, eaag2435 (2017).

X.2. Supplemental Material

Supplemental Table 1: Summary list of quantified phosphorylation sites using softwares MaxQuant and Proteome Discoverer over all MS experiments (6 experiments in total), containing details on biological variance, the number of peptide variants associated with the individual phosphorylation sites and the ratios for each individual peptide variant. According to the quantifications across the experiment types, a field-name is assigned to every phosphorylation site for easier filtering. The table also contains information on the M-track assay and the hyperosmotic sensitivity screen (see Computational Methods)

Romanov et al. (Appendix X.1) Supplemental Figure 8: Serial dilution droplet test of deletion mutants – complete dataset. Wild-type, *hog1*Δ and the corresponding dilution mutant strains were grown to mid log phase and subsequently dropped out in serial dilution steps (1:7 dilutions) onto different types of hyperosmotic stress plates: YPD +0.5M NaCl, +0.8M NaCl, +1.2M NaCl, +0.8M KCl, +1.2M KCl and +1.2M Sorbitol. A YPD plate containing no stress agent was used as negative control. Strains showing an osmosensitive phenotype are indicated (black arrow). Asterisk: weak phenotype.